1-1-2016

Proteostasis Responses to Endogenous Alpha-Synuclein Aggregation in the Brain

Scott Edward Ugras
University of Pennsylvania, scugras@sas.upenn.edu

Proteostasis Responses to Endogenous Alpha-Synuclein Aggregation in the Brain

Abstract
α-Synuclein aggregation is implicated in several neurodegenerative diseases, including Parkinson's disease (PD) and dementia with Lewy Bodies (DLB). Changes in cellular signaling pathways induced by this aggregation may contribute to cell death and disease pathogenesis. To investigate this, we used quantitative proteomics to measure the relative abundance changes of the proteome and phosphoproteome in response to aggregation of endogenous α-synuclein in the brain of a mouse model. Aggregation in this model is induced by the intrastriatal injection of α-synuclein pre-formed fibrils and recapitulates several cardinal features of human PD, including progressive aggregation concomitant with dopaminergic degeneration and motor symptoms. We quantified the relative abundance changes of 5,290 proteins and 2,763 phosphosites in wildtype mice and found significant changes in vesicle-mediated transport, RNA processing and the immune response. The immunoproteasome, an altered form of the constitutive proteasome that is induced in response to stress, was elevated in response to α-synuclein aggregation. Increased levels and activity of the immunoproteasome were found in human DLB compared with age-matched healthy controls. Additionally, the immunoproteasome degrades α-synuclein fibrils more efficiently than the constitutive proteasome. This is the first documented role of the immunoproteasome in synucleinopathies.

Degree Type
Dissertation

Degree Name
Doctor of Philosophy (PhD)

Graduate Group
Biochemistry & Molecular Biophysics

First Advisor
Harry Ischiropoulos

Keywords
Parkinson's, Proteomics, Proteostasis, Synuclein

Subject Categories
Biochemistry

PROTEOSTASIS RESPONSES TO ENDOGENOUS ALPHA-SYNUCLEIN AGGREGATION IN THE BRAIN

Scott Edward Ugras

A DISSERTATION

in

Biochemistry and Molecular Biophysics

Presented to the Faculties of the University of Pennsylvania

in

Partial Fulfillment of the Requirements for the

Degree of Doctor of Philosophy

2016

Supervisor of Dissertation

_____

Harry Ischiropoulos, Ph.D.

Research Professor, Department of Pediatrics, Children's Hospital of Philadelphia; Department of Systems Pharmacology and Translational Therapeutics, Perelman School of Medicine, University of Pennsylvania

Graduate Group Chairperson

_____

Kim A. Sharp, Ph.D.
Professor, Department of Biochemistry and Biophysics

Dissertation Committee

Yair Argon, Ph.D. Professor, Department of Pathology and Laboratory Medicine (Chair)
Walter Englander, Ph.D. Professor, Department of Biochemistry and Biophysics
Rahul Kohli, M.D., Ph.D. Assistant Professor, Department of Medicine
E. James Petersson, Ph.D. Associate Professor, Department of Chemistry

PROTEOSTASIS RESPONSES TO ENDOGENOUSE ALPHA-SYNUCLEIN AGGREGATION IN THE BRAIN

Eppur si muove

- Galileo Galilei

ACKNOWLEDGMENTS

First and foremost, I would like to thank Harry Ischiropoulos for his guidance over the past several years. Harry has consistently pushed me to be the best thinker and problem solver I can be, and has truly become a mentor to me. I look forward to continuing to receive mentorship and guidance from him in the years to come.

I would like to thank the members of my thesis committee, including Yair Argon, Rahul Kohli, Walter Englander, and James Petersson, who have helped me both inside and outside of my committee meetings.

I would like to thank members of the Ischiropoulos lab who have been scientific peers and have helped make doing research in lab fun, especially members of the 'Synuclein Data Club' including Danielle Mor, Malcolm Daniels and Dick Lightfoot.

I would like to thank my friends in the BMB program who have helped make my graduate school experience enjoyable, including Chris Yarosh, Michael Soo, Bengi Turegun, Dan Ricketts and Eric Babiash.

I am especially grateful for the support my family has provided me throughout my life, and particularly throughout graduate school. The older I get the more I appreciate all the love, support and guidance I have received from all members of my family, especially my parents, and my siblings Sandra, Steven and Stacy.

Finally I would like to thank my girlfriend Hilary. Having you in my life has taught me so much about finding balance, being confident and pursuing my passions, things I could not have learned in the classroom or at the bench. Thank for you challenging me to become a better person.

ABSTRACT

PROTEOSTASIS RESPONSES TO ENDOGENOUS ALPHA-SYNUCLEIN AGGREGATION IN THE BRAIN

Scott Edward Ugras

Harry Ischiropoulos

α-Synuclein aggregation is implicated in several neurodegenerative diseases, including Parkinson's disease (PD) and dementia with Lewy Bodies (DLB). Changes in cellular signaling pathways induced by this aggregation may contribute to cell death and disease pathogenesis. To investigate this, we used quantitative proteomics to measure the relative abundance changes of the proteome and phosphoproteome in response to aggregation of endogenous α-synuclein in the brain of a mouse model. Aggregation in this model is induced by the intrastriatal injection of α-synuclein pre-formed fibrils and recapitulates several cardinal features of human PD, including progressive aggregation concomitant with dopaminergic degeneration and motor symptoms. We quantified the relative abundance changes of 5,290 proteins and 2,763 phosphosites in wildtype mice and found significant changes in vesicle-mediated transport, RNA processing and the immune response. The immunoproteasome, an altered form of the constitutive proteasome that is induced in response to stress, was elevated in response to α-synuclein aggregation. Increased levels and activity of the immunoproteasome were found in human DLB compared with age-matched healthy controls. Additionally, the immunoproteasome degrades α-synuclein fibrils more efficiently than the constitutive proteasome. This is the first documented role of the immunoproteasome in synucleinopathies.

TABLE OF CONTENTS

LIST OF TABLES

LIST OF FIGURES

CHAPTER 1

Introduction

1.1 Proteostasis

Proteins have an intrinsic ability to adopt three-dimensional conformations that are necessary to execute proper functions[1,2]. Proteins may fail to adopt or maintain their proper conformation, however, due to errors in protein folding, mutations, or changes in binding partners, pH or concentrations[3]. To combat these potentially toxic events, cells have evolved diverse and integrated cellular machinery that maintains proper protein homeostasis through various cellular pathways. These proteostasis networks regulate protein expression, degradation, binding partners, locations and conformations[4]. A key element of proteostasis is its ability to dynamically regulate the proteome, through transcriptional and post-translational modifications[4,5].

Perturbations in the proteostasis networks, whether through age-related decline, environmental factors, or mutations, can contribute to diseases including neurodegenerative diseases[6], aging[7–9], cystic fibrosis[10], cancer[11,12] and Diabetes[13]. Intriguingly, attempts to modulate central nodes within proteostasis networks, such as the molecular chaperone Hsp90, have shown some therapeutic promise[14]. As our knowledge of proteostasis continues to advance, several other targets will emerge that have therapeutic potential[12].

The three major elements of the proteostasis network include chaperones that assist in proper protein folding[15,16], chaperone-mediated autophagy that clears misfolded proteins by translocating them into the lysosomal lumen, and the ubiquitin-proteasome system that targets specific proteins for degradation.

1.1.1 Chaperones

Despite the intrinsic ability of proteins to spontaneously adopt their native three-dimensional conformations, molecular chaperones often assist protein folding[17]. The complexity of protein folding *in vivo,* especially due to the crowded molecular environment within cells, increases the likelihood of aberrant protein aggregation[18]. Furthermore, large, multidomain proteins have a greater propensity to fold into off-pathway, misfolded intermediates[19].

Molecular chaperones assist in protein folding without being part of the final protein structure[16]. The Heat Shock Proteins (HSPs) are upregulated in times of stress or increased protein aggregation[20]. Several classes of HSPs exist and have different functions. The Hsp70 family is a group of constitutively expressed, highly conserved, ATP-dependent chaperones that assist folding of nascent proteins emerging from the ribosome and refold misfolded protein aggregates[21,22]. The Hsp90 chaperones are ATP-dependent and assist in proper protein folding events downstream of Hsp70s and are critical in many signaling events[23–26]. Another class of chaperones, chaperonins, are ATP-dependent molecular machines that include the well-studied GroEL/ES system[27,28].

1.1.2 Chaperone-Mediated Autophagy

Chaperone-mediated autophagy (CMA) is a degradation pathway that targets cytosolic proteins for lysosomal destruction[29]. CMA upregulation occurs in response to oxidative stress[30] and exposure to toxic compounds[31]. CMA substrates typically contain the pentapeptide KFERQ that is recognized by the Hsp70 member hsc70 when the motif is surface exposed. Hsc70 is part of the larger complex known as the CMA cargo recognition complex[32]. The newly formed substrate-CMA cargo recognition complex is then targeted to the lysosomal membrane for

translocation. Lysosome-associated membrane protein type 2A (LAMP-2A) is a single-span membrane protein that participates in substrate binding and translocation into the lumen of the lysosome[29,33]. The highly acidic intraluminal environment and lysosomal proteases then rapidly degrade substrate proteins.

CMA has been implicated in human pathology, including aging[34] and neurodegenerative diseases[35]. Age-related disruptions in lysosomal membrane dynamics cause a decline in total LAMP-2A levels that contribute to the decreased rate of CMA with age[36,37]. In Parkinson's disease (PD), where mutations and aggregation of α-synuclein are implicated in disease pathology, wildtype α-synuclein but not PD-linked mutant forms can be degraded by CMA[38,39]. Wildtype forms of leucine-rich repeat kinase 2 (LRKK2), another protein that is mutated in some cases of familial PD, are efficiently degraded by CMA but PD-linked mutant forms are not[40]. In Alzheimer's disease, the protein tau aggregates in the brain and forms intracellular tangles[41]. Normally, wildtype tau undergoes degradation by CMA but mutant tau undergoes differential degradation that may contribute to AD[42]. These findings suggest that the CMA arm of the proteostasis network plays a key role in maintaining functional protein networks.

1.1.3 Ubiquitin-Proteasome System

1.1.3.1 Substrate Targeting

The ubiquitin proteasome system (UPS) is the major cellular system that degrades misfolded proteins[43–45]. Proteins are targeted for degradation through a serious of sequential steps beginning with the covalent attachment of the 76-amino acid, highly conserved ubiquitin (Ub)

protein. First, the E1 Ub-activating enzyme covalently binds to Ub in an ATP-dependent process. Then, this Ub is transferred to a cysteine residue on the E2 Ub-conjugating enzyme. Then this activated E2 collaborates with the E3 enzyme to transfer the Ub to the target substrate. This mono-Ub substrate can then undergo further ubiquitination resulting in a polyubiquitinated protein. Substrates with at least four Ub are then recognized by the mature proteasome for degradation.

1.1.3.2 Constitutive Proteasome

The proteasome is composed of a 20S core catalytic subunit and two 19S regulatory caps that are responsible for substrate recognition[46–48]. The 20S core is composed of four seven-subunit rings, including two outer rings composed of seven α subunits and two inner rings composed of seven β subunits. These subunits are arranged in a $\alpha_{1\text{-}7}\beta_{1\text{-}7}\beta_{1\text{-}7}\alpha_{1\text{-}7}$ configuration. The β_1, β_2 and β_5 subunits confer the catalytic activity and specificity of the proteasome. The 19S caps regulate several steps in proteasomal degradation of substrate targets in an ATP-dependent manner, including entry into the 20S core, disassembly of the polyubiquitin chains, and binding to substrate[46].

1.1.3.3 Immunoproteasome

The immunoproteasome is an alternative form of the constitutive proteasome that is expressed under conditions of proinflammatory stimuli or oxidative stress[49–51]. In the 20S core of the immunoproteasome, the three catalytic subunits, β_1, β_2 and β_5, are replaced with Lmp2, MECL-1

and Lmp7 (also known as β_1i, β_2i and β_5i), respectively[52] (Figure 1.1). β_2 and MECL-1 each exhibit trypsin-like activity and β_5 and Lmp7 each exhibit chymotrypsin-like activity. Lmp2 and β_1 differ, however, in that Lmp2 exhibits chymotrypsin-like activity whereas β_1 exhibits caspase-like activity[53]. Assembly of the immunoproteasome by incorporation of the catalytic subunits occurs in response to interferon gamma (IFNγ) and is 4-fold faster than assembly of the constitutive proteasome[54]. Additionally, the immunoproteasome has a greater degradation efficiency of basic proteins compared with the constitutive proteasome[55]. These differences result in distinct kinetics and cleavage site preference of the immunoproteasome, resulting in the generation of antigenic peptides that are presented to major histocompatibility (MHC) class I molecules[56,57].

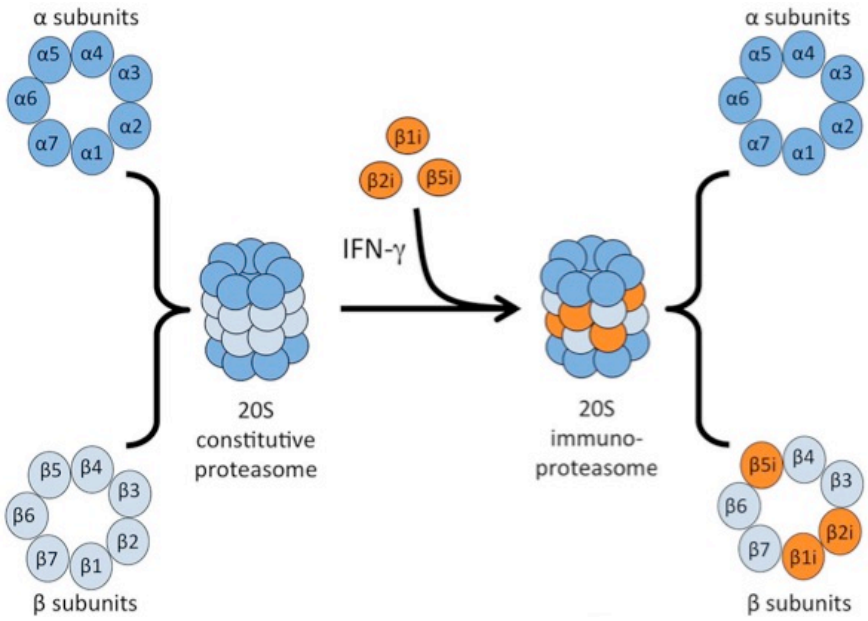

Figure 1.1 Subunit composition of the constitutive proteasome and the immunoproteasome. Representation of the subunits present in the constitutive proteasome and the immunoproteasome. Upon stimulation with cytokines such as IFNγ, the catalytic subunits of the immunoproteasome, Lmp2, MECL-1 and Lmp7 (also known as β_1i, β_2i and β_5i), replace the catalytic subunits of the constitutive proteasome, namely β_1, β_2 and β_5. Figure adopted from McCarthy and Weinberg[58].

The immunoproteasome has been implicated in a number of human diseases[59], including autoimmune diseases[60] and neurodegenerative diseases. Mutations in the *PSMB8* gene that encodes Lmp7 have been found to cause chronic atypical neutrophilic dermatosis with lipodystrophy and elevated temperature (CANDLE)[61] and joint contractures, muscle atrophy, microcytic anemia, and panniculitis-induced childhood-onset lipodystrophy (JMP)[62]. Immunoproteasome levels and activity were found to be elevated in the brains of patients who had Huntington's disease[63]. Lmp2-positive staining was also found predominantly within neurons and overlapped with 5% of cortical aggregates. Levels of the immunoproteasome have been found to be increased in the Alzheimer's disease (AD) brain compared with age-matched healthy brain[64]. Subsequent studies found that this increase is predominantly found in reactive glia that surrounds amyloid-β plaques in the AD brain[65].

1.2 Protein Misfolding in Neurodegeneration

1.2.1 Spreading of Protein Aggregates

Neurodegenerative diseases include a broad-array of progressive diseases afflicting the central nervous system (CNS)[66]. They are a major burden on older people and are predicted to increase in prevalence as populations continue to age[67]. Though these diseases affect different neuronal populations and manifest with different symptoms, they share a common feature of the accumulation of insoluble protein aggregates. These culpable proteins include amyloid-β and tau in AD, TDP43 and FUS in Amyotrophic Lateral Sclerosis (ALS), and α-synuclein in PD. These aggregates come in two major forms, either amyloid fibrils or amorphous aggregates.

While amorphous aggregates do not contain any regular structural characteristics, amyloid fibrils are highly ordered polymers that are rich in β-sheets[68]. Proteins have an intrinsic ability to adopt the amyloid conformation, though the proteostasis network prevents most from doing so[69]. These fibrils contain filaments of parallel β-strands that run perpendicular to the fibrillar axis, forming a cross-β structure[70]. The hydrogen bonds that form between the backbones of these strands provide the stability that is a characteristic of amyloid fibrils. This stability makes amyloid fibrils particularly recalcitrant to proteostasis pathways that degrade misfolded proteins. Amyloid fibrils are generated through a self-templating process composed of a nucleation phase followed by a growth phase[71]. In this process, oligomers of amyloid fibrils form first, and then recruit soluble forms of the same protein to grow at their ends. Once a critical nucleus is formed, growth rapidly proceeds until all available protein is consumed, resulting in a thermodynamically stable amyloid fibril.

This self-templating process, also known as seeding, is thought to underlie the predictable pathological spread of protein aggregates seen in neurodegenerative diseases, including AD, ALS and PD[67]. Strong evidence for seeding in neurodegenerative diseases comes from studies in PD patients who received fetal nigral transplants. In one study, human fetal neurons that were transplanted into a 61-year old patient contained Lewy Body-like aggregates characteristic of the PD brain only fourteen years after transplantation[72]. In another study, two patients who received fetal mesencephalic dopaminergic neurons developed α-synuclein positive, Lewy Body-like aggregates in the grafted neurons[73]. These studies provide evidence that in humans, protein aggregates can spread from host to graft, supporting the theory of cell-to-cell transmission in protein aggregation disorders. Additionally, studies in model organisms also support this theory, especially a recently developed mouse model of progressive α-synuclein aggregation[74]. In this

model, preformed fibrils of α-synuclein are intrastriatally injected into the right striatum of a non-transgenic mouse, resulting in progressive aggregation of endogenous α-synuclein concomitant with dopaminergic degeneration and motor phenotype. Critically, injection into α-synuclein-null mice does not result in degeneration or motor phenotype, providing evidence for the progressive aggregation of endogenous α-synuclein as being critical for pathology. This model of progressive aggregation of endogenous α-synuclein driven by a seeding mechanism has been reproduced in both mice[75,76] and rats[77].

1.2.2 Neurodegenerative Disease

1.2.2.1 Alzheimer's Disease

AD is the most common neurodegenerative disease worldwide, affecting over 45 million people in 2015 and is expected to grow to 115 million people by 2050[78]. An estimated 9.9 million new cases of AD occur each year, and the risk of developing AD increases exponentially with age[78]. Accumulation of extracellular aggregates of amyloid-β and cytoplasmic aggregates of tau are the pathological hallmarks of AD[79]. There is strong evidence for the progressive spreading of aggregates in the AD brain.

The major form of aggregated amyloid-β in the AD brain is a 42 amino acid peptide formed from the cleavage of amyloid precursor protein (APP)[80,81]. Recombinant forms of this peptide form amyloid fibrils, and these fibrils are capable of accelerating the aggregation of soluble forms of the same protein[82]. Injection of brain extracts from AD patients into APP transgenic mice induces progressive spread of pathology in the brain[83]. Additionally, inoculation with synthetic

amyloid-β aggregates induced aggregation in the APP transgenic mouse brain[84]. The aggregation of tau, a protein that binds to and stabilizes microtubules, is linked to AD and other tauopathies[85,86]. Injection of lysate from human brain that suffered from tauopathy into transgenic mouse that expressed human tau resulted in the development of tau-positive aggregates[87]. Collectively, these data support the notion that spreading of aggregates in the brain contributes to the pathogenesis of AD.

1.2.2.2 Amyotrophic Lateral Sclerosis

ALS (also known as Lou Gehrig's Disease) is a progressive motor degenerative disorder with a prevalence of 4-6 per 100,000 that is uniformly fatal within 1-5 years of disease onset[88]. Mutations in the RNA-binding proteins[89] TDP43[90–94] and FUS[95,96] cause familial forms of ALS. Cytoplasmic inclusions containing these proteins have been found in ALS patients, indicating that aggregation may contribute to disease[97]. Recombinant TDP43 forms non-amyloid aggregates *in vitro* under standard aggregating conditions[98]. The ALS-linked mutations Q331K and M337V accelerate this aggregation in cell-free systems and are toxic when expressed in cells[98]. Similarly, FUS also rapidly misfolds into non-amyloid, amorphous aggregates, and is toxic when expressed in cells[99]. Postmortem analysis of ALS patients reveals that tissues directly connected to the cortex develop TDP43 inclusions once the cortex does, but those tissues not connected do not[100]. These findings support a role for protein aggregation and spreading in the pathology of ALS.

1.3 Parkinson's disease

1.3.1 Disease Overview

PD is a neurodegenerative disorder of the CNS that afflicts over 50 million people worldwide[101]. First described in an 1817 essay by the English surgeon James Parkinson[102], it is currently the second most common neurodegenerative disease worldwide[103]. Degeneration of dopamine producing neurons in the substantia nigra pars compacta is a defining feature of PD[104]. This degeneration contributes to both motor and non-motor symptoms that PD patients exhibit. The five major motor symptoms of PD include bradykinesia, resting tremor, muscle rigidity, postural change and gait. Non-motor symptoms include cognitive changes, sleep and sensory deprivations, and constipation. PD patients may also experience dementia, particularly at later stages of the disease[105]. Estimates of the prevalence of dementia with patients who are diagnosed with PD vary, but most studies estimate 30%-40%[106,107]. Similar to other neurodegenerative diseases, age is the greatest risk factor for developing PD. Approximately 10% of PD cases are familial versus 90% that are sporadic[108].

1.3.2 Pathology of Parkinson's disease

The histopathological hallmark of PD is dense, cytoplasmic inclusions known as Lewy Bodies (LBs)[104]. The presence of LBs in different brain regions defines the progression of PD, starting from the olfactory bulb in stage 1 and progressing to the neocortex in stage 6[109]. Though some exceptions to this progression have been found[110,111], most cases follow this staging scheme[112,113]. LBs contain hyperphosphorylated α-synuclein fibrils[114] (more on α-synuclein in

Chapter 2). The aggregation of α-synuclein and formation of LBs is thought to contribute to the degeneration of dopamine-producing neurons in PD[115]. Additionally, α-synuclein mutations that cause PD have been identified[116–120], along with gene multiplications[121–123]. These data strongly implicate a role for α-synuclein aggregation in the pathogenesis of PD.

1.3.3 Treatments

PD is currently incurable and no disease modifying therapies exist. Most current therapies aim at elevating dopamine levels or potentiating dopamine pathways. The first therapy shown to be effective at mitigating PD symptoms was levodopa in 1967[124]. Levodopa, a precursor to dopamine that is able to cross the blood-brain barrier, is part of the current therapeutic regime. It is typically administered along with carbidopa, a dopa decarboxylase inhibitor, and is often the first line treatment for patients over 55 years of age. This regime is usually effective for 5 years at delaying motor symptoms of PD[125]. For patients under 55 years of age, a dopamine agonist, such as ropinirole or rotigotine, is typically the first line treatment. Selective type B monoamine oxidase inhibitors can also be administered and function by decreasing the conversion of dopamine to 3,4-Dihydroxyphenylacetic acid (DOPAC). At more advanced stages of PD, deep brain stimulation of the subthalamic nucleus is more effective at managing symptoms in the majority of patients compared with medical treatment alone, though the risk of adverse effects is greater[126].

References

1. Anfinsen, C. Principles that Govern the Folding of Protein Chains. *Science* **181,** 223–230 (1973).

2. Karplus, M., Dobson, C. M. & Andrej, S. Protein folding — a perspective from theory and experiment. *Angew. Chem. Int. Ed.* **37,** 868–893 (1998).
3. Díaz-villanueva, J. F., Díaz-molina, R. & García-González, V. Protein Folding and Mechanisms of Proteostasis. *Int. J. Mol. Sci.* **16,** 17193–17230 (2015).
4. Balch, W. E., Morimoto, R. I., Dillin, A. & Kelly, J. W. Adapting Proteostasis for Disease Intervention. *Science* **319,** 916 – 919 (2008).
5. Powers, E. T. & Balch, W. E. Diversity in the origins of proteostasis networks — a driver for protein function in evolution. *Nat. Rev. Mol. Cell Biol.* **14,** 237–248 (2013).
6. Tanaka, K. & Matsuda, N. Proteostasis and neurodegeneration: The roles of proteasomal degradation and autophagy. *BBA - Mol. Cell Res.* **1843,** 197–204 (2014).
7. Douglas, P. M. & Dillin, A. Protein homeostasis and aging in neurodegeneration. *J. Cell Biol.* **190,** 719–729 (2010).
8. Kikis, E. A., Gidalevitz, T. & Morimoto, R. I. Protein Homeostasis in Models of Aging and Age-Related Conformational Disease. *Adv Exp Med Biol* **694,** 138 – 159 (2010).
9. Vilchez, D., Saez, I. & Dillin, A. Organismal ageing and age-related diseases. *Nat. Commun.* **5,** 1–13 (2014).
10. Balch, W. E., Roth, D. M. & Hutt, D. M. Emergent Properties of Proteostasis in Managing Cystic Fibrosis. *Cold Spring Harb. Perspect. Biol.* 1–17 (2011).
11. Mendillo, M. L. *et al.* HSF1 Drives a Transcriptional Program Distinct from Heat Shock to Support Highly Malignant Human Cancers. *Cell* **150,** 549–562 (2012).
12. Powers, E. T., Morimoto, R. I., Dillin, A., Kelly, J. W. & Balch, W. E. Biological and Chemical Approaches to Diseases of Proteostasis Deficiency. *Annu. Rev. Biochem.* **78,** 959–991 (2009).
13. Back, S. H. & Kaufman, R. J. Endoplasmic Reticulum Stress and Type 2 Diabetes. *Annu. Rev. Biochem.* **81,** 767–793 (2012).
14. Trepel, J., Mollapour, M., Giaccone, G. & Neckers, L. Targeting the dynamic HSP90 complex in cancer. *Nat. Rev. Cancer* **10,** 537–549 (2010).
15. Hartl, F. U., Bracher, A. & Hayer-Hartl, M. Molecular chaperones in protein folding and proteostasis. *Nature* **475,** 324–32 (2011).
16. Kim, Y. E., Hipp, M. S., Bracher, A., Hayer-hartl, M. & Hartl, F. U. Molecular Chaperone Functions in Protein Folding and Proteostasis. *Annu. Rev. Biochem.* **82,** 323–355 (2013).
17. Doyle, S. M., Genest, O. & Wickner, S. Protein rescue from aggregates by powerful molecular chaperone machines. *Nat. Rev. Mol. Cell Biol.* **14,** 617–629 (2013).
18. White, D. A., Buell, A. K., Knowles, T. P. J., Welland, M. E. & Dobson, C. M. Protein Aggregation in Crowded Environments. *J. Am. Chem. Soc.* **132,** 5170–5175 (2010).
19. Herbst, R., Scha, U. & Seckler, R. Equilibrium Intermediates in the Reversible Unfolding of Firefly (Photinus pyralis) Luciferase. *J. Biol. Chem.* **272,** 7099–7105 (1997).
20. Verghese, J., Abrams, J., Wang, Y. & Morano, K. A. Biology of the Heat Shock Response and Protein Chaperones: Budding Yeast (Saccharomyces cerevisiae) as a Model System. *Microbiol. Mol. Biol. Rev.* **76,** 115–158 (2012).
21. Mayer, M. P. & Bukau, B. Cellular and Molecular Life Sciences Hsp70 chaperones: Cellular functions and molecular mechanism. *Cell. Mol. Life Sci.* **62,** 670–684 (2005).
22. Kampinga, H. H. & Craig, E. A. The HSP70 chaperone machinery: J proteins as drivers of functional specificity. *Nat. Rev. Mol. Cell Biol.* **11,** 579 – 592 (2010).
23. Pearl, L. H. & Prodromou, C. Structure and Mechanism of the Hsp90 Molecular Chaperone Machinery. *Annu. Rev. Biochem.* **75,** 271 – 294 (2006).

24. Li, J., Soroka, J. & Buchner, J. The Hsp90 chaperone machinery: Conformational dynamics and regulation by. *BBA - Mol. Cell Res.* **1823,** 624–635 (2012).
25. Li, J. & Buchner, J. Structure , Function and Regulation of the Hsp90 Machinery. *Biomed J.* **36,** 106–117 (2012).
26. Taipale, M., Jarosz, D. F. & Lindquist, S. HSP90 at the hub of protein homeostasis: emerging mechanistic insights. *Nat. Rev. Mol. Cell Biol.* **11,** 515–528 (2010).
27. Chen, Dong-Hua, Madan, Damian, Weaver, Jeremy, Lin, Zong, Schroder, Gunnar, Chiu, Wah, Rye, H. Visualizing GroEL / ES in the Act of Encapsulating a Folding Protein. *Cell* **153,** 1354–1365 (2008).
28. Georgescauld, F. *et al.* GroEL / ES Chaperonin Modulates the Mechanism and Accelerates the Rate of TIM-Barrel Domain Folding. *Cell* **157,** 922–934 (2014).
29. Kon, M. & Cuervo, A. M. Chaperone-mediated autophagy in health and disease. *FEBS Lett.* **584,** 1399–1404 (2010).
30. Kiffin, R., Christian, C., Knecht, E. & Cuervo, A. M. Activation of Chaperone-mediated Autophagy during Oxidative Stress. *Mol. Biol. Cell* **15,** 4829–4840 (2004).
31. Fred, J., Cuervo, A. N. A. M., Knecht, E. & Maria, A. Activation proteolysis of a selective pathway of lysosomal in rat liver by prolonged starvation. *Am. J. Physiol. Cell Physiol.* 200–208 (1995).
32. Chiang, H., SR, T., Plant, C. & Dice, J. A role for a 70-kilodalton heat shock protein in lysosomal degradation of intracellular proteins. *Science* **246,** 382–385 (1989).
33. Cuervo, A. M. & Dice, J. F. A Receptor for the Selective Uptake and Degradation of Proteins by Lysosomes. *Sci. Reports* **273,** 501 – 503 (1996).
34. Cuervo, A. M. & Wong, E. Chaperone-mediated autophagy: roles in disease and aging. *Cell Res.* **24,** 92–104 (2013).
35. Wang, G. & Mao, Z. Chaperone-mediated autophagy: roles in neurodegeneration. *Transl. Neurodegener.* **3,** 1–7 (2014).
36. Kiffin, R. *et al.* Altered dynamics of the lysosomal receptor for chaperone-mediated autophagy with age. *J. Cell Sci.* 782–791 (2007). doi:10.1242/jcs.001073
37. Cuervo, A. M. & Dice, J. F. Age-related Decline in Chaperone-mediated Autophagy. *J. Biol. Chem.* **275,** 31505–31513 (2000).
38. Cuervo, A. M., Stefanis, L., Fredenburg, R., Lansbury, P. T. & Sulzer, D. Impaired Degradation of Mutant α-Synuclein by Chaperone-Mediated Autophagy. *Sci. Reports* **305,** 1292 – 1295 (2004).
39. Vogiatzi, T., Xilouri, M., Vekrellis, K. & Stefanis, L. Wild Type a-Synuclein Is Degraded by Chaperone-mediated Autophagy and Macroautophagy in Neuronal Cells. *J. Biol. Chem.* **283,** 23542–23556 (2008).
40. Orenstein, S. J. *et al.* Interplay of LRRK2 with chaperone-mediated autophagy. *Nat. Neurosci.* **16,** 394–406 (2013).
41. Lee, V. M., Goedert, M. & Trojanowski, J. Q. Neurodegenerative tauopathies. *Annu. Rev. Neurosci.* **24,** 1121 – 1159 (2001).
42. Kaushik, S. *et al.* Tau fragmentation , aggregation and clearance : the dual role of lysosomal processing. *Hum. Mol. Genet.* **18,** 4153–4170 (2009).
43. Schwartz, A. L. & Ciechanover, A. The Ubiquitin-Proteasome Pathway and Pathogenesis. *Ann. Rev. Med.* **50,** 57–74 (1999).
44. Ravid, T. & Hochstrasser, M. Diversity of degradation signals in the ubiquitin–proteasome system. *Nat. Rev. Mol. Cell Biol.* 679 – 689 (2008). doi:10.1038/nrm2468

45. Wang, J. & Maldonado, M. A. The Ubiquitin-Proteasome System and Its Role in Inflammatory and Autoimmune Diseases. *Cell. Mol. Immunol.* **3,** 255–261 (2006).
46. Besche, H. C., Peth, A. & Goldberg, A. L. Getting to First Base in Proteasome Assembly. *Cell* **3,** 26–29 (2009).
47. Murata, S., Yashiroda, H. & Tanaka, K. Molecular Mechanisms of Proteasome Assembly. *Nat. Rev. Mol. Cell Biol.* **10,** 104 – 115 (2009).
48. Xie, Y. Structure, Assembly and Homeostatic Regulation of the 26 S Proteasome. *J. Mol. Cell Biol.* 308–317 (2010).
49. Ciehanover, A., Hod, Y. & Rershkol, A. A heat-stable polypeptide component of an ATP-dependent proteolytic system from reiculocytes. *Biochem. Biophys. Res. Commun.* **81,** 1100–1105 (1978).
50. Etlinger, J. D. & Goldberg, A. L. A soluble ATP-dependent proteolytic system responsible for the degradation of abnormal proteins in reticulocytes. *Proc. Natl. Acad. Sci. U. S. A.* **74,** 54–58 (1977).
51. Brown, Michael, Driscoll, James, Monaco, J. Structural and serological similarity of MHC-linked LMP and proteasome (multicatalytic proteinase) complexes. *Nature* **353,** 355 – 357 (1991).
52. Ferrington, D. A. & Gregerson, D. S. Immunoproteasomes: Structure, Function, and Antigen Presentation. *Prog. Mol. Biol. Transl. Sci.* **109,** 75–112 (2012).
53. Marques, J., Palanimurugan, R., Matias, A. C., Ramos, P. C. & Ju, R. Catalytic Mechanism and Assembly of the Proteasome. *Chem. Rev.* **109,** 1509–1536 (2009).
54. Heink, S., Ludwig, D., Kloetzel, P. & Kru, E. IFN-y-induced immune adaptation of the proteasome system is an accelerated and transient response. *Proc. Natl. Acad. Sci. U. S. A.* **102,** 9241–9246 (2005).
55. Raule, M., Cerruti, F. & Cascio, P. Enhanced rate of degradation of basic proteins by 26S immunoproteasomes. *BBA - Mol. Cell Res.* **1843,** 1942–1947 (2014).
56. Gaczynska, Maria, Rock, Kenneth, Goldberg, A. y-Interferon and expression of MHC genes regulate peptide hydrolysis by proteasomes. *Nature* 264 – 267 (1993).
57. Rock, K. L. *et al.* Inhibitors of the Proteasome Block the Degradation of Most Cell Proteins and the Generation of Peptides Presented on MHC Class I Molecules. *Cell* **78,** 761–771 (1994).
58. Mccarthy, M. K. & Weinberg, J. B. The immunoproteasome and viral infection: a complex regulator of inflammation. *Front. Mol. Biol.* **6,** 1–16 (2015).
59. Huber, E. M. & Groll, M. Inhibitors for the Immuno- and Constitutive Proteasome: Current and Future Trends in Drug Development Angewandte. *Angew. Chemie* **51,** 8708–8720 (2012).
60. Basler, M., Mundt, S., Bitzer, A., Schmidt, C. & Groettrup, M. The immunoproteasome: a novel drug target for autoimmune diseases. *Clin. Exp. Rheumatol.* 74–79 (2015).
61. Liu, Y. *et al.* Mutations in Proteasome Subunit B Type 8 Cause Chronic Atypical Neutrophilic Dermatosis With Lipodystrophy and Elevated Temperature With Evidence of Genetic and Phenotypic Heterogeneity. *Arthritis Rheum.* **64,** 895–907 (2012).
62. Atrophy, M. *et al.* An Autosomal Recessive Syndrome of Joint Contractures, Muscular Atrophy, Microcytic Anemia, and Panniculitis-Associated Lipodystrophy. *JCEM* **95,** 58–63 (2010).
63. Dıaz-Hernandez, M. *et al.* Neuronal Induction of the Immunoproteasome in Huntington's Disease. *J. Neurosci.* **23,** 11653–11661 (2003).

64. Mishto, M. *et al.* Immunoproteasome and LMP2 polymorphism in aged and Alzheimer's disease brains. *Neurobiol. Aging* **27,** 54–66 (2006).
65. Orre, M. *et al.* Reactive glia show increased immunoproteasome activity in Alzheimer's disease. *Brain* **136,** 1415–1431 (2013).
66. Skovronsky, D. M., Lee, V. M. & Trojanowski, J. Q. Neurodegenerative Diseases: New Concepts of Pathogenesis and Their Therapeutic Implications. *Annu. Rev. Pathol.* **1,** 151 – 170 (2006).
67. Brettschneider, J., Tredici, K. Del & Lee, V. M. Spreading of pathology in neurodegenerative diseases: a focus on human studies. *Nat. Rev. Neurosci.* **16,** 109–120 (2015).
68. Jucker, M. & Walker, L. C. Self-propagation of pathogenic protein aggregates in neurodegenerative diseases. *Nature* **501,** 45 – 51 (2013).
69. Dobson, C. M. Protein misfolding, evolution and disease. *Trends Biochem. Sci.* **24,** 329–332 (1999).
70. Nelson, R. *et al.* Structure of the cross-B spine of amyloid-like fibrils. *Nature* **435,** 773–778 (2005).
71. Wiltzius, J. J. W. *et al.* Molecular mechanisms for protein-encoded inheritance. *Nat. Struct. Mol. Biol.* **16,** 973–978 (2009).
72. Kordower, J. H., Chu, Y., Hauser, R. A., Freeman, T. B. & Olanow, C. W. Lewy body – like pathology in long-term embryonic nigral transplants in Parkinson's disease. *Nat. Med.* **14,** 504–506 (2008).
73. Li, J. *et al.* Lewy bodies in grafted neurons in subjects with Parkinson's disease suggest host-to-graft disease propagation. *Nat. Med.* **14,** 501–503 (2008).
74. Luk, K. C. *et al.* Pathological α-synuclein transmission initiates Parkinson-like neurodegeneration in nontransgenic mice. *Science* **338,** 949–53 (2012).
75. Osterberg, V. R. *et al.* Progressive Aggregation of Alpha-Synuclein and Selective Degeneration of Lewy Inclusion-Bearing Neurons in a Mouse Model of Parkinsonism. *Cell Rep.* **10,** 1252–1260 (2015).
76. Sacino, A. N. *et al.* Brain Injection of a-Synuclein Induces Multiple Proteinopathies, Gliosis, and a Neuronal Injury Marker. *J. Neurosci.* **34,** 12368–12378 (2014).
77. Paumier, K. L. *et al.* Intrastriatal injection of pre-formed mouse α-synuclein fibrils into rats triggers α-synuclein pathology and bilateral nigrostriatal degeneration. *Neurobiol. Dis.* **82,** 185–199 (2015).
78. Prince, M. *et al.* World Alzheimer Report 2015. *Alzheimer's Dis. Int.* 1 – 87 (2015).
79. Duyckaerts, C., Delatour, B. & Potier, M. Classification and basic pathology of Alzheimer disease. *Acta Neuropathol* **118,** 5–36 (2009).
80. Iwatsubo, T., Odaka, A., Suzuki, N. & Mizusawa, H. Visualization of AB42(43) and AP40 in Senile Plaques with End-Specific AB Monoclonals: Evidence That an Initially Deposited Species Is AB42(43). *Neuron* **13,** 45–53 (1994).
81. Glenner, G. G. & Wong, C. W. Alzheimer's Disease: Initial Report of the Purification and Charactrization of a Novel Cerebrovascular Amyloid Protein. *Biochem. Biophys. Res. Commun.* **120,** 885–890 (1984).
82. Kenyon, C. *et al.* Self-Propagating, Molecular-Level Polymorphism in Alzheimer's Beta-Amyloid Fibrils. *Science* **307,** 262 – 265 (2005).
83. Meyer-luehmann, M. *et al.* Exogenous Induction of Cerebral B-Amyloidogenesis is Governed by Agent and Host. *Science* **313,** 1781 – 1784 (2006).

84. Stöhr, J. *et al.* Purified and synthetic Alzheimer's amyloid beta (Aβ) prions. *PNAS* **109,** 11025 – 11030 (2012).
85. Cleveland, D. W., Hwo, S.-Y. & Kirschner, M. W. Purification of Tau, a Microtubule-associated Protein that Induces Assembly of Microtubules from Purified Tubulin. *J. Mol. Biol.* **116,** 207 – 225 (1977).
86. Ballatore, C., Lee, V. M.-Y. & Trojanowski, J. Q. Tau-mediated neurodegeneration in Alzheimer's disease and related disorders. *Nat. Rev. Neurosci.* **8,** 663 – 672 (2007).
87. Clavaguera, F. *et al.* Brain homogenates from human tauopathies induce tau inclusions in mouse brain. *Proc. Natl. Acad. Sci. U. S. A.* **110,** 9535–9540 (2013).
88. Pasinelli, P. & Brown, R. H. Molecular biology of amyotrophic lateral sclerosis: insights from genetics. *Nat. Rev. Neurosci.* **7,** 18–23 (2006).
89. Ugras, S. E. & Shorter, J. RNA-Binding Proteins in Amyotrophic Lateral Sclerosis and Neurodegeneration. *Neurol. Res. Int.* **2012,** 1 – 5 (2012).
90. Bo, R. Del *et al.* TARDBP (TDP-43) sequence analysis in patients with familial and sporadic ALS: identification of two novel mutations. *Eur. J. Neurol.* **16,** 727–732 (2009).
91. Deerlin, V. M. Van *et al.* TARDBP mutations in amyotrophic lateral sclerosis with TDP-43 neuropathology: a genetic and histopathological analysis. *Lancet* **7,** 409–416 (2008).
92. Pesiridis, G. S., Lee, V. M. & Trojanowski, J. Q. Mutations in TDP-43 link glycine-rich domain functions to amyotrophic lateral sclerosis. *Hum. Mol. Genet.* **18,** 156–162 (2009).
93. Rutherford, N. J. *et al.* Novel Mutations in TARDBP (TDP-43) in Patients with Familial Amyotrophic Lateral Sclerosis. *PLoS Genet.* **4,** 1–8 (2008).
94. Sreedharan, J. *et al.* TDP-43 Mutations in Familial and Sporadic Amyotrophic Lateral Sclerosis. *Science* **319,** 1668 –1672 (2008).
95. Hosler, B. A., Cortelli, P., Jong, P. J. De, Yoshinaga, Y. & Haines, J. L. Mutations in the FUS/TLS Gene on Chromosome 16 Cause Familial Amyotrophic Lateral Sclerosis. *Science* **323,** 1205–1209 (2009).
96. Nishimura, A. L. *et al.* Mutations in FUS, an RNA Processing Protein, Cause Familial Amyotrophic Lateral Sclerosis Type 6. *Science* **323,** 1208 –1211 (2009).
97. Parakh, S. & Atkin, J. D. Protein folding alterations in amyotrophic lateral sclerosis. *Brain Res.* 1–17 (2016).
98. Johnson, B. S. *et al.* TDP-43 Is Intrinsically Aggregation-prone, and Amyotrophic Lateral Sclerosis-linked Mutations Accelerate Aggregation and Increase Toxicity. *J. Biol. Chem.* **284,** 20329–20339 (2009).
99. Sun, Z. *et al.* Molecular Determinants and Genetic Modifiers of Aggregation and Toxicity for the ALS Disease Protein FUS / TLS. *PLoS Biol.* **9,** 1 – 25 (2011).
100. Brettschneider, J. *et al.* Stages of pTDP-43 Pathology in Amyotrophic Lateral Sclerosis. *Ann. Neurol.* **74,** 20–38 (2013).
101. Mortality, G. B. D. & Collaborators, D. Global, regional, and national age – sex specific all-cause and cause-specific mortality for 240 causes of death, 1990 – 2013: a systematic analysis for the Global Burden of Disease Study 2013. *Lancet* **385,** 117–171 (2014).
102. Parkinson, J. An essay on shaking palsy. *Whiitngham Rowl. London* (1817).
103. de Lau, L. & Breteler, N. Epidemiology of Parkinson's disease. *Lancet Neurol.* **6,** 525–535 (2006).
104. Goedert, M., Spillantini, M. G., Tredici, K. Del & Braak, H. 100 years of Lewy pathology. *Nat. Rev. Neurol.* **9,** 13–24 (2012).
105. Irwin, D. J., Lee, V. M. & Trojanowski, J. Q. Parkinson's disease dementia: convergence of

α-synuclein, tau and amyloid-β pathologies. *Nat. Rev. Neurosci.* **14,** 626–636 (2013).
106. Aarsland, D., Zaccai, J. & Brayne, C. A Systematic Review of Prevalence Studies of Dementia in Parkinson's Disease. *Mov. Disord* **20,** 1255–1263 (2005).
107. Aarsland, D. & Kurz, M. W. The Epidemiology of Dementia Associated with Parkinson's Disease. *Brain Pathol.* **20,** 633–639 (2010).
108. Elbaz, A. *et al.* Familial aggregation of Parkinson's disease: a population-based case-control study in Europe. *Neurology* **52,** 1876 – 1882 (1999).
109. Braak, H. *et al.* Staging of brain pathology related to sporadic Parkinson's disease. *Neurobiol. Aging* **24,** 197–211 (2003).
110. Braak, H. & Al, E. Pathology associated with sporadic Parkinson's disease—where does it end? *J. Neural Transm.* **70,** 89–97 (2006).
111. Uchikado, H., Lin, W., Delucia, M. W. & Dickson, D. W. Alzheimer Disease With Amygdala Lewy Bodies: A Distinct Form of a-Synucleinopathy. *J. Neuropathol. Exp. Neurol.* **65,** 685–697 (2006).
112. Dickson, D. W., Uchikado, H., Fujishiro, H. & Tsuboi, Y. Evidence in favour of Braak staging of Parkinson's disease. *Mov. Disord* **25,** S78–S82 (2010).
113. Halliday, G., McCann, H. & Shepherd, C. Evaluation of the Braak hypothesis: how far can it explain the pathogenesis of Parkinson's disease? *Expert Rev. Neurother.* **12,** 673–686 (2012).
114. Spillantini, M. *et al.* Alpha-Synuclein in Lewy bodies. *Nature* 839–840 (1997).
115. Bendor, J. T., Logan, T. P. & Edwards, R. H. The Function of a-Synuclein. *Neuron* **79,** 1044–1066 (2013).
116. Zarranz, J. J. *et al.* The new mutation, E46K, of alpha-synuclein causes Parkinson and Lewy body dementia. *Ann. Neurol.* **55,** 164–73 (2004).
117. Polymeropoulos, M. H. *et al.* Mutation in the α-Synuclein Gene Identified in Families with Parkinson's Disease. *Sci. Reports* **276,** 2045 – 2047 (1997).
118. Lesage, S. *et al.* G51D α-synuclein mutation causes a novel parkinsonian-pyramidal syndrome. *Ann. Neurol.* **73,** 459–471 (2013).
119. Appel-Cresswell, S. *et al.* Alpha-synuclein p.H50Q, a novel pathogenic mutation for Parkinson's disease. *Mov. Disord.* **28,** 811–3 (2013).
120. Krüger, R. *et al.* Ala30Pro mutation in the gene encoding α-synuclein in Parkinson's disease. *Nat. Genet.* **18,** 106–108 (1998).
121. Chartier-Harlin, M.-C. *et al.* A-synuclein locus duplication as a cause of familial Parkinson's disease. *Lancet* **07,** 1167–1169 (2004).
122. Singleton, A. B. *et al.* Alpha-Synuclein locus triplication causes Parkinson's disease. *Science* **302,** 841 (2003).
123. Ferese, R. *et al.* Four Copies of SNCA Responsible for Autosomal Dominant Parkinson's Disease in Two Italian Siblings. *Parkinsons. Dis.* **2015,** 1–6 (2015).
124. Cotzias, G. C., Van Woert, M. H. & Schiffer, L. M. Aromatic amino acids and modification of parkinsonism. *NEJM* **276,** 374 – 379 (1967).
125. Fahn, S. *et al.* Levodopa and the progression of Parkinson's disease. *NEJM* **351,** 2498 – 2508 (2004).
126. Bötzel, K. *et al.* A Randomized Trial of Deep-Brain Stimulation for Parkinson's Disease. *NEJM* 896 – 908 (2006).

CHAPTER 2

Dynamic Structural Flexibility of α-Synuclein

Danielle E. Mor[1*], Scott E. Ugras[2*], Malcolm J. Daniels[3*] and Harry Ischiropoulos[1,2,3,4#]

Biomedical graduate studies in [1]Neuroscience, [2]Biochemistry and Molecular Biophysics and [3]Pharmacology, Raymond and Ruth Perelman School of Medicine at the University of Pennsylvania, PA 19104. [4]Children's Hospital of Philadelphia Research Institute and Departments of Pediatrics and Systems Pharmacology and Translational Therapeutics, the Raymond and Ruth Perelman School of Medicine at the University of Pennsylvania, PA 19104

[*]Authors contributed equally.

[#]to whom correspondence should be addressed. E-mail: ischirop@mail.med.upenn.edu

(Published in Neurobiology of Disease, April 2016. Volume 88, Page 66-74)

2.1 Abstract

α-Synuclein is a conserved, abundantly expressed protein that is partially localized in pre-synaptic terminals in the central nervous system. The precise biological function(s) and structure of α-synuclein are under investigation. Recently, the native conformation and the presence of naturally occurring multimeric assemblies have come under debate. These are important deliberations because α-synuclein assembles into highly organized amyloid-like fibrils and non-amyloid amorphous aggregates that constitute the neuronal inclusions in Parkinson's disease and related disorders. Therefore understanding the nature of the native and pathological conformations is pivotal from the standpoint of therapeutic interventions that could maintain α-synuclein in its physiological state. In this review, we will discuss the existing evidence that define the physiological states of α-synuclein and highlight how the inherent structural flexibility of this protein may be important in health and disease.

2.2 Introduction

α-Synuclein is a soluble protein that is highly conserved in vertebrates and abundantly expressed in nervous tissue (Jakes et al., 1994). It was first discovered in 1988 in association with purified synaptic vesicles from the *Torpedo* electric ray (Maroteaux et al., 1988). Soon afterward α-synuclein was found to be widely distributed across the mammalian brain and localized to presynaptic nerve terminals, suggesting functions related to neurotransmission (Iwai et al., 1995). Independent of these reports, α-synuclein was identified as the precursor to a hydrophobic peptide found in Alzheimer's disease senile plaques, termed the non-Aβ component of Alzheimer's disease amyloid (NAC) (Uéda et al., 1993). The α-synuclein gene was

also dynamically regulated during song learning in zebra finch, supporting a role in synaptic plasticity (George et al., 1995).

The discovery of a mutation in the α-synuclein gene that was associated with autosomal dominant inheritance of Parkinson's disease (PD) provided the impetus for a major shift in α-synuclein research (Polymeropoulos et al., 1997). PD is a neurodegenerative disorder primarily characterized by the loss of dopamine-producing neurons in the substantia nigra pars compacta resulting in motor impairment. Since the original publication of the A53T mutation, several mutations, as well as multiplications of the α-synuclein gene have been linked to PD (Chartier-Harlin et al., 2004; Krüger et al., 1998; Lesage et al., 2013; Pasanen et al., 2014; Proukakis et al., 2013; Singleton et al., 2003; Zarranz et al., 2004; Ferese et al. 2015) Furthermore, several antibodies against α-synuclein robustly detect the well-known pathoanatomical features of PD, Lewy bodies and Lewy neurites, in postmortem brain tissue from patients with sporadic PD as well as other related neurodegenerative disorders (Baba et al., 1998; Spillantini et al., 1997; Takeda et al., 1998). The finding that wildtype α-synuclein was detected in Lewy bodies and Lewy neurites prompted the publication of numerous studies that investigated the biochemistry and biology of α-synuclein. Despite the rather impressive body of work several fundamental questions remain: What is the physiological function of α-synuclein? What is the structure of native α-synuclein? What factors contribute to the induction of aggregation-competent conformational states of α-synuclein? In this review, we will briefly review the evidence for the different biological functions and discuss ongoing efforts to precisely define physiological structures of α-synuclein.

2.3 The physiological function(s) of α-synuclein

The initial studies indicated that α-synuclein is not required for neuronal development or synapse formation, but instead may modulate synaptic activity. In rodents, α-synuclein is detected close to the time of birth and continues to increase until one month of age, when it reaches a steady-state level that is maintained throughout adulthood (Shibayama-Imazu et al., 1993). Similarly, in cultured rat neurons the development of synapses precedes α-synuclein expression and translocation to axonal terminals (Murphy et al., 2000; Withers et al., 1997). The hypothesis that α-synuclein regulates synaptic activity was directly tested in mice lacking α-synuclein. α-Synuclein null mice develop normal brain architecture and synaptic contacts, and do not exhibit gross behavioral phenotypes (Abeliovich et al., 2000). However, subtle abnormalities in activity-dependent neurotransmitter release have been observed. Upon repeated stimulation, dopaminergic synapses from α-synuclein null mice sustain highly elevated dopamine release (Abeliovich et al., 2000; Yavich et al., 2004). Functional redundancy among α-synuclein and the other synuclein family members, β- and γ-synuclein, may account for the mild phenotypes observed in the single knockout. In α/β-synuclein double knockout mice, synaptic plasticity appears unaltered relative to α-synuclein single knockouts, although dopamine levels in the striatum are reduced (Chandra et al., 2004). The importance of synucleins is particularly highlighted by α/β/γ-synuclein triple knockouts, which have decreased life span and late-onset synaptic dysfunction compared with wildtype mice (Burré et al., 2010; Greten-Harrison et al., 2010). Triple knockouts in another study had motor deficits and decreased striatal dopamine, along with abnormal dopamine neurotransmission (Anwar et al., 2011). Collectively, these reports emphasize the important role of the synucleins in long-term synaptic maintenance and plasticity.

Synaptic vesicle trafficking. Examination of the role of α-synuclein in the synaptic vesicle cycle has yielded conflicting results. Depletion of α-synuclein from rodent hippocampal neurons both *in vivo* and *in vitro* induces a significant loss of undocked synaptic vesicles, suggesting that α-synuclein acts to replenish or maintain the resting and/or reserve vesicle pools (Cabin et al., 2002; Murphy et al., 2000). In contrast, another study found that increasing α-synuclein in rodent hippocampal neurons reduces the recycling pool of vesicles (Nemani et al., 2010). The effect of α-synuclein on vesicles docked at the plasma membrane prior to exocytosis is similarly unclear. Knockout or knockdown of α-synuclein in rodent hippocampal neurons results in either a decrease or no change in the number of docked vesicles (Cabin et al., 2002; Murphy et al., 2000). Conversely α-synuclein expression in PC12 cells causes an accumulation of vesicles at the plasma membrane and impairment of exocytosis (Larsen et al., 2006). However, in mice modestly overexpressing α-synuclein (levels are not associated with neurotoxicity), hippocampal synapses display a redistribution of vesicles away from the active zone. The density of vesicles in synaptic boutons is also reduced, consistent with α-synuclein-mediated inhibition of vesicle clustering. This is supported by α-synuclein-induced defects in vesicle re-clustering following endocytosis in rat hippocampal neurons (Nemani et al., 2010). Still, opposing results have been obtained from yeast, in which α-synuclein expression results in massive accumulations of vesicles that co-localize with Rab GTPases (Gitler et al., 2008; Soper et al., 2008). Likewise, α-synuclein has been shown to restrict vesicle diffusion away from synapses in mouse hippocampal neurons (Wang et al., 2014). Several lines of evidence, therefore, support the participation of α-synuclein in synaptic vesicle trafficking, though the specific steps for which it may be most important, i.e. vesicle docking, recycling and/or re-clustering, remain unclear.

Chaperone-like activity and neurotransmitter release. α-Synuclein and the other synuclein family members may act as molecular chaperones, facilitating neurotransmitter release. Cysteine-string protein α (CSPα) is a chaperone that is essential for synaptic health; its deletion in mice leads to a decrease in SNARE protein complexes, nerve terminal degeneration, motor impairment and death. When expressed in CSPα-deficient mice, α-synuclein is able to rescue this degenerative phenotype and restore levels of SNARE complexes in synaptic terminals. Moreover, mice lacking both α-synuclein and CSPα exhibit an exacerbated phenotypic decline (Chandra et al., 2005). These findings suggest that α-synuclein is able to complement the activity of CSPα in promoting synapse integrity. Direct evidence for the interaction of α-synuclein with SNARE complexes was documented by co-immunoprecipitation of α-synuclein with SNARE proteins and specific binding to the vesicle-associated SNARE protein synaptobrevin-2. In mammalian cells and purified *in vitro* systems, α-synuclein dose-dependently facilitates SNARE complex assembly (Burré et al., 2010). Additional support for chaperone-like activity includes sequence homology between α-synuclein and 14-3-3 protein chaperones as well as the association of α-synuclein with 14-3-3 and its binding partners in rat brain (Ostrerova et al., 1999). α-, β-, and γ-synucleins are also able to prevent the aggregation of denatured proteins *in vitro* (Souza et al., 2000a), further supporting a conserved chaperone-like function of synucleins and the existence of several protein-protein interactions that facilitate synaptic function.

Putative role in neurotransmitter synthesis and reuptake. Published evidence indicates that α-synuclein-mediated protein-protein interactions may modulate dopamine synthesis and recycling. α-Synuclein may inhibit the activity of tyrosine hydroxylase (TH), the rate-limiting enzyme in dopamine synthesis. α-Synuclein and TH co-immunoprecipitate from rat striatal

tissue and MN9D dopaminergic cells and α-synuclein was shown to inhibit TH activity in MN9D and PC12 cells, potentially through PP2A phosphatase-mediated reduction of serine 40 phosphorylation of TH (Peng et al., 2005; Perez et al., 2002). α-Synuclein may also interact with and inhibit the activity of aromatic amino acid decarboxylase, which catalyzes the conversion of L-DOPA to dopamine (Tehranian et al., 2006). Thus, α-synuclein may serve as a negative regulator of dopamine synthesis, though further validation of these findings is necessary. Several reports have also implicated α-synuclein in the regulation of the dopamine transporter (DAT), though the evidence is conflicting with regards to the functional consequences. Direct binding of α-synuclein to DAT has been demonstrated in multiple studies. However, α-synuclein does not appear to alter DAT function, but rather in various cellular contexts can promote or inhibit DAT trafficking to the plasma membrane (Oaks and Sidhu, 2011). Elucidating the relationship between α-synuclein and DAT requires further investigation.

2.4 α-Synuclein structural flexibility

Primary sequence. The primary sequence of α-synuclein consists of 140 amino acids with a predicted molecular mass of 14,460.16 Da and an isoelectric point of 4.67 (figure 1). The sequence of α-synuclein is composed of three functionally defined domains. The N-terminal region (amino acids 1-60) is characterized by the presence of unique and highly conserved sequence of imperfect tandem repeats with a central consensus motif of **K**(A)-**T**(A,V)-**K**(V)-**E**(Q,T)-**G**(Q)-**V**(A). These motifs spanning residues 10-86 are projected to form two amphipathic α-helices and are characteristic of several proteins such as apolipoproteins that bind reversibly to membranes (George et al., 1995; Maroteaux et al., 1988). Indeed the structure of membrane bound α-synuclein contains two α-helices (amino acids 3-37 and 45-92) in a roughly antiparallel

arrangement with a short linking region (Ulmer et al., 2005). These helices are stabilized by interaction with a variety of phospholipid bilayers, though α-synuclein interacts preferentially with membranes of high curvature and an abundance of acidic phospholipids, properties consistent with those of synaptic vesicles (Davidson et al., 1998; Zhu et al., 2003). Upon interaction with membranes of low curvature α-synuclein adopts a distinct secondary structure characterized by a single extended helix that includes both previously described helical domains and the linker region (amino acids 38-44) (Ferreon et al., 2009; Georgieva et al., 2010; Trexler and Rhoades, 2009). All known mutations associated with familial PD (A30P, E46K, H50Q, G51D, A53E, and A53T) are found in the N-terminal domain (Krüger et al., 2008; Lesage et al., 2013; Pasanen et al., 2014; Polymeropoulos et al., 1997; Proukakis et al., 2013; Zarranz et al., 2004). These mutations, with the exception of G51D, A53E, and A30P, increase the propensity of α-synuclein to form insoluble aggregates and produce morphologically distinct aggregate species (Ghosh et al., 2014; Giasson et al., 1999; Greenbaum et al., 2005; Lesage et al., 2013; Mahul-Mellier et al., 2015; Narhi et al., 1999). Though the precise mechanism by which these mutations promote aggregation has not been conclusively shown, evidence implicate an accelerated formation of oligomers (Conway et al., 2000) likely due to the destabilization of the native N-terminal conformation (Bertoncini et al., 2005a; Burré et al., 2015; Coskuner and Wise-Scira, 2013; Dettmer et al., 2015).

Amino acids 61-95 compose the hydrophobic NAC domain (Uéda et al., 1993). This region contains a sequence of amino acids (71-82) necessary and sufficient for α-synuclein self-assembly into amyloid fibrils (Giasson et al., 2001). Recently the crystal structures of residues 68-78 (termed NACore), and residues 47-56 (PreNAC) were resolved by the use of micro-

electron diffraction, revealing that strands in this region stack in-register into β-sheets that are typical of amyloid assemblies (Rodriguez et al., 2015).

The C-terminal domain (96-140) is rich in negatively charged amino acids (contains 10 glutamate and 5 aspartate residues) and was originally proposed to be essential for maintaining the solubility of the protein. The presence of 5 proline residues, which are known to induce turns and disrupt secondary protein structure, suggested that this region is devoid of secondary structure (George et al., 1995; Ulmer et al., 2005). However, the C-terminus was shown to form transient, long-range interactions with the N-terminus resulting in the formation of multiple compact monomeric structures (Bertoncini et al., 2005a; Dedmon et al., 2005). These compacted structures of α-synuclein are temperature sensitive and are resistant to aggregation. The data also indicated that at elevated temperatures the C-terminus assumes an extended conformation that liberates N-terminal associations and enables aggregation (Bertoncini et al., 2005b; Dedmon et al., 2005). Moreover, C-terminally truncated forms of α-synuclein aggregate faster than full length protein (Hoyer et al., 2004; Li et al., 2005). Truncated α-synuclein has been detected in the brains of both control (non-disease) and PD patients. Cleavage of full-length protein at residues D115, D119, N122, D125 and Y133 was documented in α-synuclein extracted from LBs (Anderson et al., 2006).

The C-terminus appears to be important for the interaction of α-synuclein with other proteins and for the interaction with small molecules (Burre et al., 2012; Burré et al., 2010; Conway et al., 2001; Mazzulli et al., 2006; Souza et al., 2000b; Woods et al., 2007). Additionally, it contains the major sites of metal binding and post-translational modifications. Binding of iron, copper, and other metals has been shown to influence α-synuclein function and aggregation (Uversky et al., 2001a). Addition of Fe(III), but not Fe(II) to preformed oligomers of α-synuclein accelerates

aggregation, raising the question of metal binding at different points during the aggregation process (Kostka et al., 2008). Cu(II) is unique among metals at accelerating aggregation of α-synuclein at physiologically relevant concentrations. The sole histidine residue H50 in α-synuclein was found to be critical for Cu(II) binding (Rasia et al., 2005) whereas other divalent metal ions, including Mn(II), Co(II), Ni(II) and Fe(II), preferentially bind to the C-terminus of α-synuclein at residues D121, N122, and E123 (Binolfi et al., 2006).

Post-translational modifications. α-Synuclein undergoes a number of post-translational modifications, including N-terminal acetylation, serine and tyrosine phosphorylation, lysine ubiquitination and tyrosine nitration (Oueslati et al., 2010; Barrett & Greenamayer 2015). α-Synuclein purified under mild conditions is acetylated in the N-terminus. The N-terminal acetylation may account for the formation of an oligomeric form of the protein with partial α-helical structure (Trexler and Rhoades, 2012). However, semisynthetic production of N-terminally acetylated α-synuclein demonstrated that modified and unmodified versions of the protein share similar secondary structure, aggregation propensities, and membrane binding (Fauvet et al., 2012a). NMR studies indicated that the first 12 residues undergo a chemical shift due to N-terminal acetylation. This modification also appears to stabilize the helicity of the N-terminus within the context of the full-length protein, and increases the affinity of α-synuclein for lipids (Dikiy and Eliezer, 2014).

Mass spectrometry-based methodologies revealed that α-synuclein extracted from human Lewy bodies was phosphorylated at S129 (Fujiwara et al., 2002). An antibody raised against phosphorylated S129 was then used to show that α-synuclein was phosphorylated at this site only in subjects with disease and that S129 phosphorylated α-synuclein was present only in the Triton-X- and Sarkosyl-insoluble, urea soluble fraction. These data indicated that some form(s)

of aggregated α-synuclein and not the soluble protein is targeted for phosphorylation at S129. Indeed *in vitro* data showed that purified fibrils of α-synuclein are substrates for casein kinase 1 or 2 (Waxman and Giasson, 2008). Other data indicated that polo-like kinase (PLK) 2-mediated phosphorylation of S129 increased autophagy-mediated degradation of α-synuclein, suggesting that phosphorylation may be a neuroprotective mechanism to accelerate clearance of aggregated protein (Oueslati et al., 2013). In addition to the monomeric α-synuclein, S129 phosphorylated bands with apparent molecular weight of 22 kDa and 29 kDa were observed in the detergent insoluble extract (Hasegawa et al., 2002). These bands were also immunoreactive with anti-ubiquitin antibodies suggesting that S129 phosphorylated α-synuclein is also targeted for mono- and di-ubiquitination. It has long been established that the core of Lewy bodies stains positive for both α-synuclein and ubiquitin whereas the surrounding halo is immunoreactive for α-synuclein (Hasegawa et al., 2002). Of the 15 lysine residues in α-synuclein, the major sites of LB-derived α-synuclein undergoing ubiquitination were residues K12, K21, and K23 (Anderson et al., 2006; Hasegawa et al., 2002; Sampathu et al., 2003).

A number of spectroscopic methodologies (CD and NMR) were employed to explore the effect of S129 phosphorylation on the structure of α-synuclein. CD data revealed that phosphorylation of S129 did not affect secondary structure, such that both non-phosphorylated and phosphorylated S129 exhibited random coil structure (Paleologou et al., 2008). NMR data revealed a number of chemical shifts that occur due to phosphorylation. While the residues surrounding S129 exhibited the greatest perturbation, residues 1-90 also exhibited detectable chemical shifts (Paleologou et al., 2008) This likely reflects the previously documented long-range interactions of the C- and N-termini. The potential effects of phosphorylation of S129 on the structure of the protein were not faithfully reproduced by mutation of S129 to either E or D,

two common phosphomimics used to study the structural consequences of phosphorylation. For example, phosphorylation at S129 increased the hydrodynamic radius of the protein, whereas S129 E/D mutants did not (Paleologou et al., 2008).

Subsequent studies found additional sites of phosphorylation. Elevated levels of phosphorylated α-synuclein at residue S87 were detected in human brains with Alzheimer's disease, Lewy Body disorders, and multiple system atrophy (Paleologou et al., 2010). S87 phosphorylation alters the biophysical properties of α-synuclein, including inhibition of fibril formation and reduction in membrane binding (Paleologou et al., 2010). Additionally, phosphorylated α-synuclein at residue Y125 was detected in Drosophila expressing human wildtype α-synuclein as well as in human brains, though levels were decreased in disease compared with aged-matched healthy controls (Chen et al., 2009).

The proximity of the α-synuclein phosphorylation sites to the metal binding sites raised the question of how phosphorylation may affect metal ion interactions. This was investigated by the use of C-terminal peptides containing residues 119-132 that were either unmodified, phosphorylated at Y125 or at S129 (Liu and Franz, 2005). By exploiting the luminescence properties of Tb^{3+}, it was found that phosphorylated Y125 showed enhanced Tb^{3+} binding relative to wildtype or phosphorylated S129. Additionally, phosphorylated Y125 preferentially bound to trivalent rather than divalent metal ions. To investigate this further, longer C-terminal fragments comprised of residues 107-140 that were either unmodified of monophosphorylated at Y125 or S129 were tested for their affinity to various metal ions. By using a fluorescence quenching assay, the dissociation constants of the metal ion complexes and the α-synuclein peptides were determined. These data indicate that either phosphorylation at Y125 or S129 increases the binding affinity for Cu (II) and Fe(II), but not Fe(III). Furthermore, phosphorylated

Y125 has a greater affinity for Pb(II) than wildtype, but phosphorylated S129 has an even greater affinity than phosphorylated Y125. Additionally, tandem MS indicated that phosphorylation causes the metal ion binding sites to shift towards the C-terminal end of α-synuclein (Lu et al., 2011).

α-Synuclein within Lewy bodies is nitrated on all four tyrosine residues (Giasson et al., 2000). Chemical nitration of α-synuclein results in the formation of both tyrosine nitrated monomers and nitrated dimers (Souza et al. 2000b). Immunoelectron microscopy confirmed that nitrated monomers and dimers are incorporated into amyloid fibrils. Purified nitrated α-synuclein monomer by itself was unable to form fibrils, whereas the nitrated dimer accelerated aggregation of unmodified α-synuclein (Hodara et al., 2004). Additionally, nitration at residue Y39 in the N-terminus decreased binding to synthetic vesicles and prevented the protein from adopting α-helical conformation (Hodara et al., 2004). These observations were recently confirmed and elegantly expanded by the generation of site-specifically nitrated α-synuclein using protein semisynthetic chemistries (Burai et al. 2015). Using the synthetic nitrated α-synuclein the data showed that nitration did not interfere with phosphorylation of S129 by PLK3 and reaffirmed that intermolecular interactions between the N- and C-terminal regions of α-synuclein are critical in directing nitration-induced oligomerization of α-synuclein (Burai et al. 2015).

Native conformation(s) of α-synuclein. Figure 2 depicts the rapid growth in the number of publications identified in PubMed using the term synuclein and highlights key studies that explored the native structure and conformation of the protein. Early biochemical studies of α-synuclein isolated from bacterial expression systems or α-synuclein expressed in rodent tissues indicated that it is monomeric with limited secondary structure. Electrophoretic separation of

α-synuclein purified without heating on 6, 10, or 14% acrylamide gels estimated an apparent molecular weight of 20±3 kDa. However, the values of sedimentation coefficient ($S_{20,w}$ = 1.7S), stokes radius (34 Å), analysis on native gels and derivation of the frictional coefficient (f/f_o=2.09) indicated an apparent molecular weight in the range 57-58 kDa (Weinreb et al., 1996). To reconcile this apparently anomalous behavior it was proposed that monomeric α-synuclein achieves minimal structure in simple solutions and this rather extended unstructured conformation resembles a globular protein with a larger apparent molecular weight. This assumption was further corroborated by examination of purified monomeric α-synuclein by CD, FTIR and small angle X-ray scattering, which failed to identify significant secondary structural features. Furthermore, minimal shifts in the spectroscopic features of α-synuclein were observed when the protein was placed in solutions that would increase hydrophobicity and neutralize negative charges indicating that the protein is natively unstructured, joining a growing group of proteins sharing similar biochemical and biophysical characteristics (Uversky et al., 2001b). NMR and CD data, however, indicated that α-synuclein assumes increasingly folded secondary structure when exposed to conditions that promote aggregation (low pH and high temperature) or upon interaction with phospholipids. Collectively these data indicated that native α-synuclein is primarily an unstructured monomer, which can assume different compact conformations that resist aggregation, adopts α-helical conformation upon binding to lipids and undergoes conformational changes prior to oligomerization and formation of amyloid fibrils (Uversky et al., 2001b). However, the methodologies employed to quantify the molecular weight of α-synuclein in these elegant studies were not based on first principles and therefore a lingering uncertainty remains regarding the native size of the protein. Moreover, crosslinking experiments in both intact cells expressing α-synuclein and lipid-free lysates revealed the

stabilization of high molecular weight α-synuclein multimers (consistent with dimers, trimers, and larger multimers). These multimers were not reduced by dilution of lysates before crosslinking, nor by reducing the concentration of crosslinker from 1 mM to 8 μM, suggesting that they represented endogenous protein complexes (Cole et al., 2002).

Examination of the α-synuclein native state was reignited in 2011 with the publication of results indicating that α-synuclein exists natively as a tetramer, rather than a monomer. Methodologies that are based on first principles were employed to examine the molecular weight and size of α-synuclein extracted under non-denaturing conditions from human red blood cells. Analytical ultracentrifugation produced a sedimentation equilibrium value of 4.78 S, indicating a molecular weight of 57.8 kDa. Analysis of particle geometry by scanning transmission electron microscopy revealed the presence of roughly spherical molecules with a diameter of approximately 3.0-3.5 nm. Automated sampling of 1000 α-synuclein particles showed a distribution of molecular weights between 10 and 175 kDa with a peak distribution at 55 kDa. These findings constitute the most direct measurements of the native molecular weight of α-synuclein. The tetrameric species were shown to have α-helical conformation and were resistant to aggregation (Bartels et al., 2011).

Complimentary observations were made using recombinant GST-tagged α-synuclein purified from bacterial expression systems under non-denaturing conditions. Single-particle electron microscopy of purified α-synuclein revealed complexes of sizes and internal geometries consistent with trimers and dimers, which were corroborated by measurements of the hydrodynamic radii and elution on native state PAGE. As observed previously, these species were more resistant to aggregation than denatured monomer. CD also showed that several α-synuclein mutations associated with early onset PD (A30P, E46K, A53T) exist in less ordered

conformations than wildtype α-synuclein. These mutants were also more prone to aggregation (Wang et al., 2011). However, using the same α-synuclein construct that contains a 10-residue N-terminal extension, which forms multimers when isolated from E. coli, NMR studies indicated that only a small fraction of α-synuclein assembles into α-helical trimers and tetramers and the majority remains as a disordered monomer (Gurry et al., 2013). These data indicated that several potential conformers of α-synuclein may exist in equilibrium. The observation that α-helical trimers and tetramers constitute only a small fraction of the total α-synuclein may explain other studies in which in-cell NMR was used to probe for the structure of α-synuclein and reported primarily the presence of unstructured monomer. NMR data of α-synuclein in intact cells failed to detect stable or highly populated α-synuclein multimers and confirmed the intrinsically disordered nature of the protein in *E. coli* regardless of its purification method (Binolfi et al., 2012). Collectively these studies generated an apparent controversy and stimulated several additional studies that explored the native size and structure of α-synuclein.

A re-examination of the native state of α-synuclein reasserted that the behavior of α-synuclein from various sources was consistent with a disordered monomer. This behavior was observed with protein extracted and isolated under both denaturing and non-denaturing conditions. CD spectra previously attributed to tetrameric assemblies were not reproduced using isolated monomer, but were replicated with the addition of small unilamellar vesicles. Natively isolated α-synuclein before or after boiling that disrupts secondary structure migrated as high molecular weight α-synuclein bands in native PAGE, which was attributed to the rather expanded size of the unstructured monomer in solution. These findings reaffirmed that the majority of native α-synuclein is a monomer with minimal secondary structure (Fauvet et al., 2012a). Further support was provided by similar explorations in the mouse brain, which indicated that the

predominant native form of α-synuclein is an unstructured monomer. α-Synuclein exhibited random coil structure in solution, readily aggregated over time, and adopted α-helical structure only upon membrane binding (Burré et al., 2013).

α-Synuclein multimers were detected in postmortem non-diseased human brain using mild protein extraction methods, but no further purification. These α-synuclein multimers had Stokes radii ranging from 33.2-37.5 Å, sedimentation coefficients ranging from 1.4S to 3.8S and apparent molecular weights ranging from 53-70 kDa in native gradient gels. The multimers were detected by anti-α-synuclein antibodies that recognize different epitopes and the multimer identity was confirmed by mass spectrometry. Consistent with previous observations, melting point thermostability analysis showed progressive loss of the α-synuclein multimers and heating of the brain extracts above 55 ^{o}C collapsed the higher molecular weight α-synuclein conformers into the 53 kDa species, which corresponds to the unstructured monomer. These data indicated the presence of α-synuclein conformers, defined as conformationally diverse α-synuclein multimers, in the human brain. Therefore it appears that both monomer and metastable multimers coexist and that interactions with lipids, other proteins, or small molecules may transiently stabilize these species (Gould et al., 2014). This was further supported by controlled bimolecular fluorescence complementation methodologies in different cell types that found α-synuclein metastable conformers assembled in synapses. It was suggested that the function of these multimeric α-synuclein conformers is to restrict recycling of synaptic vesicles and thus reduce neurotransmitter release (Wang et al. 2014).

Additional support for native multimeric species comes from recent studies in which serial purification of α-synuclein from non-pathological human cortical tissue was performed. Removal of lysate components other than protein followed by sequential removal of proteins

though size exclusion, anion chromatography, and thiopropyl sepharose 6b separation, resulted in the isolation of >90% pure α-synuclein. Each step of serial purification resulted in a progressive loss of α-synuclein immunoreactive high molecular weight bands observed after disuccinimidyl glutarate crosslinking and SDS-PAGE separation. Analysis of α-synuclein secondary structure by CD found that the sequentially purified protein had greater α-helical content than the recombinant α-synuclein. However, a high degree of variability in secondary structure was observed between purified samples raising questions about the stability of these helical conformations (Luth et al., 2015). Furthermore, crosslinking experiments conducted in brain tissue from mice expressing wildtype or A53T human α-synuclein in the absence of mouse α-synuclein showed that the A53T mutation reduced the presence of soluble multimeric α-synuclein (Dettmer et al., 2015).

2.5 Concluding remarks and perspectives.

Collectively the studies on the native structure indicate a remarkable conformational plasticity and structural flexibility of α-synuclein. The ability of the protein to adopt N-terminal α-helical conformation through its association with lipids has been well documented. The association with lipids has been shown to prevent fibril formation (Martinez et al., 2007; Zhu and Fink, 2003) and may also stabilize physiological multimeric species that together with the monomer regulate SNARE complex assembly and recycling of synaptic vesicles (Burré et al., 2014; Wang et al. 2014). However, other groups have demonstrated a role for phospholipid membranes in promoting pathological α-synuclein aggregation, potentially by acting as a scaffold for amyloid nucleation. This event may preferentially occur at low lipid to protein ratios, when monomeric

α-synuclein is free in solution and can participate in nucleation (Galvagnion et al., 2015; Ysselstein et al., 2015).

In figure 3 we propose a model which incorporates and summarizes the existing knowledge regarding α-synuclein biology and structure. The steady state levels of α-synuclein are carefully regulated by protein synthesis and removal by several pathways such as the ubiquitin-proteasome pathways and autophagy (Webb et al., 2003). Controlling the steady state levels of this protein by regulating synthesis and degradation may be the first critical defense in preventing aggregation. Conformational change to α-helical rich structures, and stabilization of metastable multimers is achieved by specific interactions with vesicular phospholipids and proteins. The sequestration of α-synuclein in association with membrane vesicles and with other proteins may be of critical importance for preventing aggregation. Therefore these dynamic equilibria maintain functionality and promote assemblies that are resistant to aggregation. Catastrophic events that may include inappropriate post-translational modifications will disassemble the multimers as well as transform aggregation-incompetent monomers to aggregation-competent species. The first step in the pathway to amyloid fibril formation is the generation of a dimer that is either held together by hydrophobic interactions induced by increased conformational transition to β-sheet structure or upon covalent cross-linking. Following this nucleation event (Wood et al., 1999) the hydrophobic patch of amino acids between residues 71-82 appears to be primarily responsible for allowing additional α-synuclein monomers to assemble to form oligomeric structures. This transition is the committed rate limiting step for aggregation and must overcome a relatively large thermodynamic requirement that permits the conversion from an unstructured coil to organized β-sheet conformation. Oligomers are soluble in aqueous buffers and can appear spherical or

ring-like by atomic force and electron microscopy (Conway et al., 2000; Lashuel et al., 2002). Soluble, high molecular weight oligomers have been extracted from human brain tissue and their levels appear to be increased in PD brain (Sharon et al., 2003) as well as mouse models of α-synuclein aggregation (Tsika et al., 2010). As oligomers grow, they reach an undefined critical length and are able to assume additional quaternary structure. At this stage, these structures may continue to grow in linear β-sheets, forming polarized protofibrils and eventually fibrils. Fibrils may further arrange into protein inclusions although it remains unclear if other proteins within these inclusions anchor these fibrils. Alternatively, oligomers may remain soluble by interacting with small molecules (Conway et al., 2001) or by incorporating post-translationally modified α-synuclein molecules. These structures remain "off the amyloid fibril pathway" and may constitute what has been described in human postmortem tissue as "dots" or "dust-like" amorphous aggregates (Braak et al., 2001; Duda et al., 2002). At this juncture, it remains unclear which of these assemblies are toxic to neurons. Recent data indicate that several conformationally distinct assemblies (possibly different strains) of α-synuclein generated *in vitro* will induce the aggregation of endogenous α-synuclein resulting in neurodegeneration (Guo et al., 2013; Luk et al., 2012; Peelaerts et al., 2015; Sacino et al., 2014). The appreciation of different α-synuclein conformers and assemblies as well as their roles in disease may guide potential therapeutic approaches. For example, therapeutic strategies can be centered on preserving and stabilizing the physiological multimeric conformers as well as preventing monomers from aggregating. Alternatively, sequestration and removal of aggregation-competent monomers and oligomers can be considered.

Acknowledgements

This work was supported by the National Institutes of Health Grant AG13966; the Intellectual and Developmental Disabilities Center Gant U54 HD086984; and the National Institute of Environmental Health Sciences Center of Excellence in Environmental Toxicology Grant ES013508. DM was supported by National Institutes of Health Ruth L. Kirschstein National Research Service Award Individual Predoctoral Fellowship F31NS087779-01A1. SU was supported by the NIH Chemistry-Biology Interface Training Grant T32GM07133-08. MD was supported by National Institutes of Health Training Grant T32GM008076. HI is the Gisela and Dennis Alter Research Professor of Pediatrics.

References

Abeliovich, A., Schmitz, Y., Fariñas, I., Choi-Lundberg, D., Ho, W.H., Castillo, P.E., Shinsky, N., Verdugo, J.M., Armanini, M., Ryan, A., et al. (2000). Mice lacking alpha-synuclein display functional deficits in the nigrostriatal dopamine system. Neuron *25*, 239–252.

Anderson, J.P., Walker, D.E., Goldstein, J.M., de Laat, R., Banducci, K., Caccavello, R.J., Barbour, R., Huang, J., Kling, K., Lee, M., et al. (2006). Phosphorylation of Ser-129 is the dominant pathological modification of α-synuclein in familial and sporadic Lewy body disease. J. Biol. Chem. *281*, 29739–29752.

Anwar, S., Peters, O., Millership, S., Ninkina, N., Doig, N., Connor-Robson, N., Threlfell, S., Kooner, G., Deacon, R.M., Bannerman, D.M., et al. (2011). Functional alterations to the nigrostriatal system in mice lacking all three members of the synuclein family. J. Neurosci. *31*, 7264–7274.

Baba, M., Nakajo, S., Tu, P.H., Tomita, T., Nakaya, K., Lee, V.M., Trojanowski, J.Q., and Iwatsubo, T. (1998). Aggregation of alpha-synuclein in Lewy bodies of sporadic Parkinson's disease and dementia with Lewy bodies. Am. J. Pathol. *152*, 879–884.

Barrett, P.J., and Greenamyre, J.T. (2015). Post-translational modification of α-synuclein in Parkinson's disease. Brain Res. *1628*, 247–253.

Bartels, T., Choi, J.G., and Selkoe, D.J. (2011). α-Synuclein occurs physiologically as a helically folded tetramer that resists aggregation. Nature *477*, 107–110.

Bertoncini, C.W., Fernandez, C.O., Griesinger, C., Jovin, T.M., and Zweckstetter, M. (2005a). Familial mutants of α-synuclein with increased neurotoxicity have a destabilized conformation. J. Biol. Chem. *280*, 30649–30652.

Bertoncini, C.W., Jung, Y., Fernandez, C.O., Hoyer, W., Griesinger, C., Jovin, T.M., and Zweckstetter, M. (2005b). Release of long-range tertiary interactions potentiates aggregation of natively unstructured α-synuclein. Proc. Natl. Acad. Sci. U. S. A. *102*, 1430–1435.

Binolfi, A., Rasia, R.M., Bertoncini, C.W., Ceolin, M., Zweckstetter, M., Griesinger, C., Jovin, T.M., and Fernandez, C.O. (2006). Interaction of α-synuclein with divalent metal ions reveals key differences: A link between structure, binding specificity and fibrillation enhancement 21. J. Am. Chem. Soc. *128*, 9893–9901.

Binolfi, A., Theillet, F.-X., and Selenko, P. (2012). Bacterial in-cell NMR of human α-synuclein: a disordered monomer by nature? Biochem. Soc. Trans. *40*, 950–954.

Braak, E., Sandmann-Keil, D., Rüb, U., Gai, W.P., de Vos, R.A.I., Jansen Steur, E.N.H., Arai, K., and Braak, H. (2001). α-synuclein immunopositive Parkinson's disease-related inclusion bodies in lower brain stem nuclei. Acta Neuropathol. *101*, 195–201.

Burré, J., Sharma, M., Tsetsenis, T., Buchman, V., Etherton, M.R., and Südhof, T.C. (2010). Alpha-synuclein promotes SNARE-complex assembly in vivo and in vitro. Science *329*, 1663–1667.

Burré, J., Sharma, M., and Südhof, T.C. (2012). Systematic mutagenesis of α-synuclein reveals distinct sequence requirements for physiological and pathological activities. J. Neurosci. *32*, 15227–15242.

Burré, J., Vivona, S., Diao, J., Sharma, M., Brunger, A.T., and Südhof, T.C. (2013). Properties of native brain α-synuclein. Nature *498*, E4–E6.

Burré, J., Sharma, M., and Südhof, T.C. (2014). α-Synuclein assembles into higher-order multimers upon membrane binding to promote SNARE complex formation. Proc. Natl. Acad. Sci. *111*, E4274–E4283.

Burré, J., Sharma, M., and Südhof, T.C. (2015). Definition of a molecular pathway mediating α-synuclein neurotoxicity. J. Neurosci. *35*, 5221–5232.

Cabin, D.E., Shimazu, K., Murphy, D., Cole, N.B., Gottschalk, W., McIlwain, K.L., Orrison, B., Chen, A., Ellis, C.E., Paylor, R., et al. (2002). Synaptic vesicle depletion correlates with attenuated synaptic responses to prolonged repetitive stimulation in mice lacking alpha-synuclein. J. Neurosci. *22*, 8797–8807.

Chandra, S., Fornai, F., Kwon, H.-B., Yazdani, U., Atasoy, D., Liu, X., Hammer, R.E., Battaglia, G., German, D.C., Castillo, P.E., et al. (2004). Double-knockout mice for alpha- and beta-synucleins: effect on synaptic functions. Proc. Natl. Acad. Sci. U. S. A. *101*, 14966–14971.

Chandra, S., Gallardo, G., Fernández-Chacón, R., Schlüter, O.M., and Südhof, T.C. (2005). α-Synuclein cooperates with CSPα in preventing neurodegeneration. Cell *123*, 383–396.

Chartier-Harlin, M.-C., Kachergus, J., Roumier, C., Mouroux, V., Douay, X., Lincoln, S., Levecque, C., Larvor, L., Andrieux, J., Hulihan, M., et al. (2004). Alpha-synuclein locus duplication as a cause of familial Parkinson's disease. Lancet *364*, 1167–1169.

Chen, L., Periquet, M., Wang, X., Negro, A., McLean, P.J., Hyman, B.T., and Feany, M.B. (2009). Tyrosine and serine phosphorylation of α-synuclein have opposing effects on neurotoxicity and soluble oligomer formation. J. Clin. Invest. *119*, 3257–3265.

Cole, N.B., Murphy, D.D., Grider, T., Rueter, S., Brasaemle, D., and Nussbaum, R.L. (2002). Lipid droplet binding and oligomerization properties of the Parkinson's disease protein α-synuclein. J. Biol. Chem. *277*, 6344–6352.

Conway, K. a, Lee, S.J., Rochet, J.C., Ding, T.T., Williamson, R.E., and Lansbury, P.T. (2000). Acceleration of oligomerization, not fibrillization, is a shared property of both alpha-synuclein mutations linked to early-onset Parkinson's disease: implications for pathogenesis and therapy. Proc. Natl. Acad. Sci. U. S. A. *97*, 571–576.

Conway, K. a, Rochet, J.C., Bieganski, R.M., and Lansbury, P.T. (2001). Kinetic stabilization of the alpha-synuclein protofibril by a dopamine-alpha-synuclein adduct. Science *294*, 1346–1349.

Coskuner, O., and Wise-Scira, O. (2013). Structures and free energy landscapes of the A53T mutant-type α-synuclein protein and impact of A53T mutation on the structures of the wild-type α-synuclein protein with dynamics. ACS Chem. Neurosci. *4*, 1101–1113.

Davidson, W.S., Jonas, A., Clayton, D.F., and George, J.M. (1998). Stabilization of α-synuclein secondary structure upon binding to synthetic membranes. J. Biol. Chem. *273*, 9443–9449.

Dedmon, M.M., Lindorff-Larsen, K., Christodoulou, J., Vendruscolo, M., and Dobson, C.M. (2005). Mapping long-range interactions in α-synuclein using spin-label NMR and ensemble molecular dynamics simulations. J. Am. Chem. Soc. *127*, 476–477.

Dettmer, U., Newman, A.J., Soldner, F., Luth, E.S., Kim, N.C., von Saucken, V.E., Sanderson, J.B., Jaenisch, R., Bartels, T., and Selkoe, D. (2015). Parkinson-causing α-synuclein missense mutations shift native tetramers to monomers as a mechanism for disease initiation. Nat. Commun. *6*.

Dikiy, I., and Eliezer, D. (2014). N-terminal acetylation stabilizes N-terminal helicity in lipid- and micelle-bound α-synuclein and increases its affinity for physiological membranes. J. Biol. Chem. *289*, 3652–3665.

Duda, J.E., Giasson, B.I., Mabon, M.E., Lee, V.M.-Y., and Trojanowski, J.Q. (2002). Novel antibodies to synuclein show abundant striatal pathology in Lewy body diseases. Ann. Neurol. *52*, 205–210.

Fauvet, B., Fares, M.-B., Samuel, F., Dikiy, I., Tandon, A., Eliezer, D., and Lashuel, H.A. (2012). Characterization of semisynthetic and naturally Nα-acetylated α-synuclein in vitro and in intact cells: implications for aggregation and cellular properties of α-synuclein. J. Biol. Chem. *287*, 28243–28262.

Ferreon, A.C.M., Gambin, Y., Lemke, E.A., and Deniz, A.A. (2009). Interplay of α-synuclein binding and conformational switching probed by single-molecule fluorescence. Proc. Natl. Acad. Sci. U. S. A. *106*, 5645–5650.

Ferese R, Modugno N, Campopiano R, Santilli M, Zampatti S, Giardina E, Nardone A, Postorivo D, Fornai F, Novelli G, Romoli E, Ruggieri S, Gambardella S. (2015) Four copies of SNCA responsible for autosomal dominant Parkinson's Disease in two Italian siblings. Parkinsons Dis. 2015:546-462.

Fujiwara, H., Hasegawa, M., Dohmae, N., Kawashima, A., Masliah, E., Goldberg, M.S., Shen, J., Takio, K., and Iwatsubo, T. (2002). α-Synuclein is phosphorylated in synucleinopathy lesions. Nat. Cell Biol. *4*, 160–164.

Galvagnion, C., Buell, A.K., Meisl, G., Michaels, T.C.T., Vendruscolo, M., Knowles, T.P.J., and Dobson, C.M. (2015). Lipid vesicles trigger α-synuclein aggregation by stimulating primary nucleation. Nat. Chem. Biol. *11*, 229–234.

George, J.M., Jin, H., Woods, W.S., and Clayton, D.F. (1995). Characterization of a novel protein regulated during the critical period for song learning in the zebra finch. Neuron *15*, 361–372.

Georgieva, E.R., Ramlall, T.F., Borbat, P.P., Freed, J.H., and Eliezer, D. (2010). The lipid-binding domain of wild type and mutant α-synuclein. J. Biol. Chem. *285*, 28261–28274.

Ghosh, D., Sahay, S., Ranjan, P., Salot, S., Mohite, G.M., Singh, P.K., Dwivedi, S., Carvalho, E., Banerjee, R., Kumar, A., et al. (2014). The newly discovered Parkinson' s disease associated finnish mutation (A53E) attenuates α-synuclein aggregation and membrane binding. Biochemistry *53*, 6419–6421.

Giasson, B.I., Uryu, K., Trojanowski, J.Q., and Lee, V.M.-Y. (1999). Mutant and wild type human α-synucleins assemble into elongated filaments with distinct morphologies in vitro. J. Biol. Chem. *274*, 7619–7622.

Giasson, B.I., Duda, J.E., Murray, I. V, Chen, Q., Souza, J.M., Hurtig, H.I., Ischiropoulos, H., Trojanowski, J.Q., and Lee, V.M.-Y. (2000). Oxidative damage linked to neurodegeneration by selective alpha-synuclein nitration in synucleinopathy lesions. Science *290*, 985–989.

Giasson, B.I., Murray, I. V, Trojanowski, J.Q., and Lee, V.M.-Y. (2001). A hydrophobic stretch of 12 amino acid residues in the middle of α-synuclein is essential for filament assembly. J. Biol. Chem. *276*, 2380–2386.

Gitler, A.D., Bevis, B.J., Shorter, J., Strathearn, K.E., Hamamichi, S., Su, L.J., Caldwell, K.A., Caldwell, G.A., Rochet, J.-C., McCaffery, J.M., et al. (2008). The Parkinson's disease protein α-synuclein disrupts cellular Rab homeostasis. Proc. Natl. Acad. Sci. U. S. A. *105*, 145–150.

Gould, N., Mor, D.E., Lightfoot, R., Malkus, K., Giasson, B., and Ischiropoulos, H. (2014). Evidence of native α-synuclein conformers in the human brain. J. Biol. Chem. *289*, 7929–7934.

Greenbaum, E.A., Graves, C.L., Mishizen-Eberz, A.J., Lupoli, M.A., Lynch, D.R., Englander, S.W., Axelsen, P.H., and Giasson, B.I. (2005). The E46K mutation in alpha-synuclein increases amyloid fibril formation. J. Biol. Chem. *280*, 7800–7807.

Greten-Harrison, B., Polydoro, M., Morimoto-Tomita, M., Diao, L., Williams, a. M., Nie, E.H., Makani, S., Tian, N., Castillo, P.E., Buchman, V.L., et al. (2010). α-Synuclein triple knockout mice reveal age-dependent neuronal dysfunction. Proc. Natl. Acad. Sci. U. S. A. *107*, 19573–19578.

Guo, J.L., Covell, D.J., Daniels, J.P., Iba, M., Stieber, A., Zhang, B., Riddle, D.M., Kwong, L.K., Xu, Y., Trojanowski, J.Q., et al. (2013). Distinct α-synuclein strains differentially promote tau inclusions in neurons. Cell *154*, 103–117.

Gurry, T., Ullman, O., Fisher, C.K., Perovic, I., Pochapsky, T., and Stultz, C.M. (2013). The dynamic structure of α-synuclein multimers. J. Am. Chem. Soc. *135*, 3865–3872.

Hasegawa, M., Fujiwara, H., Nonaka, T., Wakabayashi, K., Takahashi, H., Lee, V.M.-Y., Trojanowski, J.Q., Mann, D., and Iwatsubo, T. (2002). Phosphorylated α-synuclein is ubiquitinated in α-synucleinopathy lesions. J. Biol. Chem. *277*, 49071–49076.

Hodara, R., Norris, E.H., Giasson, B.I., Mishizen-Eberz, a. J., Lynch, D.R., Lee, V.M.-Y., and Ischiropoulos, H. (2004). Functional consequences of α-synuclein tyrosine nitration: diminished binding to lipid vesicles and increased fibril formation. J. Biol. Chem. *279*, 47746–47753.

Hoyer, W., Cherny, D., Subramaniam, V., and Jovin, T.M. (2004). Impact of the acidic C-terminal region comprising amino acids 109-140 on α-synuclein aggregation in vitro. Biochemistry *43*, 16233–16242.

Iwai, A., Masliah, E., Yoshimoto, M., Ge, N., Fianagan, L., Silva, H.A.R. De, Kittei, A., and Saitoh, T. (1995). The precursor protein of non-Aβ component of Alzheimer's disease amyloid is a presynaptic protein of the central nervous system. Neuron *14*, 467–475.

Jakes, R., Spillantini, M.G., and Goedert, M. (1994). Identification of two distinct synucleins from human brain. FEBS Lett. *345*, 27–32.

Kostka, M., Hogen, T., Danzer, K.M., Levin, J., Habeck, M., Wirth, A., Wagner, R., Glabe, C.G., Finger, S., Heinzelmann, U., et al. (2008). Single particle characterization of iron-induced pore-forming α-synuclein oligomers. J. Biol. Chem. *283*, 10992–11003.

Krüger, M., Moser, M., Ussar, S., Thievessen, I., Luber, C.A., Forner, F., Schmidt, S., Zanivan, S., Fässler, R., and Mann, M. (2008). SILAC mouse for quantitative proteomics uncovers kindlin-3 as an essential factor for red blood cell function. Cell *134*, 353–364.

Krüger, R., Kuhn, W., Müller, T., Woitalla, D., Przuntek, H., Epplen, J.T., Schols, L., and Riess, O. (1998). Ala30Pro mutation in the gene encoding α-synuclein in Parkinson's disease. Nat. Genet. *18*, 106–108.

Larsen, K.E., Schmitz, Y., Troyer, M.D., Mosharov, E., Dietrich, P., Quazi, A.Z., Savalle, M., Nemani, V., Chaudhry, F.A., Edwards, R.H., et al. (2006). α-Synuclein overexpression in PC12 and

chromaffin cells impairs catecholamine release by interfering with a late step in exocytosis. J. Neurosci. *26*, 11915–11922.

Lashuel, H.A., Petre, B.M., Wall, J., Simon, M., Nowak, R.J., Walz, T., and Lansbury, P.T. (2002). α-Synuclein, especially the Parkinson's disease-associated mutants, forms pore-like annular and tubular protofibrils. J. Mol. Biol. *322*, 1089–1102.

Lesage, S., Anheim, M., Letournel, F., Bousset, L., Honoré, A., Rozas, N., Pieri, L., Madiona, K., Dürr, A., Melki, R., et al. (2013). G51D α-synuclein mutation causes a novel parkinsonian-pyramidal syndrome. Ann. Neurol. *73*, 459–471.

Li, W., West, N., Colla, E., Pletnikova, O., Troncoso, J.C., Marsh, L., Dawson, T.M., Hartmann, T., Price, D.L., and Lee, M.K. (2005). Aggregation promoting C-terminal truncation of α-synuclein is a normal cellular process and is enhanced by the familial Parkinson's disease-linked mutations. Proc. Natl. Acad. Sci. U. S. A. *102*, 2162–2167.

Liu, L.L., and Franz, K.J. (2005). Phosphorylation of an alpha-synuclein peptide fragment enhances metal binding. J. Am. Chem. Soc. *127*, 9662–9663.

Lu, Y., Prudent, M., Fauvet, B., Lashuel, H.A., and Girault, H.H. (2011). Phosphorylation of α-synuclein at Y125 and S129 alters its metal binding properties: Implications for understanding the role of α-synuclein in the pathogenesis of Parkinson's disease and related disorders. ACS Chem. Neurosci. *2*, 667–675.

Luk, K.C., Kehm, V., Carroll, J., Zhang, B., O'Brien, P., Trojanowski, J.Q., and Lee, V.M.-Y. (2012). Pathological α-synuclein transmission initiates Parkinson-like neurodegeneration in nontransgenic mice. Science *338*, 949–953.

Luth, E.S., Bartels, T., Dettmer, U., Kim, N.C., and Selkoe, D.J. (2015). Purification of α-synuclein from human brain reveals an instability of endogenous multimers as the protein approaches purity. Biochemistry *54*, 279–292.

Mahul-Mellier, A-L., Vercruysse, F., Maco, B., Ait-Bouziad, N., De Roo, M., Muller, D., and Lashuel, H. a (2015). Fibril growth and seeding capacity play key roles in α-synuclein-mediated apoptotic cell death. Cell Death Differ. *22,* 2107–2122.

Maroteaux, L., Campanelli, J.T., and Scheller, R.H. (1988). Synuclein: A neuron-specific protein localized to the nucleus and presynaptic nerve terminal. J. Neurosci. *8*, 2804–2815.

Martinez, Z., Zhu, M., Han, S., and Fink, A.L. (2007). GM1 specifically interacts with α-synuclein and inhibits fibrillation. Biochemistry *46*, 1868–1877.

Mazzulli, J.R., Mishizen, A.J., Giasson, B.I., Lynch, D.R., Thomas, S.A., Nakashima, A., Nagatsu, T., Ota, A., and Ischiropoulos, H. (2006). Cytosolic catechols inhibit α-synuclein aggregation and facilitate the formation of intracellular soluble oligomeric intermediates. J. Neurosci. *26*, 10068–10078.

Murphy, D.D., Rueter, S.M., Trojanowski, J.Q., and Lee, V.M.-Y. (2000). Synucleins are developmentally expressed, and alpha-synuclein regulates the size of the presynaptic vesicular pool in primary hippocampal neurons. J. Neurosci. *20*, 3214–3220.

Narhi, L., Wood, S.J., Steavenson, S., Jiang, Y., Wu, G.M., Anafi, D., Kaufman, S. a., Martin, F., Sitney, K., Denis, P., et al. (1999). Both familial Parkinson's disease mutations accelerate α-synuclein aggregation. J. Biol. Chem. *274*, 9843–9846.

Nemani, V.M., Lu, W., Berge, V., Nakamura, K., Onoa, B., Lee, M.K., Chaudhry, F. a, Nicoll, R. a, and Edwards, R.H. (2010). Increased expression of alpha-synuclein reduces neurotransmitter release by inhibiting synaptic vesicle reclustering after endocytosis. Neuron *65*, 66–79.

Oaks, A.W., and Sidhu, A. (2011). Synuclein modulation of monoamine transporters. FEBS Lett. *585*, 1001–1006.

Ostrerova, N., Petrucelli, L., Farrer, M., Mehta, N., Choi, P., Hardy, J., and Wolozin, B. (1999). α-Synuclein shares physical and functional homology with 14-3-3 proteins. J. Neurosci. *19*, 5782–5791.

Oueslati, A., Fournier, M., and Lashuel, H.A. (2010). Role of post-translational modifications in modulating the structure, function and toxicity of alpha-synuclein: implications for Parkinson's disease pathogenesis and therapies. Prog. Brain Res. *183*, 115–145.

Oueslati, A., Schneider, B.L., Aebischer, P., and Lashuel, H.A. (2013). Polo-like kinase 2 regulates selective autophagic α-synuclein clearance and suppresses its toxicity in vivo. Proc. Natl. Acad. Sci. *110*, E3945–E3954.

Paleologou, K.E., Schmid, A.W., Rospigliosi, C.C., Kim, H.-Y., Lamberto, G.R., Fredenburg, R. a, Lansbury, P.T., Fernandez, C.O., Eliezer, D., Zweckstetter, M., et al. (2008). Phosphorylation at Ser-129 but not the phosphomimics S129E/D inhibits the fibrillation of alpha-synuclein. J. Biol. Chem. *283*, 16895–16905.

Paleologou, K.E., Oueslati, A., Shakked, G., Rospigliosi, C.C., Kim, H.-Y., Lamberto, G.R., Fernandez, C.O., Schmid, A., Chegini, F., Gai, W.P., et al. (2010). Phosphorylation at S87 is enhanced in synucleinopathies, inhibits α-synuclein oligomerization, and influences synuclein-membrane interactions. J. Neurosci. *30*, 3184–3198.

Pasanen, P., Myllykangas, L., Siitonen, M., Raunio, A., Kaakkola, S., Lyytinen, J., Tienari, P.J., Pöyhönen, M., and Paetau, A. (2014). A novel α-synuclein mutation A53E associated with atypical multiple system atrophy and Parkinson's disease-type pathology. Neurobiol. Aging *35*, 2180.e1–e2180.e5.

Peelaerts, W., Bousset, L., Van der Perren, A., Moskalyuk, A., Pulizzi, R., Giugliano, M., Van den Haute, C., Melki, R., and Baekelandt, V. (2015). α-Synuclein strains cause distinct synucleinopathies after local and systemic administration. Nature *522*, 340–344.

Peng, X.M., Tehranian, R., Dietrich, P., Stefanis, L., and Perez, R.G. (2005). α-Synuclein activation of protein phosphatase 2A reduces tyrosine hydroxylase phosphorylation in dopaminergic cells. J. Cell Sci. *118*, 3523–3530.

Perez, R.G., Waymire, J.C., Lin, E., Liu, J.J., Guo, F., and Zigmond, M.J. (2002). A role for α-synuclein in the regulation of dopamine biosynthesis. J. Neurosci. *22*, 3090–3099.

Polymeropoulos, M.H., Lavedan, C., Leroy, E., Ide, S.E., Dehejia, A., Dutra, A., Pike, B., Root, H., Rubenstein, J., Boyer, R., et al. (1997). Mutation in the α-synuclein gene identified in families with Parkinson's disease. Science *276*, 2045–2047.

Proukakis, C., Dudzik, C.G., Brier, T., Mackay, D.S., Cooper, J.M., Millhauser, G.L., and Houlden, H. (2013). A novel α-synuclein missense mutation in Parkinson disease. Neurology *80*, 1062–1064.

Rasia, R.M., Bertoncini, C.W., Marsh, D., Hoyer, W., Cherny, D., Zweckstetter, M., Griesinger, C., Jovin, T.M., and Fernández, C.O. (2005). Structural characterization of copper (II) binding to α-synuclein: Insights into the bioinorganic chemistry of Parkinson's disease. Proc. Natl. Acad. Sci. U. S. A. *102*, 4294–4299.

Rodriguez, J.A., Ivanova, M.I., Sawaya, M.R., Cascio, D., Reyes, F.E., Shi, D., Sangwan, S., Guenther, E.L., Johnson, L.M., Zhang, M., et al. (2015). Structure of the toxic core of α-synuclein from invisible crystals. Nature *525*, 486–490.

Sacino, A.N., Brooks, M., Thomas, M.A., McKinney, A.B., Lee, S., Regenhardt, R.W., McGarvey, N.H., Ayers, J.I., Notterpek, L., Borchelt, D.R., et al. (2014). Intramuscular injection of α-synuclein induces CNS α-synuclein pathology and a rapid-onset motor phenotype in transgenic mice. Proc. Natl. Acad. Sci. *111*, 10732–10737.

Sampathu, D.M., Giasson, B.I., Pawlyk, A.C., Trojanowski, J.Q., and Lee, V.M.-Y. (2003). Ubiquitination of α-synuclein is not required for formation of pathological inclusions in α-synucleinopathies. Am. J. Pathol. *163*, 91–100.

Sharon, R., Bar-Joseph, I., Frosch, M.P., Walsh, D.M., Hamilton, J.A., and Selkoe, D.J. (2003). The formation of highly soluble oligomers of α-synuclein is regulated by fatty acids and enhanced in Parkinson's disease. Neuron *37*, 583–595.

Shibayama-Imazu, T., Okahashi, I., Omata, K., Nakajo, S., Ochiai, H., Nakai, Y., Hama, T., Nakamura, Y., and Nakaya, K. (1993). Cell and tissue distribution and developmental change of neuron specific 14 kDa protein (phosphoneuroprotein 14). Brain Res. *622*, 17–25.

Singleton, A.B., Farrer, M., Johnson, J., Singleton, A., Hague, S., Kachergus, J., Hulihan, M., Peuralinna, T., Dutra, A., Nussbaum, R., et al. (2003). α-Synuclein locus triplication causes Parkinson's disease. Science *302*, 841.

Soper, J.H., Roy, S., Stieber, A., Lee, E., Wilson, R.B., Trojanowski, J.Q., Burd, C.G., and Lee, V.M.-Y. (2008). Multiple pathways differentially regulate global oxidative stress responses in fission yeast. Mol. Biol. Cell *19*, 308–317.

Souza, J.M., Giasson, B.I., Lee, V.M.-Y., and Ischiropoulos, H. (2000a). Chaperone-like activity of synucleins. FEBS Lett. *474*, 116–119.

Souza, J.M., Giasson, B.I., Chen, Q., Lee, V.M.-Y., and Ischiropoulos, H. (2000b). Dityrosine cross-linking promotes formation of stable alpha-synuclein polymers. Implication of nitrative and oxidative stress in the pathogenesis of neurodegenerative synucleinopathies. J. Biol. Chem. *275*, 18344–18349.

Spillantini, M.G., Schmidt, M.L., Lee, V.M.-Y., Trojanowski, J.Q., Jakes, R., and Goedert, M. (1997). α-synuclein in Lewy bodies. Nature *388*, 839–840.

Takeda, A., Mallory, M., Sundsmo, M., Honer, W., Hansen, L., and Masliah, E. (1998). Abnormal accumulation of NACP/α-synuclein in neurodegenerative disorders. Am. J. Pathol. *152*, 367–372.

Tehranian, R., Montoya, S.E., Van Laar, A.D., Hastings, T.G., and Perez, R.G. (2006). Alpha-synuclein inhibits aromatic amino acid decarboxylase activity in dopaminergic cells. J. Neurochem. *99*, 1188–1196.

Trexler, A.J., and Rhoades, E. (2009). α-Synuclein binds large unilamellar vesicles as an extended helix. Biochemistry *48*, 2304–2306.

Trexler, A.J., and Rhoades, E. (2012). N-terminal acetylation is critical for forming α-helical oligomer of α-synuclein. Protein Sci. *21*, 601–605.

Tsika, E., Moysidou, M., Guo, J., Cushman, M., Gannon, P., Sandaltzopoulos, R., Giasson, B.I., Krainc, D., Ischiropoulos, H., and Mazzulli, J.R. (2010). Distinct region-specific α-synuclein oligomers in A53T transgenic mice: Implications for neurodegeneration. J. Neurosci. *30*, 3409–3418.

Uéda, K., Masliah, E., Xia, Y.U., Iwai, A., Yoshimoto, M., Otero, D.A.C., and Kondo, J.U.N. (1993). Molecular cloning of cDNA encoding an unrecognized component of amyloid in Alzheimer disease. Proc. Natl. Acad. Sci. U. S. A. *90*, 11282–11286.

Ulmer, T.S., Bax, A., Cole, N.B., and Nussbaum, R.L. (2005). Structure and dynamics of micelle-bound human α-synuclein. J. Biol. Chem. *280*, 9595–9603.

Uversky, V.N., Li, J., and Fink, A.L. (2001a). Metal-triggered structural transformations, aggregation, and fibrillation of human α-synuclein: A possible molecular link between Parkinson's disease and heavy metal exposure. J. Biol. Chem. *276*, 44284–44296.

Uversky, V.N., Li, J., and Fink, A.L. (2001b). Evidence for a partially folded intermediate in α-synuclein fibril formation. J. Biol. Chem. *276*, 10737–10744.

Wang, L., Das, U., Scott, D.A., Tang, Y., McLean, P.J., and Roy, S. (2014). α-Synuclein multimers cluster synaptic vesicles and attenuate recycling. Curr. Biol. *24*, 2319–2326.

Wang, W., Perovic, I., Chittuluru, J., Kaganovich, A., Nguyen, L.T.T., Liao, J., Auclair, J.R., Johnson, D., Landeru, A., Simorellis, A.K., et al. (2011). A soluble α-synuclein construct forms a dynamic tetramer. Proc. Natl. Acad. Sci. U. S. A. *108*, 17797–17802.

Waxman, E.A., and Giasson, B.I. (2008). Specifcity and regulation of casein kinase-mediated phosphorylation of α-synuclein. J. Neuropathol. Exp. Neurol. *67*, 402–416.

Webb, J.L., Ravikumar, B., Atkins, J., Skepper, J.N., and Rubinsztein, D.C. (2003). α-Synuclein is degraded by both autophagy and the proteasome. J. Biol. Chem. *278*, 25009–25013.

Weinreb, P.H., Zhen, W., Poon, A.W., Conway, K.A., and Lansbury, P.T. (1996). NACP, a protein implicated in Alzheimer's disease and learning, is natively unfolded. Biochemistry *35*, 13709–13715.

Withers, G.S., George, J.M., Banker, G. a., and Clayton, D.F. (1997). Delayed localization of synelfin (synuclein, NACP) to presynaptic terminals in cultured rat hippocampal neurons. Dev. Brain Res. *99*, 87–94.

Wood, S.J., Wypych, J., Steavenson, S., Louis, J., Citron, M., and Biere, A.L. (1999). α-Synuclein fibrillogenesis is nucleation-dependent. Biochemistry 19509–19512.

Woods, W.S., Boettcher, J.M., Zhou, D.H., Kloepper, K.D., Hartman, K.L., Ladror, D.T., Qi, Z., Rienstra, C.M., and George, J.M. (2007). Conformation-specific binding of alpha-synuclein to novel protein partners detected by phage display and NMR spectroscopy. J. Biol. Chem. *282*, 34555–34567.

Yavich, L., Tanila, H., Vepsäläinen, S., and Jäkälä, P. (2004). Role of α-synuclein in presynaptic dopamine recruitment. J. Neurosci. *24*, 11165–11170.

Ysselstein, D., Joshi, M., Mishra, V., Griggs, A.M., Asiago, J.M., McCabe, G.P., Stanciu, L.A., Post, C.B., and Rochet, J.-C. (2015). Effects of impaired membrane interactions on α-synuclein aggregation and neurotoxicity. Neurobiol. Dis. *79*, 150–163.

Zarranz, J.J., Alegre, J., Gómez-Esteban, J.C., Lezcano, E., Ros, R., Ampuero, I., Vidal, L., Hoenicka, J., Rodriguez, O., Atarés, B., et al. (2004). The new mutation, E46K, of α-synuclein causes Parkinson and Lewy body dementia. Ann. Neurol. *55*, 164–173.

Zhu, M., and Fink, A.L. (2003). Lipid binding inhibits α-synuclein fibril formation. J. Biol. Chem. *278*, 16873–16877.

Zhu, M., Li, J., and Fink, A.L. (2003). The association of α-synuclein with membranes affects bilayer structure, stability, and fibril formation. J. Biol. Chem. *278*, 40186–40197.

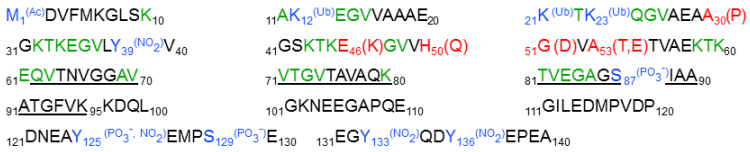

Figure 2.1. Primary sequence of human α-synuclein. Green color indicates the imperfect tandem repeats. Known mutations are indicated in red. The hydrophobic NAC domain is underlined. The major sites of posttranslational modifications identified in vivo are highlighted in blue (Ac, acetylation; Ub, ubiquitination; NO_2, nitration; and PO_3^- phosphorylation).

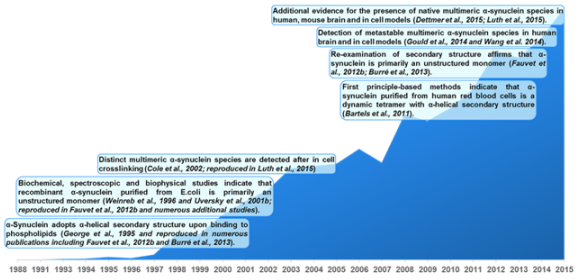

Figure 2.2. The graph depicts the number of publications retrieved from PuBMed using the search term “alpha synuclein” from a single publication in 1998 to 862 in 2015. Significant milestones that examined the native structure and conformations of α-synuclein are displayed.

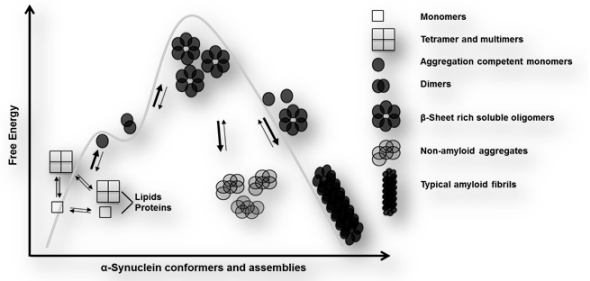

Figure 2.3. Free energy landscape of possible α-synuclein conformers and multimeric assemblies. The conversion of native α-synuclein to aggregation-competent monomers may depend on dissociation from stabilizing interactions with lipids and/or proteins as well as dissociation of the metastable tetrameric species. α-Synuclein aggregation-competent monomers can then assemble into dimers and larger oligomeric conformers. The generation of α-synuclein oligomers can rapidly lead to formation of stable amyloid fibrils, or 'off-pathway' amorphous aggregates, both of which have been observed in postmortem brain tissue from patients with PD and related disorders.

CHAPTER 3

Quantitative Proteomics Reveals Upregulation of the Immunoproteasome in Response to Endogenous α-Synuclein Aggregation

Scott Ugras[1], Kelvin Luk[2], Esteban Luma[2], Anastasia K. Yocum[3], Hua Ding[4], Chris McKennan[4,5], Steven Seeholzer[4], Perry Evans[6], and Harry Ischiropoulos[1,4,7]

[1]Biochemistry and Molecular Biophysics Graduate Group, Perelman School of Medicine, University of Pennsylvania, Philadelphia, PA 19104, USA.

[2]Center for Neurodegenerative Disease Research, Department of Pathology and Laboratory Medicine, Perelman School of Medicine, University of Pennsylvania, Philadelphia, PA 19104, USA.

[3]A2IDEA, LLC Ann Arbor, MI 48105, USA.

[4]Proteomics Core, Children's Hospital of Philadelphia Research Institute, Philadelphia, PA 19104, USA.

[5]Department of Statistics, University of Chicago, Il 60637, USA.

[6]Department of Biomedical and Health Informatics, Children's Hospital of Philadelphia, Philadelphia, PA 19104, USA.

[7]Department of Pediatrics, Children's Hospital of Philadelphia, Philadelphia, PA 19104, USA; Department of Systems Pharmacology and Translational Therapeutics, Perelman School of Medicine, University of Pennsylvania, Philadelphia, PA 19104, USA.

Electronic address: ischirop@mail.med.upenn.edu.

Manuscript in Preparation

3.1 Abstract

Aggregation of α-synuclein contributes to dopaminergic degeneration in Parkinson's disease and related neurodegenerative disorders. A decline in proteostasis is associated with protein aggregation but how α-synuclein aggregation affects the brain proteome remains undetermined. A global proteomic approach applied to wild type mouse midbrain and striatum quantified 5,290 proteins of which 311 exhibited significant change in relative abundance in response to α-synuclein aggregation induced by pre-formed fibril injection. These proteins were not affected in α-synuclein null mice, which do not undergo α-synuclein aggregation or dopaminergic neuron degeneration. Interestingly, an increase in the immunoproteasome, which is linked with preservation of proteostasis, was documented in wild type mice and in human synucleinopathies. The increase in immunoproteasome resulted in augmented proteolytic activity and improved efficiency to degrade α-synuclein fibrils. The induction of the immunoproteasome in response to α-synuclein aggregation could be exploited as a protective strategy to preserve proteostasis in α-synuclein aggregation disorders.

3.2 Introduction

Cells have developed proteostasis networks to maintain proper protein homeostasis and to combat potentially toxic protein aggregation[1]. Deficiencies in proteostasis are linked to several diseases, including cystic fibrosis[2], diabetes[3], and cancer[4,5]. Additionally, a failure in proteostasis associated with protein aggregation is considered a pathogenetic mechanism of several neurodegenerative diseases of aging such as Parkinson's disease (PD), Alzheimer's disease (AD) and Amyotrophic Lateral Sclerosis (ALS)[6–8]. The aggregated proteins in these diseases have been

identified, including α-synuclein in PD, amyloid-β and tau in AD, and SOD1, FUS, and TDP43 in ALS[9–12]. The indomitable progression of aggregation and cell death suggests that the proteostasis network is unable to cope in these neurodegenerative diseases. However, reorganization and reallocation of proteostatic resources may be a viable strategy to combat toxic protein aggregation. The effects of endogenous protein aggregation on the overall proteome have never been studied *in vivo*, and may uncover proteostatic responses to protein aggregation that could be modulated to mitigate disease.

α-Synuclein is a 140 amino acid protein that has roles in synaptic plasticity and has been linked to neurodegenerative disease[13–15]. Aggregated forms of the protein are deposited into cytoplasmic inclusions known as Lewy Bodies, which are the histopathological hallmarks of PD and several other related neurodegenerative disorders[16]. Recombinant wild type (WT) α-synuclein aggregates and forms amyloid-like fibrils[17]. Several point mutations in α-synuclein that cause early-onset PD have been identified, including A30P, E46K, H50Q, G51D and A53T[18–22]. These point mutations accelerate aggregation, supporting the role of protein aggregation in causing pathology[23–26]. Additionally, multiplications of the gene encoding α-synuclein cause PD[27–29]. Collectively, these data demonstrate a role for α-synuclein aggregation in human disease.

A recently developed mouse model of α-synuclein combines several cardinal features of PD, including endogenous α-synuclein aggregation concomitant with progressive dopaminergic degeneration and motor impairment[30]. In this model preformed fibrils (PFFs) of recombinant WT mouse α-synuclein were unilaterally injected into the striatum of non-transgenic mice. This induced a cascade whereby endogenous α-synuclein progressively aggregates, first in the regions near the injection site and then to synaptically connected regions. Eventually, the mice

exhibited dopaminergic neuron degeneration and impaired balance and motor coordination. Importantly, dopaminergic degeneration and α-synuclein inclusions were confined to the injected side and not found in the non-injected side of the brain. Additionally, injection of PFFs into α-synuclein null (*Snca -/-)* mice failed to induce these effects, indicating that the presence of endogenous α-synuclein was required. This PFF injection model has been successfully reproduced in both mice[31,32] and rats[33].

This model (both WT and *Snca -/-* injected mice) provides a unique opportunity to study, *in vivo*, the changes in the proteome upon aggregation of endogenous α-synuclein. To study these proteome responses, we used mass spectrometry (MS)-based proteomics in combination with Stable Isotope Labeling in Mammals (SILAM)[34,35] to quantify changes in the relative abundance of proteins in the brain in response to endogenous α-synuclein aggregation.

3.3 Experimental Procedures

Animals: Wild type (WT) C57BL6/C3H mice were obtained from the Jackson Laboratories (Bar Harbor, ME). *Snca -/-* mice[36] were maintained on a C57BL6 background. ^{13}C-Stable Isotope Labeling in Mammals (SILAM) mouse brain tissue (Female, L-Lysine 13C6, 97%) was purchased from Cambridge Isotope Laboratories, Inc. All housing, breeding, and procedures were performed according to the NIH Guide for the Care and Use of Experimental Animals and approved by the University of Pennsylvania Institutional Animal Care and Use Committee (IACUC).

Stereotaxic injection of PFFs: For stereotaxic injection, PFFs were first diluted in sterile PBS and fragmented using a Bioruptor bath sonicator (Diagenode; Denville, NJ). Sonication was performed at high power for 10 cycles (30s on, 30s off, at 10°C). Mice (2-3 months old) were anesthetized with ketamine hydrochloride (100 mg/kg, i.p.) and xylazine (10 mg/kg, i.p.). For each animal, PFFs were stereotaxically targeted into the ventral striatum (AP: +0.2 mm Bregma, lateral: 2.0 mm from midline, depth: 3.6 mm beneath the dura), dorsal striatum (AP: +0.2 mm, lateral: 2.0 mm, depth: 2.6 mm), and overlaying cortex (AP: +0.2 mm, lateral: 2.0 mm, depth: 0.8 mm). Injections were made through a single needle tract using 10 µL syringes (Hamilton, NV) at a rate of 0.1 µL per min (2.5 µL total per site) with the needle in place for > 5 min at each target. Animals were monitored regularly following recovery from surgery. Mice were sacrificed at 90 days post injection by overdose with ketamine/xylazine. For biochemical studies, dorsal striatum and ventral midbrain from ipsilateral and contralateral sides were dissected and stored at -80°C until used. For histological studies the brain and spinal cord were removed after transcardial perfusion with PBS and underwent overnight postfixation in either neutral buffered formalin (Fisher Scientific) or 70% ethanol (in 150 mM NaCl, pH 7.4), before being processed and embedded in paraffin.

Immunohistochemistry: Immunohistochemistry for α-synuclein phosphorylated at Ser-129 and tyrosine hydroxylase (TH) were performed on 6 µm thick coronal sections as previously described[30,37]. Digitized images of stained sections were acquired using a Perkin Elmer Lamina scanner at 20x magnification. Midbrain DA neurons belonging to the substantia nigra pars compacta (SNpc) and the ventral tegmental area (VTA) were quantified from TH-immunostained coronal sections spanning the entire extent of the midbrain (every 9th section). Immunoreactive

neurons were counted following previously described criteria for each subgroup[38]. Only intact neurons with defined nuclei were included. Statistical analysis between groups was compared using one-way ANOVA with Tukey's post-hoc test.

Sample Preparation for LC-MS/MS: For each mouse injected, the midbrain and striatum of the injected and non-injected sides were dissected and kept separate. Two midbrain and striatum regions of the injected hemisphere were combined to generate one biological sample for the proteomic analysis. The same approach was employed for the non-injected side. Four biological samples for WT and three for Snca -/- for each injected and non-injected side were analyzed through the proteomic work flow depicted in Figure 3.1C. Sample preparation was done as previously described[39]. Briefly, tissues were homogenized with a tissue grinder in cold urea buffer: 8 M urea, 75 mM NaCl, 50 mM Tris HCl pH 8.0, 1 mM EDTA, 2 µg/mL aprotinin (Sigma, A6103), 10 µg/mL leupeptin (Roche, #11017101001), 1 mM PMSF (Sigma, 78830), 10 mM NaF, 5 mM sodium butyrate, 5 mM iodoacetamide (Sigma, A3221), Phosphatase Inhibitor Cocktail 2 (1:100, Sigma, P5726), and Phosphatase Inhibitor Cocktail 3 (1:100, Sigma, P0044). Following 10 min centrifugation at 20,000*g*, protein concentration was determined by a BCA assay (Thermo, Prod# 23235) on the supernatant and then combined with ^{13}C-labeled brain lysates in a 1:1 ratio (5µg:5µg) in a mini scale. Samples were reduced for 45 min with 5 mM dithiothreitol followed by alkylation with 20 mM iodoacetamide for 45 min. Samples were then diluted 1:4 with 50 mM Tris HCl pH 8.0 (to reduce urea concentration to 2 M), then digested overnight with Trypsin (Promega, Cat# V5111) at 37°C overnight. 1% formic acid was added to the digests to remove urea by pelleting. The tryptic peptides were desalted by ultraMicroSpin Vydac C18 column (Nestgroup, Inc, cat# SUMSS18V). The peptides were analyzed by mass

spectrometry (MS) and the data was analyzed with MaxQuant (described below). The SILAC ratio of injected/non-injected was calculated by dividing the injected/heavy ratio by the non-injected/heavy ratio. The SILAC ratio of light/heavy generated from the MaxQuant was converted to $\log_2$ scale and the median of the SILAC ratios therefore was calculated. If the SILAC ratio was close to 1:1, a larger scale sample prep was performed similarly as described above. Protein (2 mg:2 mg, heavy:light) was digested with Trypsin/Lys-C mix (Promega, Cat# V5073) at 1:25 (enzyme:protein, w:w). The peptide fragments were desalted on tC18 SepPak cartridge (Waters, cat# WAT036815) and the peptides were lyophilized and stored in -80°C. For reverse phase (RP)-HPLC, the peptides were reconstituted in 20 mM ammonium formate, pH 10.0. Peptide concentration was determined by UV280 before they were separated by high-pH reverse phase chromatography to 72 fractions detected at UV-214 nm via ACQUITY UPLC H-Class instrument (Waters). Solvent A (2% acetonitrile, 5mM ammonium formate, pH10) and solvent B (90% acetonitrile, 5mM ammonium formate, pH 10) were used to separate peptides with a ZPRBAX 300Extend-C18 column (4.6mmx250mm, 5 Micron, Agilent). The gradient for separation was 1mL/min flow rate as at 9 min, 100% A; 13 min, 94% A; 63 min, 71.5% ; 68.5 min, 66% A; 81.5 min, 40% A; 83 min; 0% A; at 88-120 min with 1.2mL/min with 100% A. 5% of samples were taken and recombined in a concatenated pattern into 24 fractions for proteomics analysis.

LC-MS/MS: Peptide digests were analyzed on a hybrid LTQ Orbitrap mass spectrometer (Thermofisher Scientific, San Jose, CA) coupled with a NanoLC Ultra (Eksigent Technologies) as previously described[40]. Briefly, peptides were separated by RP-HPLC. Mobile phase A consisted of 1% methanol/0.1% formic acid and mobile phase B consisted of 1% methanol/0.1% formic

acid/79% acetonitrile. Peptides were eluted into the MS at 200 nL/min with each RP-LC run comprising a 15 min sample load at 3% B and a 90 min linear gradient from 5 to 45% B. The mass spectrometer repetitively scanned m/z from 300 to 1800 (R = 100,000 for LTQ-Orbitrap). FTMS full scan maximum fill time was set to 500 ms, while ion trap MSn fill time was 50 ms; microscans were set at one. FT preview mode, charge state screening, and monoisotopic precursor selection were all enabled with rejection of unassigned and 1+ charge states.

MS Database Searching and Data Processing: Protein identification was performed with MaxQuant (1.5.1.2) using a mouse UniProt database. Carbamidomethyl was defined as a fixed modification. The False Discovery Rate for peptides was set at 1%. Fragment ion tolerance was set to 0.5 Da. The MS/MS tolerance was set at 20 ppm. The minimum peptide length was set at 7 amino acids. The requantification option was left unchecked and the match-between-runs was turned on. For a protein to be quantified, the peptide must be identified at least once in light and once in heavy. To calculate the injected/non-injected ratio, the heavy/non-injected ratio was divided by the heavy/injected ratio.

Construction of the Mouse Brain Reference Proteome: To make a unified set of literature and experimental proteins, UniProt accessions were cross-referenced by gene or protein name. UniProt's retrieve function was used to get protein and gene names for all UniProt accessions. For literature proteins, we selected several studies[41–44] that used MS-based proteomics to identify proteins in the unperturbed mouse brain. Proteins identified in at least 3 of 4 biological replicates in the non-injected side of WT mice were checked for presence in the literature list using gene and protein names rather than UniProt accessions. Genes and proteins not found in

the experimental protein list are included as literature-only proteins. Multiple UniProt accessions can annotate one gene or protein name.

Statistical Analyses: The Heavy/Light (H/L) ratio in the non-injected side was divided by the H/L ratio in the injected side to compute the injected/non-injected ratio of ratios. A protein was considered quantified in WT if this ratio of ratios was computed in at least 3 of the 4 biological replicates; it was considered quantified in *Snca -/-* if this ratio of ratios was computed in all 3 biological replicates. This resulted in 5,290 proteins quantified in WT (of which 3,331 were also quantified in *Snca -/-*, and 1,959 were quantified only in WT), and 3,335 proteins quantified in *Snca -/-*. A separate statistical analysis was performed for these two groups of proteins. For the 3,331 proteins quantified in both WT and *Snca -/-*, the ratio of ratios were scaled using the standard z-score. p-Values were determined for each protein with the z-scaled values using a Welch's T-Test. The Welch's T-Test was employed rather than a simple Students T-Test because the samples sizes between the WT and *Snca -/-* experiments were unequal (4 replicates in WT and 3 in *Snca -/-*). p-Values < 0.05 were considered significant, yielding 201 proteins for those quantified in both WT and *Snca -/-*. Of the 1,959 proteins quantified only in the WT experiments, the H/L ratios in the injected side and the H/L ratios in the non-injected sides were scaled using the standard z-score. A paired Student's T-Test was performed to calculate p-values, comparing the injected to non-injected sides. p-Values < 0.05 were considered significant, resulting in 110 proteins. Thus the relative abundance of a total of 311 proteins were found to significantly change (201 from those quantified in WT and *Snca -/-*, and 110 from those only quantified in WT).

Heat Map Generation: Heat maps are undirected clustering of experimental values, z-scaled ratio of ratios with a p-value < 0.05. Heat maps were created using pHeatmap in Rstudio (version 1.0.8). Clustering distances were calculated by row and column with Euclidean math and clustered by the Ward.D2 methodology. The scale and intensity of color, blue to white to red, is representative of the direction and degree of differential expression.

Mouse Immunoblot Analysis: Mouse brain samples were extracted using the same method described above for the MS analysis. For each analysis, 5-20 µg of sample was added per lane and separated in a 12% Bis-Tris Pre-Cast gel (ThermoFisher) and transferred to a PVDF membrane and blocked using 7.5% BSA in TBS. Primary antibody (Table 3.1) was used overnight. Antigens-antibody complexes were detected using an Odyssey LC scanner (LiCor) after incubation with appropriate secondary antibodies. Densitometry was used to quantify intensity of protein bands.

Gene Ontology Enrichment Analysis: DAVID Bioinformatics Resources 6.7 was used for enrichment analysis. The 5,290 proteins quantified in WT were used as background. The 311 significantly changed proteins were separated into the 159 that decreased and the 152 that increased. Each was separately used as a list and the enrichment of Biological Processes was examined. Those with p-values < 0.05 were considered significant, and fold-changes were determined using the DAVID software.

Cellular Compartment Localization Analysis: The 159 and 152 proteins that significantly decreased and increased, respectively, were separately entered into UniProtKB/Swiss-Prot to

obtain the subcellular localizations. Percentages of proteins mapped to each cellular compartment were calculated by dividing the number of proteins mapped to a given cellular compartment by the total number of annotated proteins entered.

Human Immunoblot Analysis: Human brain samples were extracted using high salt buffer containing 1% Triton-X100 (150 mM NaCl, 50 mM Tris, pH 7.6). Brain samples from Dementia with Lewy Bodies and non-disease brain were obtained[45]. Protease inhibitors were added to buffer prior to use. To collect triton-soluble fractions, samples were homogenized, sonicated and sedimented at 15,000 rpm for 30 min. 500 µl of buffer was added to each sample. Protein concentrations were determined by BCA assay (Thermo Fisher). Samples were separated in a 12% Bis-Tris Pre-Cast gel (ThermoFisher) and transferred to a PVDF membrane and blocked using 7.5% BSA in TBS. For each analysis 40 µg of sample was added per lane. Primary antibody (Table SX) was used overnight. Antigen-antibody complexes were detected using LiCor after incubation with appropriate secondary antibodies. Densitometry was used to quantify intensity of protein bands.

Proteasome Activity Assay: Human brain samples were extracted using high salt buffer containing 1% Triton-X100 (150 mM NaCl, 50 mM Tris, pH 7.6). Protease inhibitors were excluded from buffer. To collect triton-soluble fractions, samples were homogenized, sonicated and sedimented at 15,000 rpm for 30 min. 500 µl of buffer was added to each sample. Protein concentrations were determined by BCA assay (Thermo Fisher). Proteasome Activity Fluorometric Assay Kit (BioVision K245) was used to assay proteasome activity. Assays were performed in a 96-well plate at 37°C according to the manufacturer's protocol. 5 µg of lysates

were added per experimental condition. Each condition was done with or without proteasome inhibitor. At the final time point (60 min), the fluorescence with inhibitor was subtracted from the fluorescence without inhibitor per condition. Three biological replicates were quantified for each experimental condition.

In Vitro Degradation Assay: Recombinant human WT α-synuclein was purified as previously described[46]. Purified human WT α-synuclein was aggregated at 5 mg/ml for 7 days at 1,400 rpm at 37°C. The fibrils generated from the aggregation of α-synuclein were used as substrate for the *in vitro* degradation assays. Myelin Basic Protein (Sigma M1891) was used at 25 μM and α-synuclein was used at 1 mg/ml. Human Immunoproteasome 20S (Enzo BML-PW8720) and Human Constitutive Proteasome 20S (Enzo BML-PW9645) were used at a ratio of 0.11:1 proteasome:α-synuclein. Human Proteasome Activator 11S complex (BML-PW9420) was added at a final concentration of 500 nM. Reactions were incubated at 37°C agitating at 600 rpm, and samples were removed at indicated time points. Samples were separated in a 12% Bis-Tris Pre-Cast gel (ThermoFisher) and stained with colloidal blue. Densitometry was used to quantify protein degradation of monomer bands of α-synuclein. Initial time point was considered 100% for each experimental condition. Three biological replicates were quantified for each experimental condition.

In Vitro Aggregation Assay: Reactions from the *in vitro* degradation assay were stopped by freezing samples and storing at -20°C. These samples were thawed, and used as templates by adding 5% of these samples to soluble recombinant human WT α-synuclein. At indicated time points, sample was removed and centrifuged at 15,000 rpm for 30 minutes at -4°C. Supernatant

was removed and equal volume PBS was added to pellet and re-suspended. Samples were loaded onto a 12% Bis-Tris Pre-Cast gel (ThermoFisher) and stained with colloidal blue. Densitometry was used to quantify monomer bands of α-synuclein. Protein in the supernatant at initial time point was considered 100% soluble. Three biological replicates were analyzed for each experimental condition.

Table 3.1: List of Antibodies

Protein	Catalog Number	Working Dilution
NSE	ab53025	1:1000
α-Synuclein	D37A6	1:1000
Lmp7	ab3329	1:1000
β5	PA1-977	1:1000
PKC-β2	Ab33206	1:1000
DAT	MAB369	1:1000
Addc	Ab3905	1:1000
Akt	9272	1:1000
Tyrosine Hydroxylase	657012	1:1000

3.4 Results

Mouse Model of Endogenous α-Synuclein Aggregation

To identify proteomic perturbations induced by the aggregation of endogenous α-synuclein, a modified version of a recently developed and independently verified mouse model[30] was employed whereby α-synuclein pre-formed fibrils (PFFs) were unilaterally injected into three locations (cortex, dorsal and ventral striatum) of non transgenic mice. The injection of PFFs into the WT mouse brain induces progressive aggregation of endogenous mouse α-synuclein that is

associated with loss of dopamine producing neurons in the injected side. To confirm conversion of endogenous α-synuclein occurred, the substantia nigra was stained with an antibody that recognizes phosphorylated α-synuclein at Ser-129 (Figure 3.1A), a marker of α-synuclein inclusions in human synucleinopathies[47,48]. In WT mice 90 days post injection, dense Lewy body-like inclusions immunoreactive for phosphorylated Ser-129 were abundant in the injected side but not detectable in the contralateral, non-injected side. Additionally, biochemical extraction of brain lysates showed increased levels of insoluble α-synuclein in the injected side of the WT mice compared with the non-injected side, corroborating the phosphorylated Ser-129 staining and reaffirming that α-synuclein aggregation occurred in the injected side of WT mice (Supplementary Figure 3.1).

Progressive aggregation of α-synuclein and dopaminergic degeneration has been documented in WT but not in *Snca -/-* mice that are injected in the same manner with PFFs[30]. To confirm this in triple-injected mice, staining was also performed in *Snca -/-* mice. As expected, no staining for phosphorylated Ser-129 α-synuclein in the injected or non-injected sides was observed in the substantia nigra of *Snca -/-* mice (Figure 3.1A). Thus, *Snca -/-* mice are an important control that enables us to separate the effect of changes in the mouse brain proteome due to PFF injection from those due to α-synuclein aggregation and neuron loss.

Tyrosine hydroxylase (TH) staining in both the injected and non-injected sides of WT mice was performed in order to quantify the loss of dopaminergic neurons (Figure 3.1B). Quantification of TH+ neurons in the substantia nigra of WT mice revealed a 19% loss in the injected versus non-injected side that approached statistical significance (p-value = 0.0507). Quantification in *Snca -/-* mice, on the other hand, revealed no significant TH+ neuron loss in the injected side. Collectively these data indicate that α-synuclein aggregation is predominantly occurring in the

injected side of WT mice, leading to TH+ neuron loss, consistent with previous findings using this model[30].

Midbrain Proteome Depth, Quantification and Quality

To quantify the changes in the relative abundance of proteins in both the WT and *Snca -/-* mice, we employed a quantitative proteomic workflow depicted in Figure 3.1C. The method incorporated the use of ^{13}C-Stable Isotope Labeling in Mammals (SILAM)[34,35] as an internal standard for the quantitative analysis of the relative abundance of proteins. Four biological replicates for the injected and non-injected sides for the WT mouse and three biological replicates for each side of the *Snca -/-* mice were analyzed. Combined analysis of the replicates in WT mice applying a false discovery rate of 1% resulted in the identification of 7,021 proteins in the injected side, 6,949 proteins in the non-injected side, with 6,706 proteins identified in both sides (Figure 3.1C, Supplementary Table 1). Analysis in the *Snca -/-* mice resulted in the identification of 4,739 proteins in the injected side, 4,913 proteins in the non-injected side, with 4,446 proteins identified in both sides (Figure 3.1C; Supplementary Table 2).

For a subset of the proteins identified we also detected the cognate isotopically labeled peptide, allowing the determination of the heavy/light (H/L) ratio. The H/L ratio of 5,623 proteins in the injected side (Supplementary Table 3) and 5,588 proteins in the non-injected side of WT mice were obtained (Supplementary Table 4). In *Snca -/-* mice, the H/L ratio for 3,519 proteins in the injected side (Supplementary Table 5) and 3,625 proteins in the non-injected side was determined (Supplementary Table 6). We employed a ratiometric method (dividing the H/L ratio of the non-injected side by the H/L ratio in the injected side) to quantify changes in the relative abundance of proteins in the injected side compared with the non-injected side.

Completion of this analysis resulted in the quantification of the relative abundance of 5,290 proteins in WT (Supplementary Table 7) and 3,335 proteins in *Snca -/-* (Figure 3.1C; Supplementary Table 8).

Construction of a global mouse brain proteome was completed and used as a reference to determine whether the proteins quantified are reflective of the proteins expressed in the mouse brain (Supplementary Table 9). For the reference proteome we combined proteins identified by mass spectrometry in the unperturbed mouse brain from several existing studies that we then curated through UniProt with the 6,949 proteins identified in our study in the WT non-injected side. This reference proteome is comprised of 11,055 proteins, of which 76 were proteins contributed by our study.

To evaluate the quality of the quantified proteome (5,290 proteins in WT and 3,335 proteins in *Snca -/-*), we compared these proteins with this reference mouse brain proteome. The distribution of the quantified proteins based on their molecular weight was representative of the whole mouse brain proteome covering the entire range of >10 kDa to >400 kDa (Figure 3.1D). Gene set enrichment using biological process and KEGG Pathways revealed a compatible distribution of the quantified proteome among major biological processes with the whole brain proteome (Figure 3.1E). Moreover, Gene Ontology enrichment analysis using cellular components showed that the cellular location of the quantified proteins was representative of the whole mouse brain proteome (Figure 3.1F). Collectively, these analyses suggest that the proteins quantified here are representative of the proteins in the mouse brain.

Statistical Analysis of Proteomic Changes

The frequency distribution of quantified proteins in WT and *Snca -/-* each showed a unimodal distribution centered at Log_2=0 (Figures 3.2A and B). To identify the proteins that exhibited a significant change in relative abundance due to α-synuclein aggregation, the following statistical analyses were performed. For the 3,331 proteins quantified in both WT and *Snca -/-*, the ratio of ratios were z-scaled and a Welch's T-Test was applied to compute p-values. (Figure 3.2C). Using a p-value of less than 0.05, 201 proteins were significantly changed. For the 1,959 proteins that were quantified in WT only, a paired Student's T-Test was used to compare the injected to the non-injected side, and any p-values less than 0.05 were accepted as significant, totaling an additional 110 proteins. Combined, this resulted in 311 proteins (152 that increase and 159 that decrease in the injected side) that the relative abundance changed significantly due to α-synuclein aggregation (Supplementary Table 10). A summary of the breakdown of these 311 proteins is depicted in Supplementary Figure 3.2.

Heatmaps generated for the significant proteins quantified in both WT and *Snca -/-* show that proteins with increased or decreased relative abundance in the injected side cluster together in WT versus *Snca -/-* across all biological replicates (Figure 3.2D). The scale and intensity of color, blue to white to red, is representative of the direction and degree of differential expression. Furthermore, this clustering persists in the injected versus non-injected side for those proteins quantified only in WT (Figure 3.2E). These data demonstrate the consistency in the relative abundance changes of the 311 proteins across all biological replicates.

Validation of the Proteomic Changes

The documented 19% loss of TH+ neurons in the injected side of WT mice (Figure 3.1B) provides a benchmark whereby proteins selectively expressed in dopaminergic neurons can be leveraged

to validate the quantified changes in the proteome. Indeed four of the 159 proteins that significantly declined in the injected side were TH, aromatic-L-amino-acid decarboxylase (Addc), synaptic vesicular amine transporter-2 (VMAT2), and dopamine transporter (DAT) (Figure 3.3A and B). These four proteins are selectively expressed in dopaminergic neurons and participate in the biosynthesis, vesicular transport and recycling of dopamine. The levels of Slc10a4, a protein that is specifically expressed in catecholaminergic neurons though its function is not well understood, also declined in the injected side[49,50]. Notably, the relative abundance of proteins such as monoamine oxidase A (MAO-A) and catechol-O-methyl transferase (COMT), that are expressed in glial cells as well as dopaminergic neurons, varied from 6.0-6.2% and did not change significantly (Figure 3.3B). These findings demonstrate the sensitivity and precision of our method used to quantify relative changes in protein abundance.

The changes in the levels of TH, DAT, and Addc quantified by SILAM-MS-based methodology were further validated by semi-quantitative western blot analysis. The western blot analysis was entirely consistent with the MS-based quantification showing a decline of 33-51% in the levels of TH, DAT, and Addc in the injected versus the non-injected side (Figure 3.3C). Importantly, and consistent with the need of endogenous α-synuclein aggregation for the loss of dopaminergic neurons, the levels of TH, DAT, and Addc do not decline in the injected side of *Snca -/-* mice quantified by either the MS-based or western blot methods (Figure 3.3B and C). Additional confirmation and validation of the MS-based quantification was obtained by probing for proteins such as α-synuclein, NSE, PKC-β2 and Akt, which showed no change in the levels between injected and non-injected side (Figure 3.3D; Supplementary Figure 3.3). Overall, these findings provide confidence that the quantitative methodology delivered robust and precise changes in the proteome in this model of endogenous α-synuclein aggregation.

Enrichment Analysis of α-Synuclein Responsive Proteins

Enrichment analyses were performed to examine the effects of α-synuclein aggregation and dopaminergic degeneration on biological processes within the midbrain and striatal proteomes. The analysis used the 5,290 proteins quantified in WT mice as background and was separately performed for the 159 and 152 proteins whose relative abundance decreased or increased, respectively. Subcellular localizations of the significantly changed proteins were analyzed using UniProtKB/Swiss-Prot to retrieve the Gene Ontology-annotated cellular compartments. Cytoplasmic proteins accounted for the greatest percent, with 52% and 65% of the significant proteins that increased or decreased, respectively (Figure 3.4A). The cell membrane accounted for 44% of each dataset, and the nucleus for 29% and 27% (note that each protein can have more than one localization). The mitochondria, endoplasmic reticulum, Golgi apparatus, and extracellular space accounted for 6%-10% of the datasets. This analysis indicates that the proteomic disturbances are impacting all major cellular compartments, although endogenous α-synuclein aggregates are predominantly cytoplasmic.

Consistent with dopaminergic neuron loss, catecholamine metabolism was a functional category enriched by 15 fold among the proteins whose relative abundance decreased (Figure 3.4B). Furthermore, ion transmembrane transport, microtubule organization, and vesicle-mediated transport were all significantly enriched by 2-7 fold. The enrichment of these biological processes suggests that cellular communication, membrane conductance, and cytoskeletal dynamics may all be disrupted. Importantly, these functions have all been previously linked to α-synuclein aggregation[51–56], reinforcing the robustness of the quantitative approach used in our analysis of proteome wide changes.

Of the proteins that increased in the injected side, glycoprotein metabolism, mRNA transport and the immune response were significantly enriched by 4-6 fold. Interestingly, the four proteins that displayed the greatest increase in relative abundance among the 311 significant proteins are functionally linked to immune responses.

Finally, a global pathway analysis of the 311 significantly changed proteins was performed using the Reactome pathway database (Figure 3.4C). This analysis highlighted and confirmed the enrichment of several distinct pathways within vesicle mediated transport, programmed cell death, gene expression, neuronal expression and the immune system. Given that the immune response was identified in both the biological enrichment analysis and this pathway analysis, we further investigated its role in α-synuclein aggregation.

α-Synuclein Aggregation Upregulates the Immunoproteasome

The novel finding that Lmp7 is the protein with the highest relative abundance increase was probed further because Lmp7 is one of the three subunits that comprise the catalytic core of the immunoproteasome[57]. The immunoproteasome is an altered form of the constitutive proteasome that is upregulated in response to interferon-gamma (IFNγ) and exhibits different peptide cleavage activity[58–61] than the constitutive proteasome. It has been proposed as an adaptive response for the maintenance of proteostasis upon protein aggregation and has been implicated in other neurodegenerative diseases, including Huntington's disease[62] and AD[63,64], but not in α-synuclein aggregation disorders.

The increase in relative abundance of Lmp7 quantified by the proteomic analysis was validated by western blot analysis (Figure 3.5A). We then examined whether a similar increase of the immunoproteasome occurs in human disease characterized by aggregation of α-synuclein. The

levels of Lmp7 in the brains of dementia with Lewy Bodies (DLB), which contain aggregated α-synuclein, and control non-disease subjects were evaluated by semi-quantitative western blot analysis. The analysis documents a 2-fold increase in the levels of Lmp7 in DLB as compared to controls (Figure 3.5B). To further evaluate if the increase in protein levels correlates with activity, chymotrypsin-like activity, which is selectively elevated in the immunoproteasome, was quantified (Figure 3.5C). Indeed, an 80% increase in the chymotrypsin-like activity was measured in the DLB brain homogenates as compared with controls. These data demonstrate that the activation of the immunoproteasome quantified in response to α-synuclein aggregation in the WT mouse also occurs in human disease driven by α-synuclein aggregation.

The Immunoproteasome Degrades α-Synuclein Fibrils

Since the immunoproteasome and constitutive proteasome have different proteolytic activities, the possibility that the immunoproteasome and the constitutive proteasome differ in their ability to degrade α-synuclein fibrils was evaluated. First, myelin basic protein (MBP), a protein previously shown to be degraded more efficiently by the immunoproteasome than the constitutive proteasome[61], was incubated with purified immunoproteasome or constitutive proteasome. After 22 hours, 96% of MBP was degraded by the immunoproteasome compared with 69% by the constitutive proteasome (Supplementary Figure 3.4). These data document the previously known differential activity of the immunoproteasome compared with the constitutive proteasome and enable us to compare the catalytic efficiency against α-synuclein fibrils.

α-Synuclein fibrils were generated by a standard protocol that included continuous agitation of soluble α-synuclein at 37°C at 1,400 rpm for 7 days. These aggregates exhibited an increase in Thioflavin-T fluorescence (Supplementary Figure 3.5A), turbidity (Supplementary Figure 3.5B)

and sedimentation analysis revealed a shift from the supernatant to the pellet (Supplementary Figure 3.5C). Finally, circular dichroism revealed typical β-sheet secondary structure (Supplementary Figure 3.5D). These amyloid-like fibrils were used as a substrate for the constitutive proteasome, and the immunoproteasome. (Figure 3.5D). After 7 days of incubation, 100% of α-synuclein fibrils were degraded by the immunoproteasome compared with 57% by the constitutive proteasome. Thus, the immunoproteasome degrades α-synuclein fibrils more rapidly compared with the constitutive proteasome in a cell-free system.

Next the products of these degradation reactions were tested for their ability to accelerate the aggregation of recombinant human α-synuclein. Intact preformed α-synuclein fibrils, the constitutive proteasome products or the immunoproteasome products were added to soluble monomeric α-synuclein and an aggregation reaction was performed. Typically, addition of 5% PFFs in a solution of monomeric α-synuclein accelerates the aggregation as compared with no PFFs as shown in Figure 3.5E. Similar with α-synuclein fibrils, addition of products generated by the constitutive proteasome accelerated the aggregation of monomeric α-synuclein. In contrast, the products from the degradation of α-synuclein fibrils by the immunoproteasome did not accelerate the aggregation of monomeric α-synuclein. After 2 days of incubation, 90% of the monomeric α-synuclein had aggregated in the presence of products derived from the constitutive proteasome as compared to 66% from the immunoproteasome (Figure 3.5E). These data indicate the immunoproteasome degrades α-synuclein fibrils to generate products that will not template and accelerate the aggregation of soluble α-synuclein.

3.5 Discussion

The proteostasis network consists of integrated cellular machinery that coordinates activities against the harmful effects of aging, environmental stresses, and infections[1]. Dynamic regulation of proteostasis pathways in response to disease-associated protein aggregation is crucial to maintaining cellular homeostasis[7,65–67]. This regulation is achieved through altering protein expression, turnover, localization, and post-translational modifications. Despite recognition of the importance of proteostasis networks, it remains unknown how the proteome responds to protein aggregation in neurodegenerative diseases. Here, we utilize α-synuclein, a protein that aggregates in a spectrum of neurodegenerative diseases[13–15], to quantitatively study proteostatic regulation of the proteome in response to endogenous protein aggregation.

The present study quantified the changes in relative abundance of proteins in response to endogenous aggregation of α-synuclein in the mouse brain using a quantitative proteomics approach. A mouse model of endogenous α-synuclein aggregation caused by the intrastriatal injection of pre-formed fibrils (PFFs) of α-synuclein was used[30]. In this model, at 90 days post injection α-synuclein pathology and dopaminergic degeneration is restricted to one side of the mouse brain, allowing us to use the non-injected side as an internal control. Furthermore, α-synuclein-null mice (*Snca -/-)* fail to develop any pathology, providing a control for proteome responses to the injection of PFFs alone. Our quantitative proteomic approach was both comprehensive and selective. We compared the 5,290 and 3,335 proteins we quantified in WT and *Snca -/-*, respectively, to a mouse brain reference proteome that we constructed by curating previous mass spectrometry-based studies. This analysis revealed that the proteins quantified here do not substantially differ from previously identified proteins, demonstrating that there is no significant bias in our quantified proteome. Critically, proteins participating in dopamine synthesis and transport were among the 311 proteins whose relative abundance significantly

changed. Given the documented degeneration of dopaminergic neurons in this model, this provides confidence for our approach. If mice analyzed 180 days post injection were analyzed, we would expect to document a similar set of proteins whose relative abundance significantly changed, along with greater dopaminergic neuron loss.

The data revealed that Lmp7, one of the three cardinal subunits of the immunoproteasome, exhibited the greatest increase in relative abundance in response to α-synuclein aggregation. The immunoproteasome is a derivative of the constitutive proteasome that is upregulated primarily by IFNγ and in response to pro-inflammatory stimuli[57,68]. The immunoproteasome is formed via the replacement of the three catalytic subunits of the constitutive proteasome, β_1, β_2 and β_5, with the three catalytic subunits of the immunoproteasome, namely Lmp2, MECL-1 and Lmp7, respectively[57]. The primary function of the immunoproteasome is the generation of peptides that are presented by MHC class I molecules on the cell surface for recognition by CD8+ T cells[69]. Mice deficient in all three catalytic subunits of the immunoproteasome had substantially reduced presentation of the majority of MHC class I epitopes during viral infection as compared with WT mice[70]. The reduced presentation and differences in the repertoire of MHC class I antigens contributed to the rejection of wild type splenocytes by the triple knockout mice, which were otherwise healthy, viable and fertile[70]. The vast differences in the peptides detected by mass spectroscopy in the presence versus the absence of the immunoproteasome are consistent with previous reports indicating altered enzyme kinetics and cleavage site preferences for the immunoproteasome[71]. The immunoproteasome usually cleaves proteins after nonpolar residues, resulting in the generation of peptides with hydrophobic C-terminal residues that preferentially interact with and are transported to plasma membranes by MHC class I molecules[72–74]. Additionally, there is elevated chymotrypsin-like activity relative to the

constitutive proteasome[71].

Although the importance of the immunoproteasome for the host-mediated antiviral immune response is clearly documented, additional proposed functions of the proteasome are currently debated. Critical for neurodegenerative disorders is the debate regarding the function of the immunoproteasome in the degradation of ubiquitinated proteins, which result from oxidative protein modifications[75–77]. The association between oxidized proteins and increased immunoproteasome has been reported[78] and oxidative stress has been considered in the pathological cascade of neurodegenerative diseases including PD and related α-synuclein aggregation disorders[79,80]. However, a link between upregulation of the immunoproteasome in response to endogenous α-synuclein aggregation, potentially mediated by oxidative stress, has not been made. In this study, we report elevated levels and activity of the immunoproteasome in the DLB brain compared with healthy brain (Figures 3.5B and C). Moreover, mass spectrometry-based analysis documents a similar increase in Lmp7 in mouse brain undergoing endogenous α-synuclein aggregation. Data in Figure 3.5D demonstrates that the immunoproteasome has an enhanced ability to degrade α-synuclein fibrils compared with the constitutive proteasome. Furthermore, we found that the products derived for the degradation by the immunoproteasome are unable to accelerate the aggregation of soluble α-synuclein (Figure 3.5E).

Immunoproteasome levels and activity were also found to be elevated in postmortem brains of patients with Huntington's and Alzheimer's disease[62–64]. In Huntington's disease Lmp2-positive staining was predominantly within neurons and overlapped with approximately 5% of cortical huntingtin protein aggregates[62]. In the Alzheimer's disease increased labeling for immunoproteasome was associated with reactive glia that surrounded amyloid-β plaques[64].

Collectively these studies suggest that coordinated and reversible activation of immunoproteasome may influence the progression of neurodegenerative disorders and aging consistent with the observation that primates and mice with longer lifespans have elevated levels of the immunoproteasome[81].

Of interest is the recent report documenting expression of MHC I in dopaminergic neurons in control (non-disease) and PD post mortem tissues[82]. Moreover, the same report showed that the expression of MHC I in murine dopaminergic neurons was induced by IFNγ and by oxidative stress. These data in part corroborate our findings indicating induction of the immunoproteasome in the substantia nigra and striatum. This report proposes a mechanism linking neuroinflammation, MHC I expression and dopaminergic degeneration. Aggregated α-synuclein activates microglia leading to the release of IFNγ that induces neuronal expression of MHC I. Additionally, cytosolic dopamine causes oxidative stress that contributes to MHC I expression. This MHC I is then loaded with antigens and presented on the cell surface for detection by cytotoxic T cells (CTLs), resulting in the selective destruction of dopaminergic neurons. What is missing from this model is how the IFNγ or oxidative stress causes antigen loading onto MHC I molecules for CTL detection. Our data here provide this link. Upon stimulation by IFNγ from microglial and/or oxidative stress from cytosolic dopamine levels, dopaminergic neurons express the immunoproteasome. The immunoproteasome is then able to degrade α-synuclein more efficiently than the constitutive proteasome, leading to the generation of distinct peptides that may preferentially be loaded onto MHC I. Thus, the degradation of α-synuclein by the immunoproteasome may accelerate cell death by CTLs and thus exacerbate dopaminergic degeneration.

Overall, we establish a role for the immunoproteasome in disease driven by α-synuclein aggregation. Ultimately, modulation of the immunoproteasome may have therapeutic potential in mitigating α-synuclein-mediated neurotoxicity.

References

1. Balch, W. E., Morimoto, R. I., Dillin, A. & Kelly, J. W. Adapting Proteostasis for Disease Intervention. *Science* **319,** 916 – 919 (2008).
2. Balch, W. E., Roth, D. M. & Hutt, D. M. Emergent Properties of Proteostasis in Managing Cystic Fibrosis. *Cold Spring Harb. Perspect. Biol.* 1–17 (2011).
3. Back, S. H. & Kaufman, R. J. Endoplasmic Reticulum Stress and Type 2 Diabetes. *Annu. Rev. Biochem.* **81,** 767–793 (2012).
4. Mendillo, M. L. *et al.* HSF1 Drives a Transcriptional Program Distinct from Heat Shock to Support Highly Malignant Human Cancers. *Cell* **150,** 549–562 (2012).
5. Powers, E. T., Morimoto, R. I., Dillin, A., Kelly, J. W. & Balch, W. E. Biological and Chemical Approaches to Diseases of Proteostasis Deficiency. *Annu. Rev. Biochem.* **78,** 959–991 (2009).
6. Skovronsky, D. M., Lee, V. M. & Trojanowski, J. Q. Neurodegenerative Diseases: New Concepts of Pathogenesis and Their Therapeutic Implications. *Annu. Rev. Pathol.* **1,** 151 – 170 (2006).
7. Tanaka, K. & Matsuda, N. Proteostasis and neurodegeneration: The roles of proteasomal degradation and autophagy. *BBA - Mol. Cell Res.* **1843,** 197–204 (2014).
8. Aguzzi, A. & Connor, T. O. Protein aggregation diseases: pathogenicity and therapeutic perspectives. *Nat. Rev. Drug Discov.* **9,** 237 – 248 (2010).
9. Irwin, D. J., Lee, V. M. & Trojanowski, J. Q. Parkinson's disease dementia: convergence of α-synuclein, tau and amyloid-β pathologies. *Nat. Rev. Neurosci.* **14,** 626–636 (2013).
10. Brettschneider, J., Tredici, K. Del & Lee, V. M. Spreading of pathology in neurodegenerative diseases: a focus on human studies. *Nat. Rev. Neurosci.* **16,** 109–120 (2015).
11. Kwong, L. K., Trojanowski, J. Q. & Lee, M. TDP-43 Proteinopathies: Neurodegenerative Protein Misfolding Diseases without Amyloidosis. *Neurosignals* 41–51 (2008). doi:10.1159/000109758
12. Lee, E. B., Lee, V. M. Y. & Trojanowski, J. Q. Gains or losses: molecular mechanisms of TDP43 - mediated neurodegeneration. *Nat. Publ. Gr.* **13,** 38 – 50 (2011).
13. Lashuel, H. A., Overk, C. R., Oueslati, A. & Masliah, E. The many faces of α-synuclein: from structure and toxicity to therapeutic target. *Nat. Rev. Neurosci.* **14,** 38 – 48 (2013).
14. Bendor, J. T., Logan, T. P. & Edwards, R. H. The Function of a-Synuclein. *Neuron* **79,** 1044–1066 (2013).
15. Goedert, M. Alpha-Synuclein and Neurodegenerative Diseases. *Nat. Rev. Neurosci.* **2,** 492–501 (2001).
16. Spillantini, M. G. *et al.* α-synuclein in Lewy bodies. *Nature* **388,** 839–840 (1997).
17. Giasson, B. I., Uryu, K., Trojanowski, J. Q. & Lee, V. M.-Y. Mutant and wild type human α-

synucleins assemble into elongated filaments with distinct morphologies in vitro. *J. Biol. Chem.* **274,** 7619–7622 (1999).

18. Polymeropoulos, M. H. *et al.* Mutation in the α-Synuclein Gene Identified in Families with Parkinson's Disease. *Sci. Reports* **276,** 2045 – 2047 (1997).
19. Krüger, R. *et al.* Ala30Pro mutation in the gene encoding α-synuclein in Parkinson's disease. *Nat. Genet.* **18,** 106–108 (1998).
20. Zarranz, J. J. *et al.* The new mutation, E46K, of alpha-synuclein causes Parkinson and Lewy body dementia. *Ann. Neurol.* **55,** 164–73 (2004).
21. Appel-Cresswell, S. *et al.* Alpha-synuclein p.H50Q, a novel pathogenic mutation for Parkinson's disease. *Mov. Disord.* **28,** 811–3 (2013).
22. Lesage, S. *et al.* G51D α-synuclein mutation causes a novel parkinsonian-pyramidal syndrome. *Ann. Neurol.* **73,** 459–471 (2013).
23. Conway, K. a, Harper, J. D. & Lansbury, P. T. Accelerated in vitro fibril formation by a mutant alpha-synuclein linked to early-onset Parkinson disease. *Nat. Med.* **4,** 1318–20 (1998).
24. Narhi, L. *et al.* Both familial Parkinson's disease mutations accelerate α-synuclein aggregation. *J. Biol. Chem.* **274,** 9843–9846 (1999).
25. Conway, K. A., Harper, J. D. & Lansbury, P. T. Fibrils Formed in Vitro from R-Synuclein and Two Mutant Forms Linked to Parkinson ' s Disease are Typical Amyloid †. *Biochemistry* 2552–2563 (2000).
26. Greenbaum, E. a *et al.* The E46K mutation in alpha-synuclein increases amyloid fibril formation. *J. Biol. Chem.* **280,** 7800–7 (2005).
27. Chartier-Harlin, M.-C. *et al.* A-synuclein locus duplication as a cause of familial Parkinson's disease. *Lancet* **07,** 1167–1169 (2004).
28. Singleton, A. B. *et al.* Alpha-Synuclein locus triplication causes Parkinson's disease. *Science* **302,** 841 (2003).
29. Ferese, R. *et al.* Four Copies of SNCA Responsible for Autosomal Dominant Parkinson's Disease in Two Italian Siblings. *Parkinsons. Dis.* **2015,** 1–6 (2015).
30. Luk, K. C. *et al.* Pathological α-synuclein transmission initiates Parkinson-like neurodegeneration in nontransgenic mice. *Science* **338,** 949–53 (2012).
31. Osterberg, V. R. *et al.* Progressive Aggregation of Alpha-Synuclein and Selective Degeneration of Lewy Inclusion-Bearing Neurons in a Mouse Model of Parkinsonism. *Cell Rep.* **10,** 1252–1260 (2015).
32. Sacino, A. N. *et al.* Brain Injection of a-Synuclein Induces Multiple Proteinopathies, Gliosis, and a Neuronal Injury Marker. *Neurobiol. Dis.* **34,** 12368–12378 (2014).
33. Paumier, K. L. *et al.* Intrastriatal injection of pre-formed mouse α-synuclein fibrils into rats triggers α-synuclein pathology and bilateral nigrostriatal degeneration. *Neurobiol. Dis.* **82,** 185–199 (2015).
34. Kru, M. *et al.* Resource SILAC Mouse for Quantitative Proteomics Uncovers Kindlin-3 as an Essential Factor for Red Blood Cell Function. 353–364 (2008). doi:10.1016/j.cell.2008.05.033
35. Zanivan, S., Krueger, M. & Mann, M. In Vivo Quantitative Proteomics: The SILAC Mouse. **757,**
36. Abeliovich, A. *et al.* Mice lacking alpha-synuclein display functional deficits in the nigrostriatal dopamine system. *Neuron* **25,** 239–52 (2000).
37. Duda, J. *et al.* Immunohistochemical and Biochemical Studies Demonstrate a Distinct

Profile of a-Synuclein Permutations in Multiple System Atrophy. *J. Neuropathol. Exp. Neurol.* **59,** 830–841 (2000).

38. Fu, Y., Yuan, Y. & Halliday, G. A cytoarchitectonic and chemoarchitectonic analysis of the dopamine cell groups in the substantia nigra, ventral tegmental area, and retrorubral field in the mouse. *Brain Struct Funct* **217,** 591–612 (2012).
39. Mertins, P. *et al.* Integrated proteomic analysis of post-translational modifications by serial enrichment. *Nat. Methods* **10,** 634 – 637 (2013).
40. Wojcechowskyj, J. A., Lee, J. Y., Seeholzer, S. H. & Doms, R. W. Quantitative Phosphoproteomics of CXCL12 (SDF-1) Signaling. *PLoS One* **6,** (2011).
41. Walther, D. M. & Mann, M. Accurate Quantification of More Than 4000 Mouse Tissue Proteins Reveals Minimal Proteome Changes During Aging. *Mol. Cell. Proteomics* 1–7 (2011). doi:10.1074/mcp.M110.004523
42. Price, J. C., Guan, S., Burlingame, A., Prusiner, S. B. & Ghaemmaghami, S. Analysis of proteome dynamics in the mouse brain. *Proc. Natl. Acad. Sci. U. S. A.* **107,** 14508 –14513 (2010).
43. Sharma, K. *et al.* Cell type – and brain region – resolved mouse brain proteome. *Nat. Neurosci.* **18,** 1819 – 1831 (2015).
44. Wang, H. *et al.* Characterization of the Mouse Brain Proteome Using Global Proteomic Analysis Complemented with Cysteinyl-Peptide Enrichment. *J. Proteome Res.* 361–369 (2006).
45. Giasson, B. I. *et al.* Oxidative damage linked to neurodegeneration by selective alpha-synuclein nitration in synucleinopathy lesions. *Science (80-.).* **290,** 985–989 (2000).
46. Weinreb, P. H., Zhen, W., Poon, A. W., Conway, K. A. & Lansbury, P. T. NACP, a Protein Implicated in Alzheimer's Disease and Learning, is Natively Unfolded. *Biochemistry* **35,** 13709–13715 (1996).
47. Fujiwara, H. *et al.* Alpha-Synuclein is phosphorylated in synucleinopathy lesions. *Nat. Cell Biol.* **4,** 160–4 (2002).
48. Anderson, J. P. *et al.* Phosphorylation of Ser-129 is the dominant pathological modification of alpha-synuclein in familial and sporadic Lewy body disease. *J. Biol. Chem.* **281,** 29739–52 (2006).
49. Larhammar, M. *et al.* SLC10A4 Is a Vesicular Amine-Associated Transporter Modulating Dopamine Homeostasis. *Biol Psychiatry* **77,** 526–536 (2015).
50. Patra, K., Lyons, D. J., Bauer, P., Hilscher, M. M. & Sharma, S. A role for solute carrier family 10 member 4, or vesicular aminergic-associated transporter, in structural remodelling and transmitter release at the mouse neuromuscular junction. *Eur J Neurosci* **41,** 316–327 (2015).
51. Scott, D. A. *et al.* Neurobiology of Disease A Pathologic Cascade Leading to Synaptic Dysfunction in a-Synuclein-Induced Neurodegeneration. *Neurobiol. Dis.* **30,** 8083–8095 (2010).
52. Rebekah, L. & Kathleen, F. Dopamine and Paraquat Enhance a-Synuclein-Induced Alterations in Membrane Conductance. *Neurotox. Res.* 387–401 (2011). doi:10.1007/s12640-011-9255-x
53. Danzer, K. M. *et al.* Different Species of a-Synuclein Oligomers Induce Calcium Influx and Seeding. *Neurobiol. Dis.* **27,** 9220–9232 (2007).
54. Illes-toth, E., Ramos, M. R., Cappai, R., Dalton, C. & Smith, D. P. Distinct higher-order α-synuclein oligomers induce intracellular aggregation. *Biochem J.* 485–493 (2015). doi:10.1042/BJ20150159

55. Tosatto, L. *et al.* Alpha-synuclein pore forming activity upon membrane association. *BBA - Biomembr.* **1818,** 2876–2883 (2012).

56. Prots, I. *et al.* a-Synuclein Oligomers Impair Neuronal Microtubule-Kinesin. *J. Biol. Chem.* **288,** 21742–21754 (2013).

57. Ferrington, D. A. & Gregerson, D. S. Immunoproteasomes: Structure, Function, and Antigen Presentation. *Prog. Mol. Biol. Transl. Sci.* **109,** 75–112 (2012).

58. Cascio, P., Hilton, C., Kisselev, A. F., Rock, K. L. & Goldberg, A. L. 26S proteasomes and immunoproteasomes produce mainly N-extended versions of an antigenic peptide. *EMBO J.* **20,** 2357 – 2366 (2001).

59. Gaczynska, M., Rock, K. L., Spies, T. & Goldberg, A. L. Peptidase activities of proteasomes are differentially regulated by the major histocompatibility complex-encoded genes for LMP2 and LMP7. *PNAS* **91,** 9213–9217 (1994).

60. Huber, E. M. *et al.* Immuno- and Constitutive Proteasome Crystal Structures Reveal Differences in Substrate and Inhibitor Specificity. *Cell* **148,** 727–738 (2012).

61. Raule, M., Cerruti, F. & Cascio, P. Enhanced rate of degradation of basic proteins by 26S immunoproteasomes. *BBA - Mol. Cell Res.* **1843,** 1942–1947 (2014).

62. Dıaz-Hernandez, M. *et al.* Neuronal Induction of the Immunoproteasome in Huntington's Disease. *J. Neurosci.* **23,** 11653–11661 (2003).

63. Aso, E. *et al.* Amyloid Generation and Dysfunctional Immunoproteasome Activation with Disease Progression in Animal Model of Familial Alzheimer's Disease. **22,** 636–653 (2012).

64. Orre, M. *et al.* Reactive glia show increased immunoproteasome activity in Alzheimer's disease. *Brain* **136,** 1415–1431 (2013).

65. Díaz-villanueva, J. F., Díaz-molina, R. & García-gonzález, V. Protein Folding and Mechanisms of Proteostasis. *Int. J. Mol. Sci.* **16,** 17193–17230 (2015).

66. Douglas, P. M. & Dillin, A. Protein homeostasis and aging in neurodegeneration. *J. Cell Biol.* **190,** 719–729 (2010).

67. Kikis, E. A., Gidalevitz, T. & Morimoto, R. I. Protein Homeostasis in Models of Aging and Age-Related Conformational Disease. *Adv Exp Med Biol* **694,** 138 – 159 (2010).

68. Heink, S., Ludwig, D., Kloetzel, P. & Kru, E. IFN-y-induced immune adaptation of the proteasome system is an accelerated and transient response. *Proc. Natl. Acad. Sci. U. S. A.* **102,** 9241–9246 (2005).

69. Dalet, A., Stroobant, V. & Vigneron, N. Differences in the production of spliced antigenic peptides by the standard proteasome and the immunoproteasome. *Eur. J. Immunol.* **41,** 39–46 (2011).

70. Kincaid, E. Z. *et al.* Mice completely lacking immunoproteasomes show major changes in antigen presentation. *Nat. Immunol.* **13,** 129–135 (2012).

71. Marques, J., Palanimurugan, R., Matias, A. C., Ramos, P. C. & Ju, R. Catalytic Mechanism and Assembly of the Proteasome. *Chem. Rev.* **109,** 1509–1536 (2009).

72. Chapiro, J. *et al.* Destructive Cleavage of Antigenic Peptides Either by the Immunoproteasome or by the Standard Proteasome Results in Differential Antigen Presentation. *J. Immunol.* **176,** 1053–1061 (2006).

73. Cardozo, C. & Kohanski, R. A. Altered Properties of the Branched Chain Amino Acid-preferring Activity Contribute to Increased Cleavages after Branched Chain Residues by the 'Immunoproteasome'. *J. Biol. Chem.* **273,** 16764–16770 (1998).

74. Lei, B. *et al.* Molecular Basis of the Selectivity of the Immunoproteasome Catalytic Subunit LMP2-Specific Inhibitor Revealed by Molecular Modeling and Dynamics Simulations. *J. Phys. Chem.* 12333–12339 (2010).

75. Ebstein, F. *et al.* Immunoproteasomes Are Important for Proteostasis in Immune Responses. *Cell Corresp.* **152,** 935 – 937 (2013).

76. Nathan, J. A., Spinnenhirn, V., Schmidtke, G., Basler, M. & Groettrup, M. Matters Arising Immuno- and Constitutive Proteasomes Do Not Differ in Their Abilities to Degrade Ubiquitinated Proteins. *Cell* **152,** 1184–1194 (2013).

77. Seifert, U. *et al.* Immunoproteasomes Preserve Protein Homeostasis upon Interferon-Induced Oxidative Stress. *Cell* **142,** 613–624 (2010).

78. Teoh, C. Y. & Davies, K. J. A. Potential roles of protein oxidation and the immunoproteasome in MHC class I antigen presentation: the 'PrOxI' hypothesis. *Arch. Biochem. Biophys.* **423,** 88–96 (2004).

79. Mazzulli, J. R., Armakola, M., Dumoulin, M., Parastatidis, I. & Ischiropoulos, H. Cellular Oligomerization of a-Synuclein Is Determined by the Interaction of Oxidized Catechols with a C-terminal Sequence. *J. Biol. Chem.* **282,** 31621–31630 (2007).

80. Riederer, B., Leuba, G. & Elhajj, Z. Oxidation and ubiquitination in neurodegeneration. *Exp. Biol. Med.* **238,** 519–524 (2013).

81. Pickering, A. M., Lehr, M. & Miller, R. A. Lifespan of mice and primates correlates with immunoproteasome expression. *J. Clin. Invest.* **125,** 2059–2068 (2015).

82. Cebrian, C. *et al.* MHC-I expression renders catecholaminergic neurons susceptible to T-cell-mediated degeneration. *Nat. Commun.* **5,** 3633 (2014).

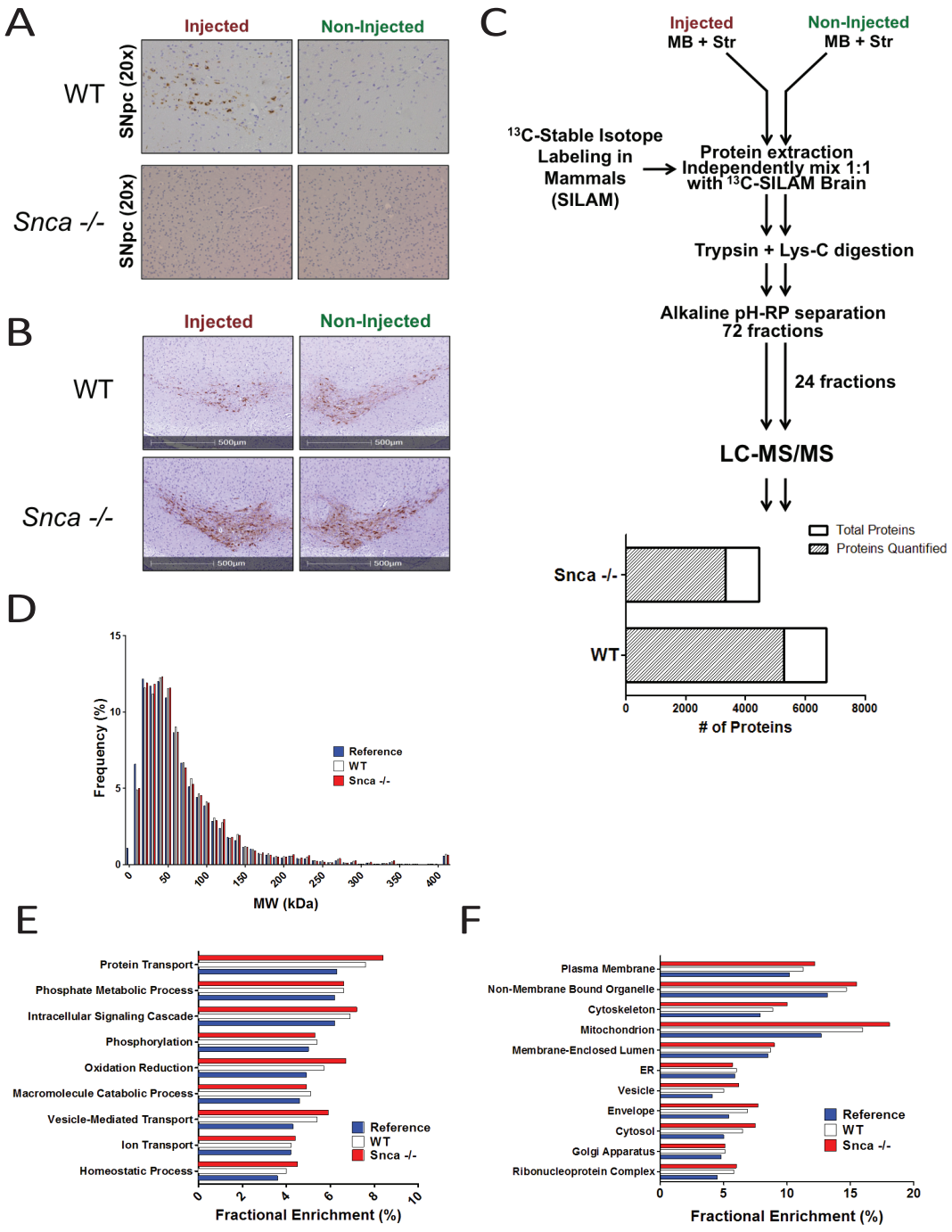

Figure 3.1. Quantitative Proteomic Workflow and Characterization of WT and *Snca -/-* Injected Mice.

(A) Staining the substantia nigra of the injected and non-injected sides of WT and *Snca -/-* mice for phosphorylated α-synuclein at Ser-129, a marker for pathology.

(B) Staining for tyrosine hydroxylase in the injected and non-injected hemispheres of WT mice (n=4; p-value = 0.0507) and *Snca -/-* mice (n=1).

(C) Overview of proteomic workflow. The midbrain and striatum of each side of the mouse brain were dissected and combined. The injected and non-injected sides were kept separate and processed throughout the workflow independently.
(D-F) A mouse brain reference proteome was constructed by combining proteins identified by mass spectrometry in the mouse brain in the literature with proteins we identified in the WT non-injected side. This was compared with the proteins we quantified in both WT and *Snca -/-* to secure that there are no significant biases based on protein MW (D), biological functions (E) or cellular compartments (F).

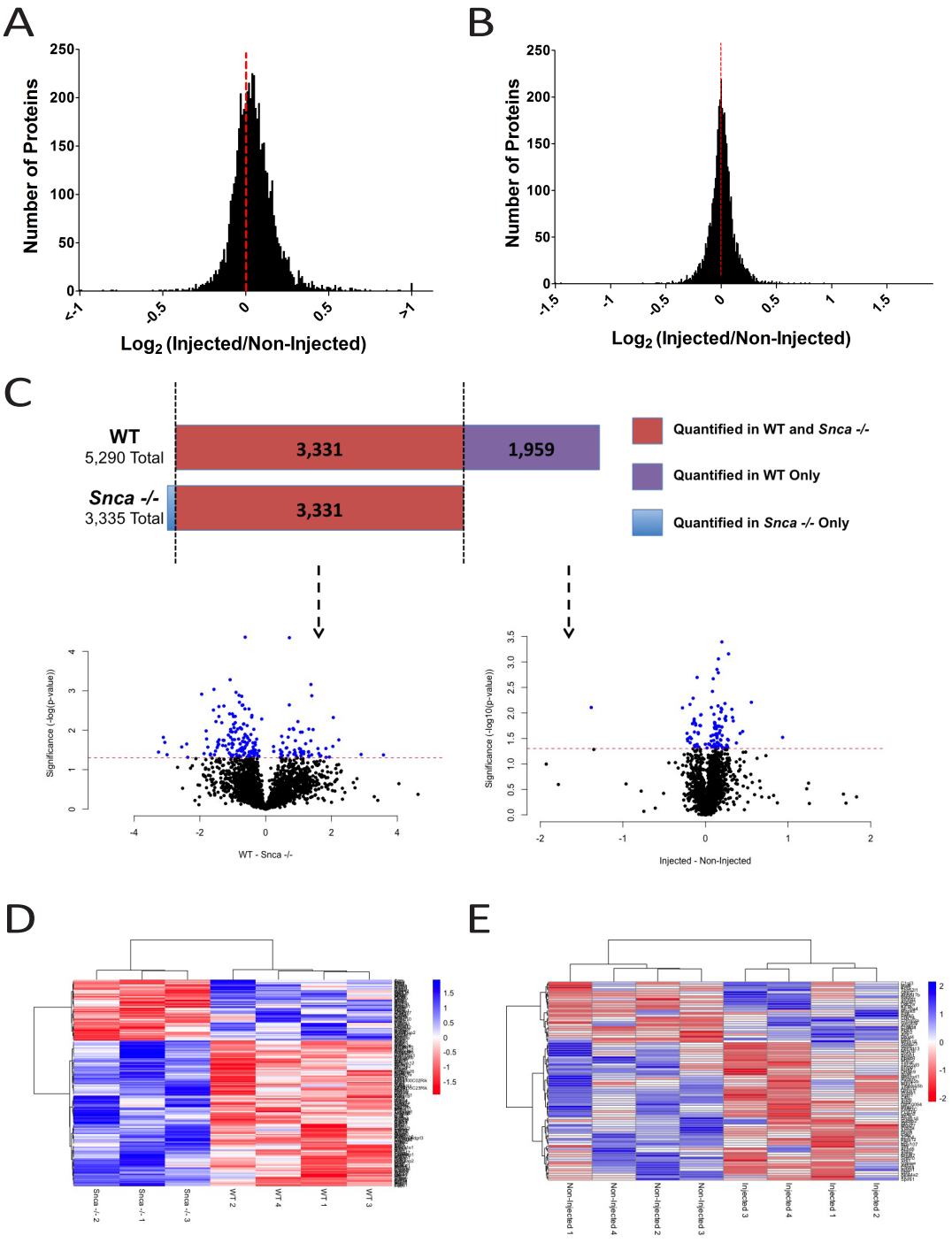

Figure 3.2. Analysis of Quantified Proteins and Identification of α-Synuclein Responsive Proteins.

(A) Frequency distribution plot of proteins quantified in WT mice.

(B) Frequency distribution plot of proteins quantified in *Snca -/-* mice.

(C) Schematic depicting methodology to identify the significantly changed proteins. Of the 3,331 proteins quantified in both WT and *Snca -/-*, 201 significantly changed. Of the 1,959 proteins quantified in WT only, 101 significantly changed. Collectively, this analysis reveals

that the relative abundance of 311 proteins significantly changed, due to endogenous α-synuclein aggregation.
(D) Heatmap depicting clustering of significantly changed proteins comparing WT to *Snca -/-*.
(E) Heatmap depicting clustering of significantly changed proteins comparing injected to non-injected sides in WT.

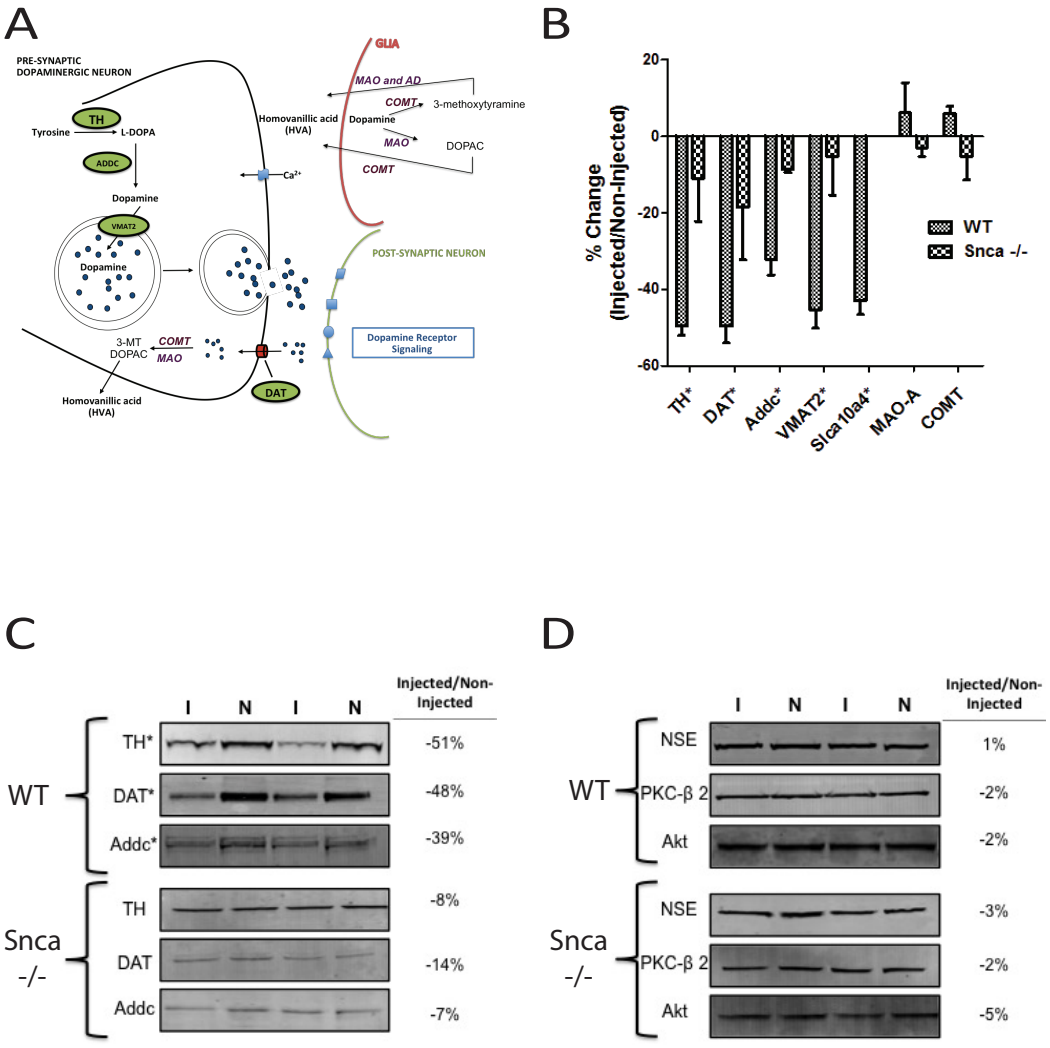

Figure 3.3. Validation of Changes in Dopamine Neuron Specific Proteins.
(A) Depictions of a dopaminergic neuron synapse and specific proteins expressed in pre-synaptic dopaminergic neurons.
(B) Selective loss of these neurons results in a significant decrease in the levels of TH, DAT, Addc and VMAT2 documented by the mass-spectrometry-based proteomic quantification.
(C) Western blot confirmation of proteins found to significantly decrease in WT but not *Snca -/-* mice.
(D) Western blot confirmation of proteins found to not significantly change, including NSE, PKC-β 2 and Akt.

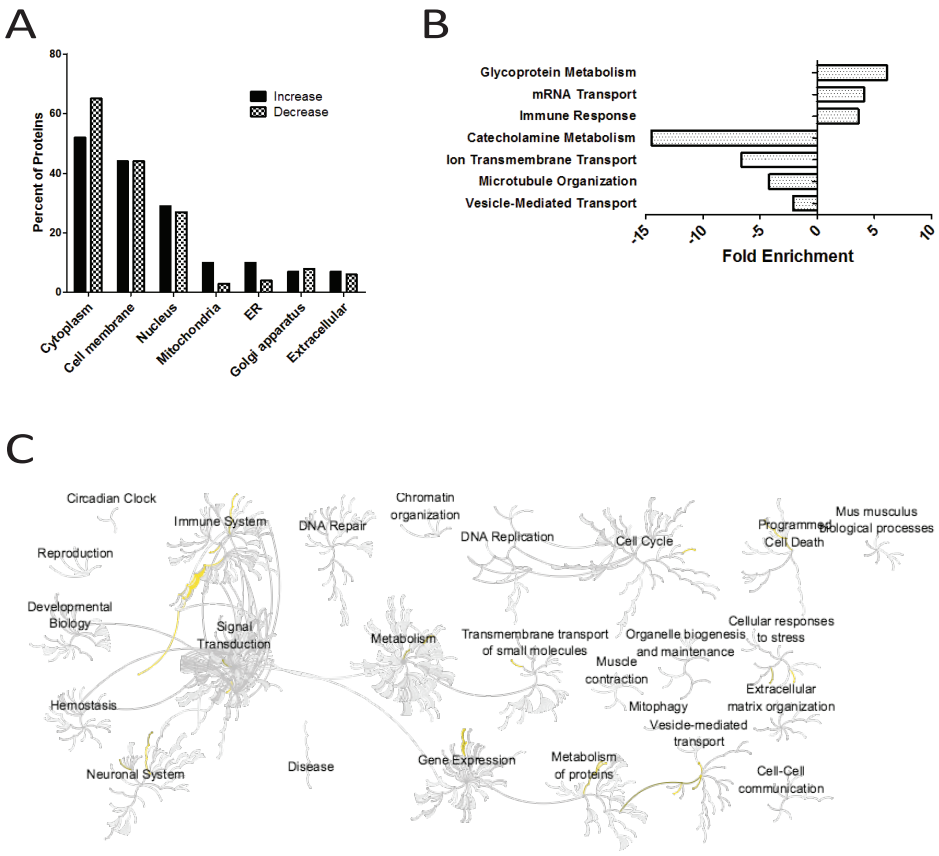

Figure 3.4. Enrichment Analysis of α-Synuclein Responsive Proteins.

(A) Percent of α-synuclein responsive proteins that either increased or decreased in the injected side that are localized to each subcellular localization.
(B) Biological processes that are significantly enriched among the α-synuclein responsive proteins that increased or decreased in the injected side. The 5,290 proteins quantified in WT were used as background to determine enrichment.
(C) Overview of pathways enriched for α-synuclein responsive proteins. Yellow lines represent pathways enriched for these proteins.

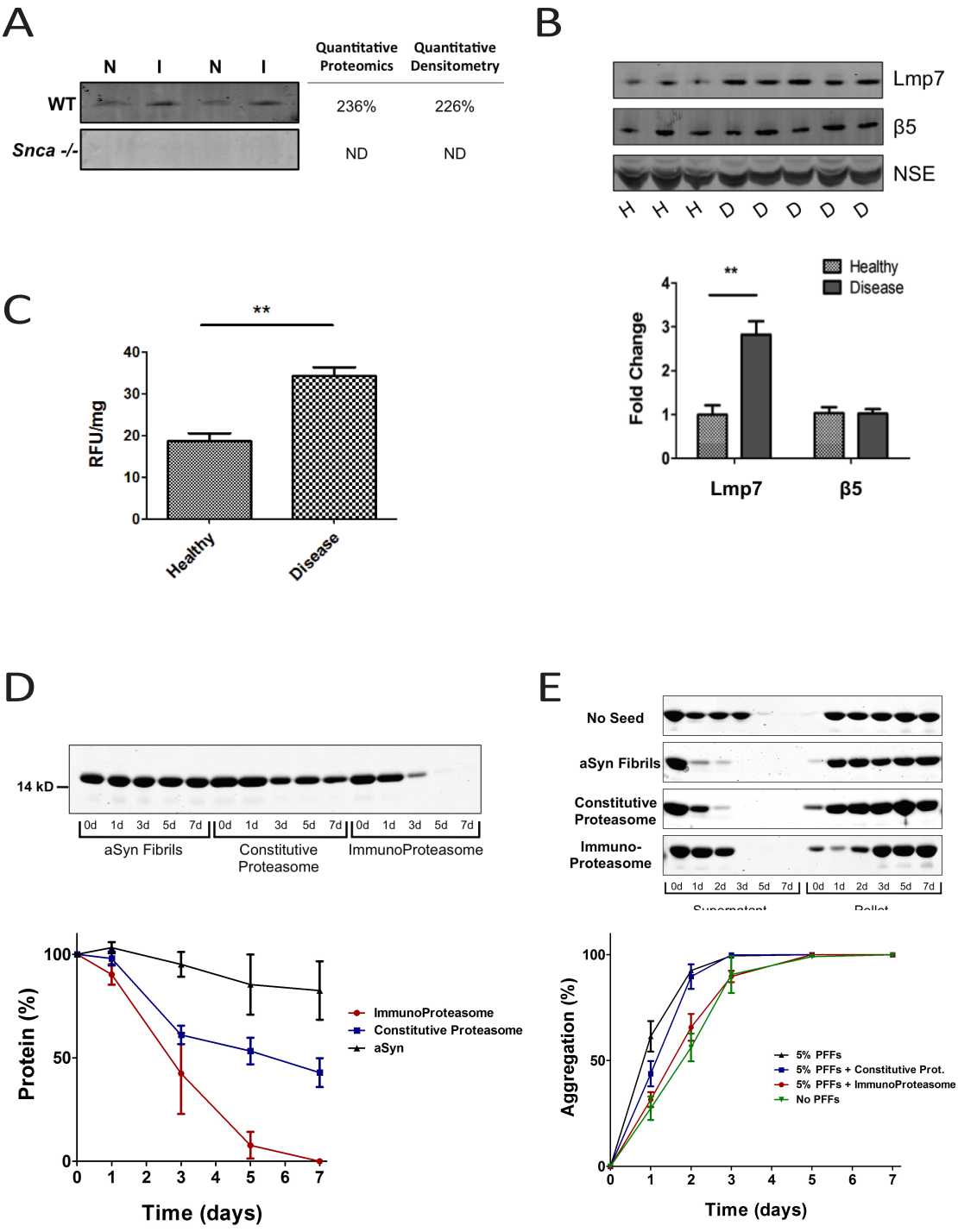

Figure 3.5. The Immunoproteasome is Implicated in Human Disease Driven by α-Synuclein Aggregation.

(A) Western blot in WT and *Snca -/-* mouse brain for Lmp7 reveals that Lmp7 is increased in the injected side by 226% compared to the non-injected side, consistent with the 236% increase found by the proteomic analysis. Lmp7 was not detected in *Snca -/-* mice by either Western blot or proteomics.

(B) Western blot analysis in human DLB brain versus healthy brain reveals that Lmp7 is increased by 297% in disease compared with healthy.
(C) Chymotrypsin-like activity, a proxy for immunoproteasome activity, is increased by 189% in disease brain compared with healthy brain. n=3.
(D) Degradation efficiencies of α-synuclein fibrils by the constitutive proteasome and the immunoproteasome were compared. After 7 days, 100% degradation was achieved by the immunoproteasome compared with only 55% by the constitutive proteasome. n=3.
(E) Efficiency of accelerating aggregation of the products from the degradation assay of the immunoproteasome and constitutive proteasome were compared with 5% fibrillar PFFs and no PFFs. n=3. Two-way ANOVA analysis with a Bonferroni post-test (*** p-value < 0.001).

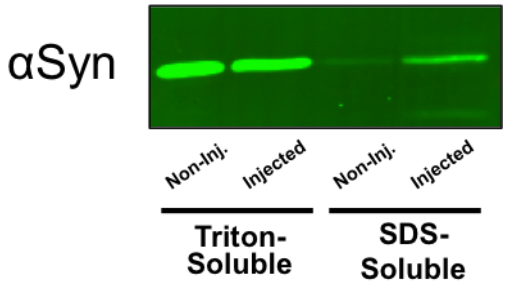

Supplementary Figure 3.1. Greater Insoluble α-Synuclein in the Injected Side than the Non-Injected Side.

Sequential biochemical extraction was performed on the combination of the midbrain and striatum from the injected and non-injected sides of the WT mouse. Samples were analyzed by Western blot to confirm that there is a greater amount of α-synuclein in the SDS-Soluble fraction in the injected side than the non-injected side.

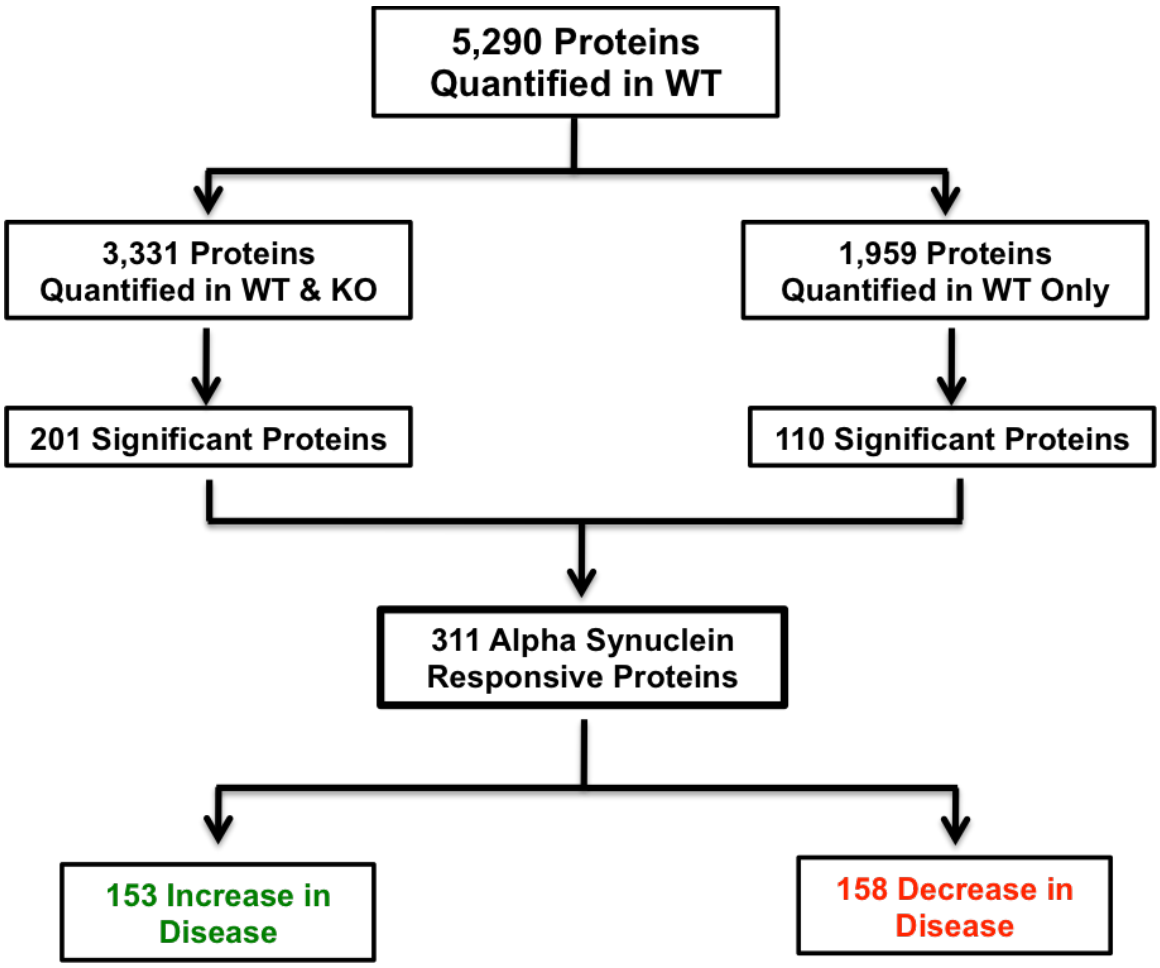

Supplementary Figure 3.2. Breakdown of 311 α-Synuclein Responsive Proteins.
All 5,290 proteins quantified in WT were analyzed to identify significantly changed proteins.

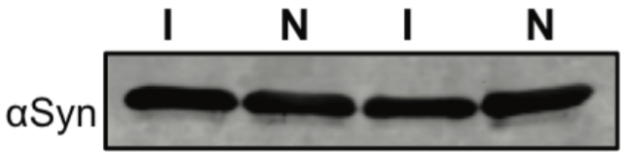

Supplementary Figure 3.3. Relative Abundance of α-Synuclein Does Not Change in WT.
Western blot confirmation of the relative abundance of α-synuclein in the injected and non-injected sides from WT mice.

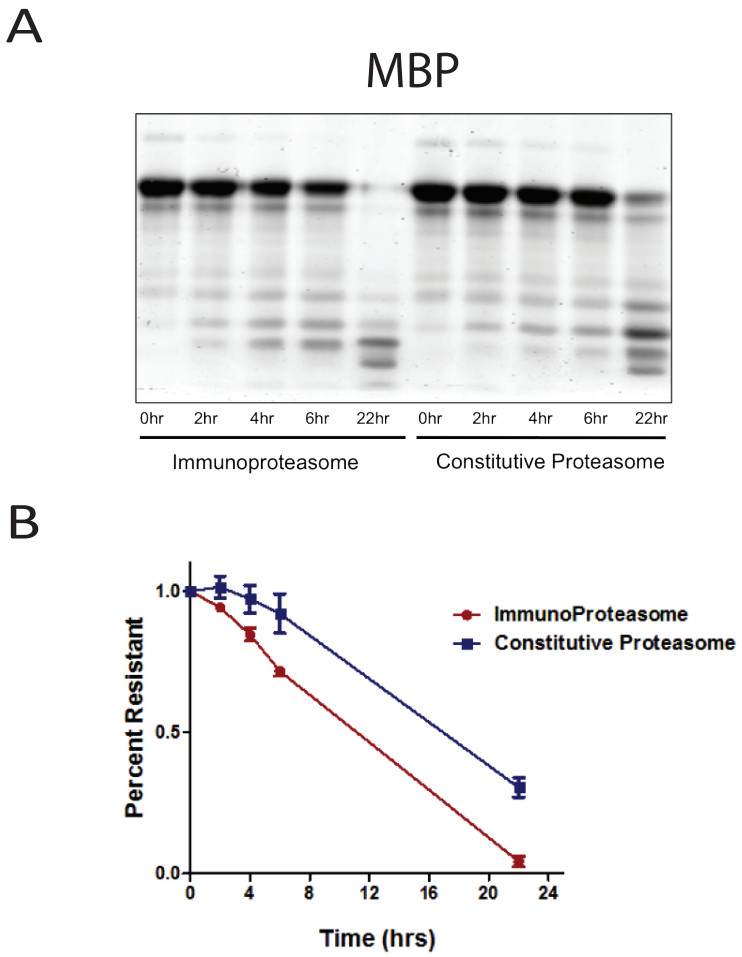

Supplementary Figure 3.4. Myelin Basic Protein is More Rapidly Degraded by the Immunoproteasome than the Constitutive Proteasome.
(A) Myelin Basic Protein was incubated with the constitutive proteasome or the immunoproteasome. At indicated time points aliquots were removed and analyzed by SDS-PAGE.
(B) Densitometry of monomeric band of MBP reveals that incubation with the immunoproteasome results in 96% degradation compared to 70% with the constitutive proteasome. n=3.

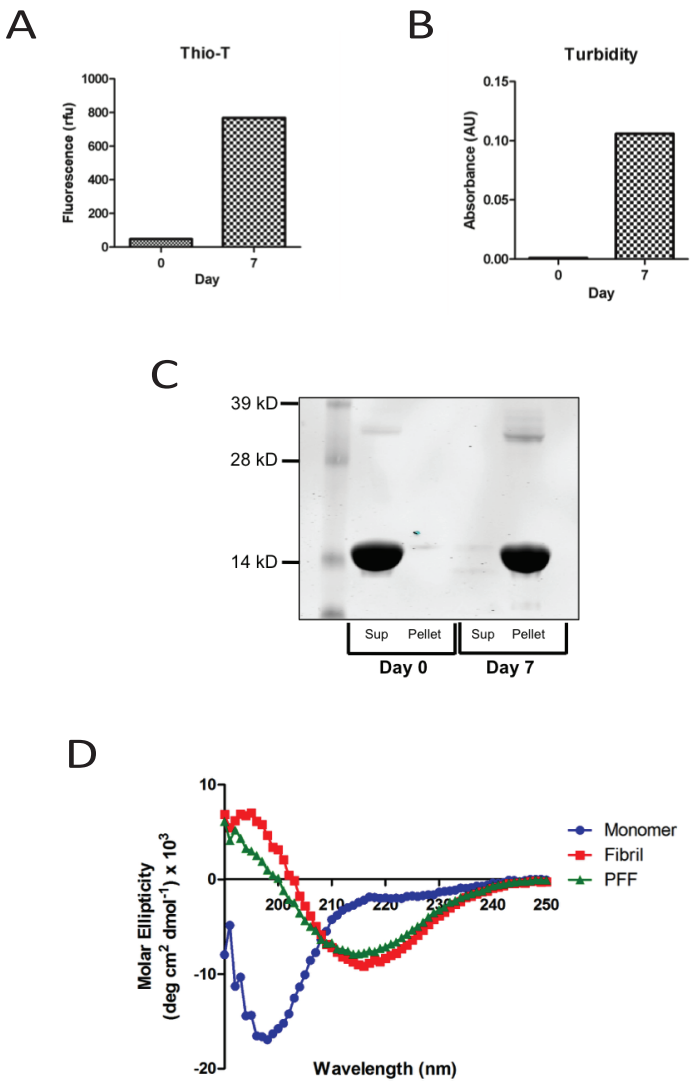

Supplementary Figure 3.5. Amyloid Characteristics of α-Synuclein Fibrils Used for Pure Proteasome Assay.
(A) Human recombinant WT α-synuclein was incubated at 37°C, agitating at 1,400 rpm at 5 mg/ml. At Day 0 and Day 7 sample was removed for Thioflavin-T analysis, an assay for the presence of β-sheet rich amyloid fibrils, revealing a >20-fold increase in fluorescence.
(B) At Day 0 and Day 7 a sample was removed for turbidity analysis, an assay for the presence of insoluble species, revealing a >30-fold increase in turbidity.
(C) At Day 0 and Day 7 a sample was removed for sedimentation analysis, revealing a shift of protein from the soluble supernatant to the insoluble pellet.
(D) At Day 7, circular dichroism analysis was done. The monomer displayed random coil, and both the fibrils and PFFs revealed β-sheet structure.

CHAPTER 4

Quantitative Phosphoproteomics Reveals Changes in Cellular Signaling in Response to Endogenous Alpha-Synuclein Aggregation

Scott Ugras[1], Kelvin Luk[2], Anastasia Yocum[3], Hua Ding[4], Chris McKennan[4,5], Steven Seeholzer[4], and Harry Ischiropoulos[6]

[1]Biochemistry and Molecular Biophysics Graduate Group, Perelman School of Medicine, University of Pennsylvania, Philadelphia, PA, 19104, USA.
[2]Center for Neurodegenerative Disease Research, Department of Pathology and Laboratory Medicine, University of Pennsylvania Perelman School of Medicine, Philadelphia, PA, 19104, USA.
[3]A2IDEA, LLC Ann Arbor, MI 48105, USA.
[4]Children's Hospital of Philadelphia Research Institute, Philadelphia, PA 19104, USA.
[5]Department of Statistics, University of Chicago, Il 60637, USA.
[6]Department of Pediatrics, Children's Hospital of Philadelphia, Philadelphia, PA 19104, USA; Department of Systems Pharmacology and Translational Therapeutics, Perelman School of Medicine, University of Pennsylvania, Philadelphia, PA 19104, USA. Electronic address: ischirop@mail.med.upenn.edu.

4.1 Abstract

α-Synuclein deposited into Lewy Bodies in Parkinson's disease and related synucleinopathies have elevated levels of Ser-129 phosphorylation compared with soluble protein. This change may be reflective of a global perturbation in cellular signaling induced by α-synuclein aggregation that contributes to neurodegeneration and disease pathogenesis. Here, we used mass spectrometry to quantify the relative abundance changes of phosphorylation sites due to endogenous α-synuclein aggregation in a mouse model of progressive α-synuclein aggregation. This resulted in the quantification of 2,763 and 2,112 phosphosites in wildtype (WT) and α-synuclein-null mice (Snca -/-), respectively. 126 and 65 phosphosites were significantly altered in WT and Snca -/- mice, respectively. The amino acid distribution of the phosphosites did not significantly deviate between the significant phosphosites and the total quantified phosphosites. Endosome transport, membrane organization and vesicle-mediated transport were enriched among the significantly altered phosphoproteins in WT, suggesting that various cellular signaling processes respond to α-synuclein aggregation. Further interrogation of the phosphorylation signaling changes that drives these processes would shed light on α-synuclein aggregation-mediated neurotoxicity.

4.2 Introduction

α-Synuclein is a 140 amino acid protein that has roles in synaptic plasticity and neurotransmitter release[1]. Progressive accumulation of α-synuclein aggregates underlies several neurodegenerative diseases, including Parkinson's disease (PD), collectively referred to as synucleinopathies. PD is the second most common neurodegenerative disease in the United

States and is characterized by dopaminergic degeneration and α-synuclein-positive intracellular inclusions known as Lewy Bodies (LBs)[2–4]. Multiplications[5–7] and point mutations[8–12] in the gene encoding α-synuclein, *SNCA*, cause PD. Additionally, purified wildtype and PD-linked mutant forms of α-synuclein rapidly fibrillize *in vitro*[13–16]. Collectively, these data implicate α-synuclein aggregation as a contributing factor in PD and related diseases.

Phosphorylation of α-synuclein deposited into LBs is increased at Ser-129 compared with soluble α-synuclein[17,18]. LBs derived from other synucleinopathies, including multiple system atrophy and dementia with Lewy Bodies, also contain abundant α-synuclein phosphorylated at Ser-129[17,18]. The biochemical consequences of this phosphorylation on aggregation, membrane binding, and neurotoxicity are unclear[19]. Studies expressing Ser-129A to prevent phosphorylation or Ser-129D to mimic phosphorylation in rodent models and drosophila have yielded conflicting results as to whether phosphorylation is neurotoxic or neuroprotective[20–24]. Using cell free systems, most studies have found that phosphorylation of Ser-129 inhibits fibrillization[25,26], though some have found that it accelerates aggregation[18].

This finding that α-synuclein phosphorylation is altered upon aggregation inspired our work. We postulated that α-synuclein aggregation induces global perturbations in cellular signaling that may contribute to neurodegeneration. To study these changes, we focused on phosphorylation because of the documented increase in Ser-129 phosphorylation of α-synuclein upon aggregation, and the importance of phosphorylation in regulating a multitude of critical cellular activities. Using a recently developed mouse model of progressive aggregation of endogenous α-synuclein[27], we employed a quantitative phosphoproteomic approach to measure the relative abundance changes of phosphosites due to α-synuclein aggregation.

4.3 Experimental Procedures

Mouse Models Used in this Study: All handling of mice were performed according to the NIH Guide for the Care and Use of Experimental Animals and approved by the University of Pennsylvania Institutional Animal Care and Use Committee (IACUC). Wildtype (WT) C57BL6/C3H mice were obtained from the Jackson Laboratories (Bar Harbor, ME). Snca -/- mice[28] were maintained on a C57BL6 background. ^{13}C-Stable Isotope Labeling in Mammals (SILAM) mouse brain tissue was purchased from Cambridge Isotope Laboratories, Inc (Female, L-Lysine 13C6, 97%).

Stereotaxic Injection of PFFs: Stereotaxic injection of pre-formed fibrils (PFFs) was performed as previously described (see Chapter 3). Briefly, human WT α-synuclein fibrils were diluted in sterile PBS and sonicated to produce PFFs. These PFFs were injected into the ventral striatum, dorsal striatum and overlaying cortex of WT and Snca -/- mice. Mice were sacrificed 90 days post injection by overdose with ketamine/xylazine.

Sample Preparation for LC-MS/MS: Briefly, the midbrain and striatum of the injected and non-injected sides were dissected and kept separate throughout the workflow. Two midbrain and striatum regions of the injected side were combined to generate one biological sample for the phosphoproteomic analysis. The same approach was employed for the non-injected side. Three biological samples for WT and Snca -/- for each injected and non-injected side were analyzed through the phosphoproteomic workflow. Sample preparation was done as previously described in Carr *et al.*[29], and in Chapter 3. After peptide separation by high-pH reverse phase chromatography, 95% of peptides were combined in a concatenated pattern into 12 fractions

for phosphoproteomic analysis. Lyophilized phosphopeptides fractions were resuspended in 50% acetonitrile/0.1% trifluoroacetic acid (TFA) and then diluted 1:1 with 100% acetonitrile/0.1% TFA. These samples were then enriched for phosphorylation by incubation with 10 µl with immobilized metal affinity chromatography (IMAC) for 30 min. Enriched IMAC beads were the loaded onto C18 silica-packed stage tips, washed twice with 50 µl of 80% acetonitrile/0.1% TFA and 100 µl of 1% formic acid. Phosphopeptides were then eluted from IMAC beads with 3 washes of 70 µl 500 mM dibasic sodium phosphate, pH 7.0, (Sigma, S9763) and 2 washes of 100 µl of 1% formic acid. Elution from stage tips was then performed with 60µl of 50% acetonitrile/0.1% formic acid. Washes were performed on a tabletop centrifuge at a maximum speed of 3,500 *g*.

LC-MS/MS and MS Database Searching and Data Processing: LC-MS/MS and MS Database Searching using MaxQuant (1.5.1.2) was performed as described in Chapter 3.

Statistical Analysis: SILAC ratios were calculated as described in Chapter 3. Briefly, The Heavy/Light (H/L) ratio in the non-injected side was divided by the H/L ratio in the injected side to compute the injected/non-injected ratio of ratios. A phosphosite was considered quantified in WT if this ratio of ratios was computed in in all 3 biological replicates; it was considered quantified in *Snca -/-* if this ratio of ratios was computed in all 3 biological replicates. This resulted in the quantification of 2,763 phosphosites (from 1,445 phosphoproteins) in WT and 2,112 phosphosites (from 1,110 phosphoproteins) in Snca -/-. A paired Student's T-Test was then used to calculate the significance of the differential expression for the phosphosites quantified in WT and Snca -/-. p-Values $\leq$ 0.05 were considered significant. This yielded 136

phosphosites (from 124 phosphoproteins) in WT and 75 phosphosites (from 69 phosphoproteins) in Snca -/- that were significant. Next, we eliminated phosphoproteins that overlapped between WT and Snca -/-, since we could not attribute the significant change to α-synuclein aggregation versus the PFF injection. There were 9 phosphoproteins that overlapped in WT and Snca -/-. Eliminating these resulted in a final significant list of 126 phosphosites (from 115 phosphoproteins) in WT and 65 phosphosites (from 60 phosphoproteins) in Snca -/-.

Heatmap Generation: Heatmaps were created using pHeatmap in Rstudio. Clustering distances were calculated by row and column with either Euclidean or Manhattan metrics, n- dimensional real vector space with fixed Cartesian coordinate system, and clustered by either ward.D2 or average linkage methodology, UPGMA.

Gene Ontology Enrichment Analysis: DAVID Bioinformatics Resources 6.7 was used for enrichment analysis. For WT, the 1,445 quantified phosphoproteins in WT were used as background. The 115 significantly changed phosphoproteins were used as a list and the enrichment of Biological Processes was examined. Similarly for Snca -/-, the 1,110 quantified phosphoproteins were used as background and the 60 significant phosphoproteins were used as a list. Those biological processes with p-values ≤ 0.05 were considered significant, and fold-changes were determined using the DAVID software.

4.4 Results

Quantitative Phosphoproteomics in PFF Mouse Model

With the goal of quantifying changes in phosphorylation signaling in the brain due to α-synuclein aggregation, we decided to use a modified version of a recently developed mouse model[27]. In this model, α-synuclein pre-formed fibrils (PFFs) are intrastriatally injected into the right hemisphere of a wildtype (WT) mouse brain. This induces a cascade of progressive α-synuclein aggregation in synaptically connected regions, concomitant with dopaminergic degeneration in the injected side only, and motor symptoms. Importantly, injection of PFFs into α-synuclein null mice (Snca -/-) does not result in this phenotype. This model has been replicated in mouse[30,31] and rats[32], and recapitulates the cardinal features of Parkinson's disease. We modified this model to accelerate pathology by injecting triple the load of PFFs. 90 days post injection (dpi), we documented a 19% loss of tyrosine hydroxylase positive neurons and increased α-synuclein aggregation in the injected side of WT mice (see Chapter 3).

To measure the relative abundance changes of phosphorylation due to α-synuclein aggregation, we employed a recently described quantitative mass spectrometry (MS) based methodology[29]. This method utilized ^{13}C-Stable Isotope Labeling in Mammals (SILAM)[33,34] as an internal standard to quantify phosphosite changes. First, we extracted the midbrain and striatum from the injected and non-injected sides of the mouse that was sacrificed 90 dpi. The tissue from the injected and non-injected sides was kept separate for the entire workflow (Figure 4.1). We combined tissue from two mice for each biological replicate in order to have enough sample for the phosphoproteomic analysis. The injected and non-injected sample from the PFF injected mouse was then independently mixed with the SILAM tissues in a 1:1 ratio, followed by homogenization, enzymatic peptide digestion, and separation by high-pH reverse phase liquid chromatography (RPLC). These peptides were then enriched for phosphopeptides with immobilized metal affinity chromatography (IMAC) followed by LC-MS/MS.

To quantify phosphosites, a ratio of ratios approach was taken whereby the SILAM/Non-Injected ratio was divided by the SILAM/Injected ratio to generate the Injected/Non-Injected ratio. This allows us to compare the relative abundance change of a given phosphosite in the injected side compared with the non-injected side. We performed three biological replicates for WT and three for Snca -/-. We used Snca -/- to account for phosphosite changes induced by the injection of PFFs. Our analysis resulted in the quantification of 2,763 phosphosites (from 1,445 phosphoproteins) in WT (Supplementary Table 11) and 2,112 phosphosites (from 1,110 phosphoproteins) in Snca -/- (Figure 4.2A, Supplementary Table 12). The distribution of the $\log_2$ transformed ratio of ratios for WT Snca -/- shows a unimodal distribution centered on $\log_2=0$ (Figures 4.2B and C).

Identification of Significantly Altered Phosphosites

To identify phosphosites whose relative abundance signififcantlty changed, several filtering steps were applied. First, a paired Student's T-Test was applied to each quantified phosphosite in WT and Snca -/-. p-Values ≤ 0.05 were considered significant, resulting in 136 (from 124 phosphoproteins) and 75 phosphosites (from 69 phosphoproteins) in WT and Snca -/-, respectively. Then, phosphosites found in both WT and Snca -/- were excluded since the change could be attributed to the injection of PFFs and not α-synuclein aggregation. After elimination of the 9 phosphoproteins found in both groups, the final significant list consisted of 126 phosphosites (from 115 phosphoproteins) and 65 phosphosites (from 60 phosphoproteins) in WT and Snca -/-, respectively (breakdown depicted in Supplementary Figure 4.1; Supplementary Table 13). Volcano plots depicting the significant phosphosites in WT and Snca -/- depict the

average differential expression versus significance (Figures 4.3A and B). Heatmaps generated show that phosphosites that either significantly increase or decrease cluster together across biological replicates, demonstrating the consistency in the relative abundance changes across replicates (Figures 4.3C and D).

Exploration of Biological Processes and Pathways that are Altered in Response to α-Synuclein Aggregation

Next, we interrogated the significantly altered phosphosites in order to elucidate changes in signaling events in response to α-synuclein aggregation. First, the distribution of phosphorylated amino acids in the significantly altered phosphosites was compared with the total quantified phosphosites (Figure 4.4A). Serine phosphorylation comprised 85% - 93% of the total phosphorylation, followed by threonine with 8% - 14% and tyrosine with 0% - 2%. Overall, no significant deviations were detected, suggesting that significant changes did not preferentially occur on a particular amino acid. Next, the enrichment of biological processes among the significant phosphoproteins in WT and Snca -/- were determined (Figure 4.4B). Among WT phosphoproteins, endosome transport, mitosis, membrane organization and neurological systems were significantly enriched 2 – 7 fold. This is consistent with disruptions in cellular signaling and the cell cycle. Among the significant Snca -/- phosphoproteins, only protein kinase-related processes were enriched, suggesting that kinases respond to the injection of PFFs. Finally, a global view of perturbed pathways in WT was determined (Figure 4.4C). This revealed that vesicle-mediated transport and the immune system respond in WT, suggesting that cellular

communication and defense systems are altered in response to endogenous α-synuclein aggregation in the brain.

4.5 Discussion

The precise mechanisms by which dysfunction in cellular signaling pathways contributes to neurodegeneration in PD and other synucleinopathies remains incompletely understood. Initially, proteostasis mechanisms aimed at maintaining proper protein homeostasis, including the ubiquitin/proteasome system, autophagy, and the unfolded protein response, are likely perturbed due to α-synuclein aggregation. Later, cell-death pathways, including p53, JNK signaling, cell-cycle reactivation, become involved[35]. Intervening with these later pathways could provide a therapeutic strategy to mitigate the neurotoxicity associated with α-synuclein aggregation in human disease

Our work aimed to shed light on changes in phosphorylation signaling induced by endogenous α-synuclein aggregation in the brain. Given the documented changes in phosphorylation of proteins implicated in PD, α-synuclein[18] and the 14-3-3 proteins[36], we reasoned that global phosphorylation may be perturbed. We documented that 126 phosphosites were significantly changed due to α-synuclein aggregation. These phosphoproteins were involved in various aspects of cellular signaling, including endosome transport, vesicle-mediated transport and neurological systems. Further investigation of these pathways may reveal phosphorylation-mediated signaling events that contribution to dopaminergic degeneration in PD.

References

1. Lashuel, H. a, Overk, C. R., Oueslati, A. & Masliah, E. The many faces of α-synuclein: from structure and toxicity to therapeutic target. *Nat. Rev. Neurosci.* **14,** 38–48 (2013).
2. Mortality, G. B. D. & Collaborators, D. Global, regional, and national age – sex specific all-cause and cause-specific mortality for 240 causes of death, 1990 – 2013: a systematic analysis for the Global Burden of Disease Study 2013. *Lancet* **385,** 117–171 (2014).
3. de Lau, L. & Breteler, N. Epidemiology of Parkinson's disease. *Lancet Neurol.* **6,** 525–535 (2006).
4. Goedert, M., Spillantini, M. G., Tredici, K. Del & Braak, H. 100 years of Lewy pathology. *Nat. Rev. Neurol.* **9,** 13–24 (2012).
5. Chartier-Harlin, M.-C. *et al.* Alpha-synuclein locus duplication as a cause of familial Parkinson's disease. *Lancet* **364,** 1167–9 (2004).
6. Singleton, A. B. *et al.* Alpha-Synuclein locus triplication causes Parkinson's disease. *Science* **302,** 841 (2003).
7. Ferese, R. *et al.* Four Copies of SNCA Responsible for Autosomal Dominant Parkinson's Disease in Two Italian Siblings. *Parkinsons. Dis.* **2015,** 1–6 (2015).
8. Appel-Cresswell, S. *et al.* Alpha-synuclein p.H50Q, a novel pathogenic mutation for Parkinson's disease. *Mov. Disord.* **28,** 811–3 (2013).
9. Krüger, R. *et al.* Ala30Pro mutation in the gene encoding α-synuclein in Parkinson's disease. *Nat. Genet.* **18,** 106–108 (1998).
10. Lesage, S. *et al.* G51D α-synuclein mutation causes a novel parkinsonian-pyramidal syndrome. *Ann. Neurol.* **73,** 459–471 (2013).
11. Polymeropoulos, M. H. *et al.* Mutation in the α-Synuclein Gene Identified in Families with Parkinson's Disease. *Sci. Reports* **276,** 2045 – 2047 (1997).
12. Zarranz, J. J. *et al.* The new mutation, E46K, of alpha-synuclein causes Parkinson and Lewy body dementia. *Ann. Neurol.* **55,** 164–73 (2004).
13. Conway, K. a, Harper, J. D. & Lansbury, P. T. Accelerated in vitro fibril formation by a mutant alpha-synuclein linked to early-onset Parkinson disease. *Nat. Med.* **4,** 1318–20 (1998).
14. Conway, K. A., Harper, J. D. & Lansbury, P. T. Fibrils Formed in Vitro from A-Synuclein and Two Mutant Forms Linked to Parkinson's Disease are Typical Amyloid. *Biochemistry* **39,** 2552–2563 (2000).
15. Greenbaum, E. a *et al.* The E46K mutation in alpha-synuclein increases amyloid fibril formation. *J. Biol. Chem.* **280,** 7800–7 (2005).
16. Narhi, L. *et al.* Both familial Parkinson's disease mutations accelerate α-synuclein aggregation. *J. Biol. Chem.* **274,** 9843–9846 (1999).
17. Anderson, J. P. *et al.* Phosphorylation of Ser-129 is the dominant pathological modification of alpha-synuclein in familial and sporadic Lewy body disease. *J. Biol. Chem.* **281,** 29739–52 (2006).
18. Fujiwara, H. *et al.* Alpha-Synuclein is phosphorylated in synucleinopathy lesions. *Nat. Cell Biol.* **4,** 160–4 (2002).
19. Oueslati, A., Fournier, M. & Lashuel, H. Role of post-translational modifications in modulating the structure, function and toxicity of alpha-synuclein: implications for Parkinson's disease pathogenesis and therapies. *Prog. Brain Res.* **183,** 115–45 (2010).
20. McFarland, N. R. *et al.* Alpha-Synuclein S129 Phosphorylation Mutants do not Alter Nigrostriatal Toxicity in a Rat Model of Parkinson Disease. *J Neuropathol Exp Neurol* **68,** 515–524 (2009).

21. Chen, L. & Feany, M. B. a-Synuclein phosphorylation controls neurotoxicity and inclusion formation in a Drosophila model of Parkinson disease. *Nat. Neurosci.* **8,** 657–663 (2005).
22. Gorbatyuk, O. S. *et al.* The phosphorylation state of Ser-129 in human a-synuclein determines neurodegeneration in a rat model of Parkinson disease. *Proc. Natl. Acad. Sci. U. S. A.* **105,** (2008).
23. Azeredo, S., Schneider, B. L., Cifuentes-diaz, C., Sage, D. & Aebischer, P. Phosphorylation does not prompt, nor prevent, the formation of a-synuclein toxic species in a rat model of Parkinson's disease. *Hum. Mol. Genet.* **18,** 10–15 (2009).
24. Chen, L. *et al.* Tyrosine and serine phosphorylation of α-synuclein have opposing effects on neurotoxicity and soluble oligomer formation. *J. Clin. Invest.* **119,** 3257–3265 (2009).
25. Paleologou, K. E. *et al.* Phosphorylation at Ser-129 but not the phosphomimics S129E/D inhibits the fibrillation of alpha-synuclein. *J. Biol. Chem.* **283,** 16895–905 (2008).
26. Waxman, E. A. & Giasson, B. I. Specificity and Regulation of Casein Kinase/Mediated Phosphorylation of Alpha-Synuclein. *J Neuropathol Exp Neurol* **67,** 402–416 (2008).
27. Luk, K. C. *et al.* Pathological α-synuclein transmission initiates Parkinson-like neurodegeneration in nontransgenic mice. *Science* **338,** 949–53 (2012).
28. Abeliovich, A. *et al.* Mice lacking alpha-synuclein display functional deficits in the nigrostriatal dopamine system. *Neuron* **25,** 239–52 (2000).
29. Mertins, P. *et al.* Integrated proteomic analysis of post-translational modifications by serial enrichment. *Nat. Methods* **10,** 634–7 (2013).
30. Osterberg, V. R. *et al.* Progressive Aggregation of Alpha-Synuclein and Selective Degeneration of Lewy Inclusion-Bearing Neurons in a Mouse Model of Parkinsonism. *Cell Rep.* **10,** 1252–1260 (2015).
31. Sacino, A. N. *et al.* Brain Injection of a-Synuclein Induces Multiple Proteinopathies, Gliosis, and a Neuronal Injury Marker. *J. Neurosci.* **34,** 12368–12378 (2014).
32. Paumier, K. L. *et al.* Intrastriatal injection of pre-formed mouse α-synuclein fibrils into rats triggers α-synuclein pathology and bilateral nigrostriatal degeneration. *Neurobiol. Dis.* **82,** 185–199 (2015).
33. Zanivan, S., Krueger, M. & Mann, M. In Vivo Quantitative Proteomics: The SILAC Mouse. *Methods Mol Biol.* **757,** 435–450 (2012).
34. Krüger, M. *et al.* Resource SILAC Mouse for Quantitative Proteomics Uncovers Kindlin-3 as an Essential Factor for Red Blood Cell Function. *Cell* **134,** 353–364 (2008).
35. Kim, E. K. & Choi, E. Pathological roles of MAPK signaling pathways in human diseases. *BBA - Mol. Basis Dis.* **1802,** 396–405 (2010).
36. Levy, O. A., Malagelada, Æ. C., Greene, L. A. & Alpha-synuclein, N. Á. Cell death pathways in Parkinson's disease: proximal triggers, distal effectors, and final steps. *Apoptosis* **14,** 478–500 (2009).

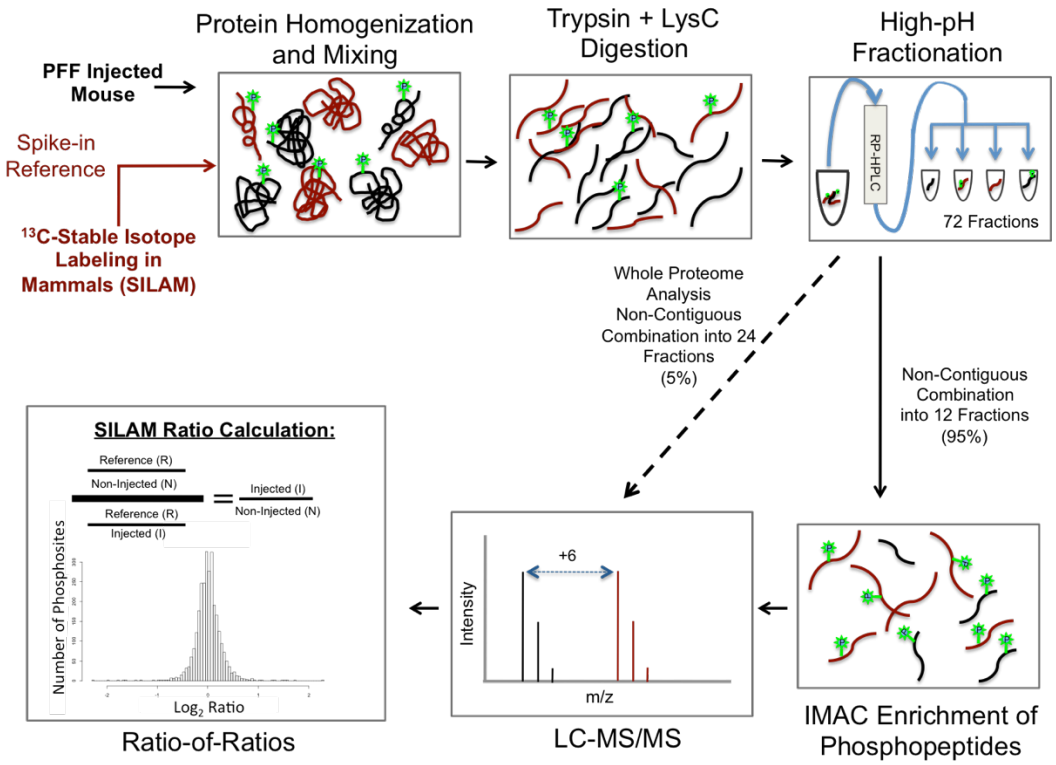

Figure 4.1 Overview of Phosphoproteomic Workflow

The midbrain and striatum from the injected side of two mice are collected and combined. The same is done from the non-injected side. These samples are then independently mixed and homogenized in a 1:1 ratio with SILAM brain tissue. The mixture is then digested with trypsin and LysC, followed by high-PH RPLC. 95% of the resulting peptides are then combined into 12 fractions in a concatenated pattern. IMAC enrichment is then used to enrich for phosphorylated peptides. Following LC-MS/MS, the relative abundance changes of the phosphopeptides are determined using a ratio of ratios calculation. Three biological replicates in both WT and Snca -/- injected mice were completed.

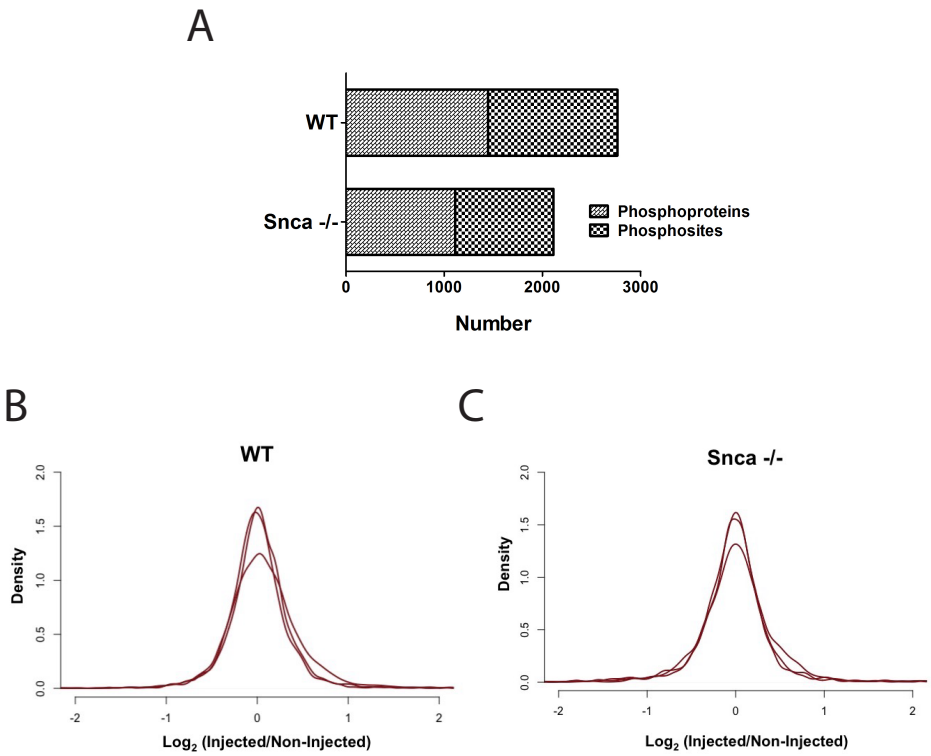

Figure 4.2 Phosphosites Quantified in WT and Snca -/-

(A) A phosphosite is considered quantified if the relative abundance change has been determined in all three replicates. Using this criterion, 2,763 phosphosites (from 1,445 phosphoproteins) and 2,112 phosphosites (from 1,110 phosphoproteins) were quantified in WT and Snca -/-, respectively.

Density plots of the $\log_2$ transformed ratio of ratios of **(B)** WT and **(C)** Snca -/-.

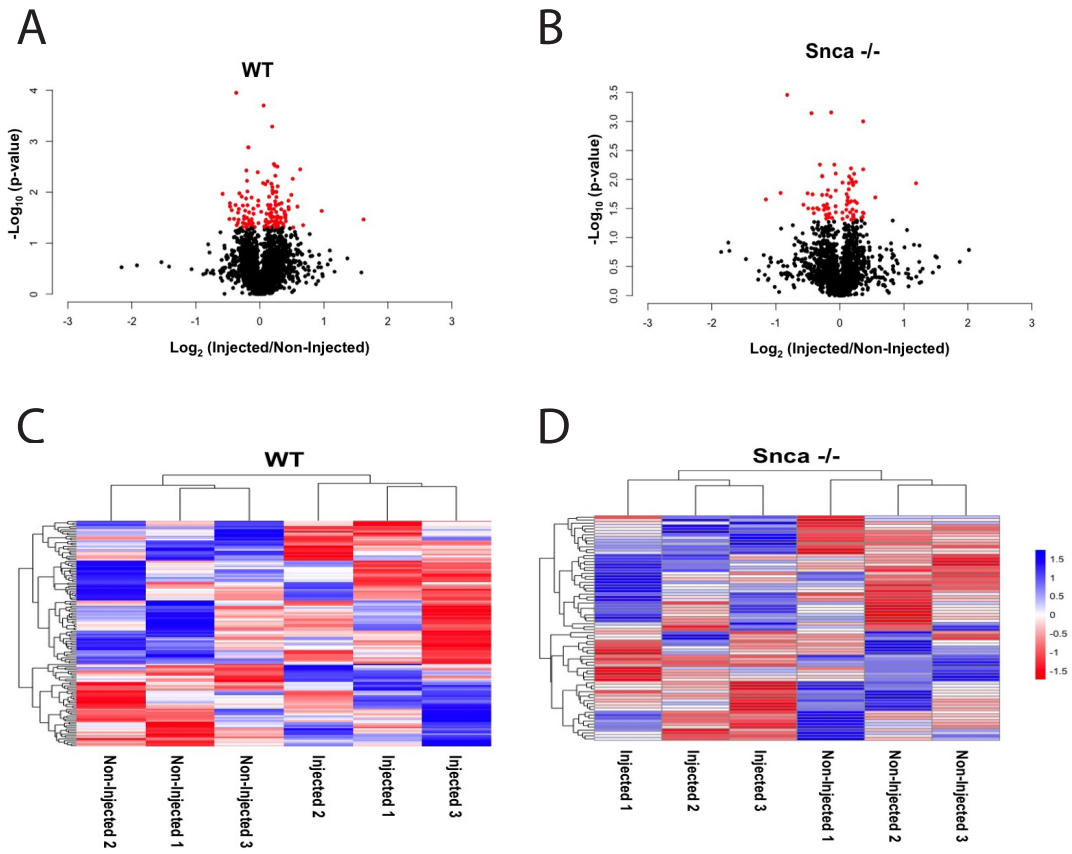

Figure 4.3 Significantly Changed Phosphosites
Volcano plots showing average differential expression verses significance for **(A)** WT and **(D)** Snca -/-. Red dots represent those phosphosites that have a p-value of $\leq$ 0.05.
Heatmaps of unidirected clustering of the phosphosites that significantly changed in **(C)** WT and **(D)** Snca -/- shows that the relative abundance changes are clustering by columns (injected versus non-injected).

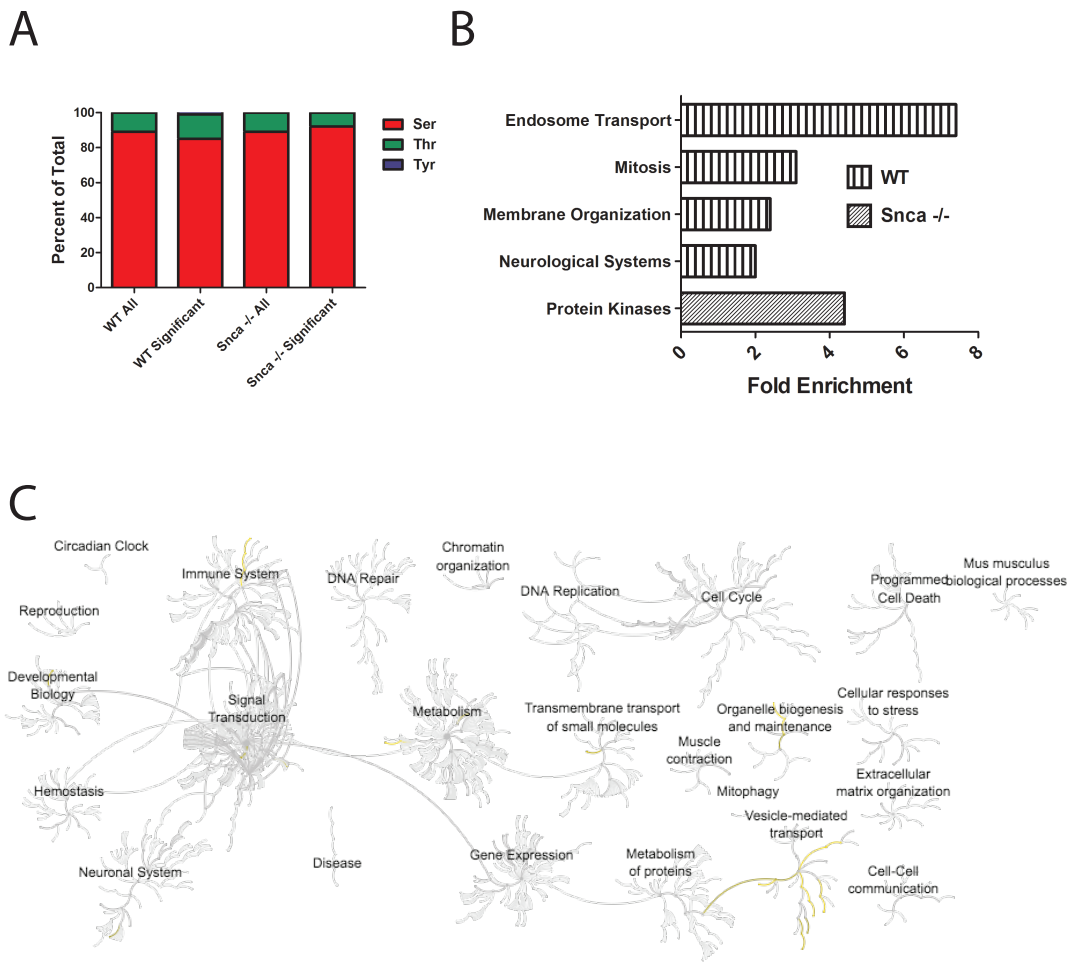

Figure 4.4 Properties, Biological Processes and Pathways of Significantly Altered Phosphoproteins

(A) Amino acid distribution of phosphosites quantified in WT, Snca -/-, including all and significant phosphosites.

(B) Enriched biological processes of the significantly altered phosphoproteins in WT and Snca -/-. In each set, the background was all the phosphoproteins quantified in that respective genotype.

(C) Global pathways that are enriched for significantly altered phosphosites in WT.

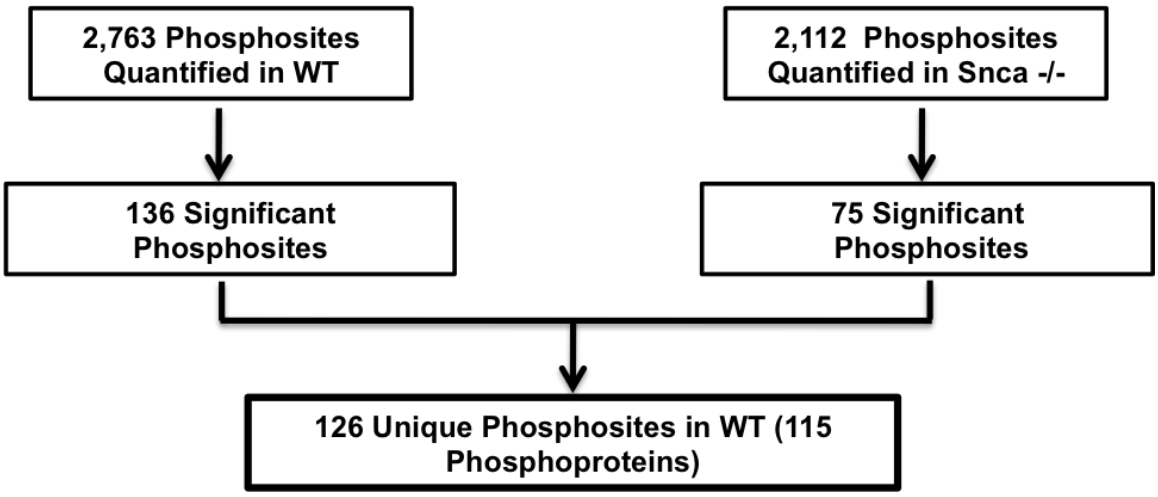

Figure 4.1 Breakdown of Significantly Changed Phosphosites
All 2,763 phosphosites quantified in WT were used to identify the 116 phosphosites that significantly changed.

CHAPTER 5

Conclusions

5.1 Summary and Conclusions

Neurodegenerative diseases present a significant challenge for healthcare systems, patients afflicted by these diseases, and scientists attempting to understand their underlying mechanisms and develop disease-modifying therapies. As populations continue to age, the burden of these diseases is expected to worsen. The number of people afflicted with dementia is expected to rise from over 46 million people today to over 130 million people by 2018[1]. The total cost associated with treatment and care is expected to rise from $818 billion today to over $1 trillion in 2018[1]. The development of effective disease-modifying therapies to treat these diseases, especially Alzheimer's disease (AD) and Parkinson's disease (PD), is urgently needed. AD is the most common neurodegenerative disease and the most common cause of dementia, accounting for 60%-80% of cases[2]. In the United States, it is the sixth leading cause of death and afflicts approximately 5.4 million people. This is expected to rise to 13.8 million people by 2050. Age is the greatest risk factor, with one in nine people over the age of 65 diagnosed. Of the top 10 causes of death in the United States, only AD cannot be prevented or delayed[3]. Early symptoms include difficulty remembering recent conversations, and apathy and depression. Later symptoms include confusion, disorientation, poor judgment and eventually impaired ability to walk, speak and eat.

PD afflicts 7-10 million people worldwide, including approximately 1 million people in the United States[4]. The lifetime risk of developing PD is 1.5%[5]. Like AD, the greatest risk factor is age, with the median onset age of 60 and 4 percent of cases being diagnosed before the age of 50[4]. Men are 50% more likely to develop PD than women[6]. Early symptoms of PD include subtle motor deficiencies, including changes in writing, impairments in dexterity, and dragging one foot while

walking[7]. As the disease progresses, symptoms include bradykinesia, resting tremor, rigidity and slurred speech.

Underlying the pathology of both AD and PD, as well as other neurodegenerative diseases including Amyotrophic Lateral Sclerosis and Huntington's disease (HD), is protein aggregation[8–10]. Though many of the proteins that misfold in these diseases have been identified, the relationship between this misfolding and neurodegeneration is unclear. Filling this gap would shed light on biological pathways and molecular targets that could be modified to mitigate cell death and thus provide a therapeutics relief. In this study, we focused on the aggregation of α-synuclein, a 140 amino acid protein that has roles in synaptic plasticity[11]. Aggregation of α-synuclein is implicated in several diseases, collectively known as synucleinopathies. Prominent among these are PD and dementia with Lewy Bodies (DLB).

In these studies we aimed to quantitatively investigate the effect of endogenous aggregation of α-synuclein on the proteostasis network of the brain. The proteostasis network refers to the diverse and integrated cellular machinery and pathways that function to maintain proper protein homeostasis, including protein localization, expression, degradation, folding and binding partners[12]. We focused on changes in both protein and phosphorylation levels to study how the proteostasis network is perturbed due to α-synuclein aggregation in the brain.

To accomplish this, we utilized a recently developed mouse model of endogenous α-synuclein that recapitulates several cardinal features of PD. Aggregation is induced in this model by intrastriatal injection of pre-formed fibrils (PFFs) of α-synuclein into non-transgenic (WT) mice[13]. This aggregation of endogenous α-synuclein is progressive, spreading from near the site of injection to synaptically connected regions over a 180-day period. Concomitant with this progressive aggregation is dopaminergic degeneration and the onset of a motor phenotype,

both cardinal features of PD. Importantly, aggregation (in the midbrain and striatum) and dopaminergic degeneration is confined to the injected side only, allowing us to use the non-injected side as an internal control. Finally, injection of PFFs into α-synuclein-null mice (Snca -/-) fails to induce this pathology, allowing us to use these mice to control for the effect of the injection on protein and phosphorylation levels. We used a modified version of this model whereby mice were triple-injected instead of single-injected in order to accelerate pathology. Before analyzing these mice further, we validated that the expected differences between the injected and non-injected sides, and between the WT and Snca -/- mice, were maintained. We found that α-synuclein phosphorylated at Ser-129, a marker for pathology[14,15], was confined to the injected side of WT mice. Additionally, we quantified a 19% loss in dopaminergic neurons in the injected side of WT mice compared with the non-injected side, versus no loss in the Snca -/- mice. After confirming these findings, employed a quantitative mass spectrometry (MS)-based approach to measure the relative abundance changes in protein and phosphorylation levels due to α-synuclein aggregation.

Our work quantified the relative abundance changes of 5,290 proteins in WT and 3,335 proteins in Snca -/- mice and 2,983 phosphorylation sites in WT and 2,112 phosphorylation sites in Snca -/-. Comparing the quantified proteins in our work to proteins identified in the mouse brain in MS-based studies in the literature[16–19] revealed no major differences in terms of molecular weight, biological function or cellular localizations. This adds confidence that the proteins quantified in our study do not significantly differ from those found in other studies. Additionally, there were significant declines in the relative abundance of proteins selectively expressed in dopaminergic neurons in WT but not Snca -/- mice, including tyrosine hydroxylase (TH), aromatic-L-amino-acid decarboxylase (Addc), synaptic vesicular amine transporter-2 (VMAT2),

and dopamine transporter (DAT). The declines in TH, Addc and VMAT2 were validated by Western blot, adding further confidence in our model and approach. Collectively, these analyses demonstrate the comprehensiveness and selectivity of our approach, and add confidence in our findings.

Statistical analysis of the quantified proteins and phosphosites resulted in the identification of 311 proteins (152 that increased and 159 that decreased in the injected side) and 133 phosphosites (from 121 phosphoproteins) whose relative abundance significantly changed. Of the proteins that significantly changed, we found that RNA transport and the immune response were enriched among the proteins that increased in the injected side, and that vesicle-mediated transport, ion transmembrane transport and microtubule organization was enriched in the proteins that decreased. Among the phosphoproteins that significantly changed, vesicle-mediated transport and membrane organization were enriched. For the phosphoproteins we did not separate the phosphosites that increased and decreased since the direction of the change in relative abundance is not necessarily indicative of the change in activity (i.e. and increase in phosphorylation does not necessarily mean an increase in activity). These enrichment analyses from the proteomics and phosphoproteomics suggest that cellular signaling is perturbed in response to α-synuclein aggregation, consistent with the documented dopaminergic degeneration in this model and data from other studies[13,20–22].

Of the 311 proteins and 135 phosphosites that significantly changed, we decided to focus on Lmp7 (also known as proteasome subunit beta 8, or psmb8) for three reasons. First, it had the greatest increase of the 152 proteins that significantly increased (236%). Second, it is involved in the immune response, a topic that has garnered increased attention as a potential mediator of α-synuclein aggregation-mediated toxicity in PD[23]. And finally, it is a catalytic subunit of the

immunoproteasome, which has been implicated in protein aggregation diseases including AD and HD[24–26], but not in synucleinopathies. We first validated the increase detected by proteomics by Western blot. Then, using human DLB samples, we found that Lmp7 levels and activity were elevated in disease compared with healthy controls. This is, to our knowledge, the first reported association between the immunoproteasome and synucleinopathies.

Lmp7 is one of the three cardinal subunits of the immunoproteasome. Upon stimulation by proinflammatory cytokines or oxidative stress, expression of the catalytic subunits of the immunoproteasome, namely Lmp2, MECL-1 and Lmp7, is elevated[27,28]. These proteins then replace the catalytic subunits of the constitutive proteasome, namely β_1, β_2 and β_5, respectively. The immunoproteasome, which has different cleavage site preferences and catalytic activity than the constitutive proteasome, generates antigenic peptides that are recognized by MHC class I molecules[29–32]. These MHC class I molecules then present these peptides on the cell surface for detection and destruction by CD8+ T cells[33].

Though the immunoproteasome has not been directly linked to synucleinopathies, a recent study found a link between MHC-I and dopaminergic neurons[34]. This study documented the expression of MHC-I in the substantia nigra of both control and PD samples leading to a proposed model that links MHC-I and dopaminergic degeneration. In this model, IFNγ induced by the aggregation α-synuclein and the oxidative stress caused by cytosolic dopamine results in the expression of MHC-I. This MHC-I is then loaded with antigenic peptides and exposed on the cell surface for destruction by cytotoxic T cells (CTLs). Though the endogenous source of these peptides was not considered, our work may provide the link.

The oxidative stress and IFNγ results in the increased expression of the immunoproteasome, as we document in our studies. The immunoproteasome then interacts with and degrades α-

synuclein fibrils more efficiently than the constitutive proteasome. This is consistent with the documented preference of the immunoproteasome to degrade basic proteins[35]. Furthermore, in our studies using cell free systems, we demonstrate that degradation of α-synuclein fibrils occurs more rapidly by the immunoproteasome than the constitutive proteasome. Furthermore, the products of this degradation reaction are unable to accelerate the aggregation of soluble α-synuclein, a feature of bona fide protein aggregates[9]. The resulting α-synuclein peptides are then loaded onto the MHC-I molecules for presentation to CTLs. Thus, dopaminergic neuron degeneration in synucleinopathies may be enhanced by accelerated degradation of α-synuclein by the immunoproteasome, leading to MHC-1 presentation on the cell surface, and recognition by CTLs.

Alternatively, the degradation of α-synuclein fibrils by the immunoproteasome could be neuroprotective. Though there is debate as to whether the aggregation of α-synuclein causes cell death via a toxic gain-of-function or a toxic loss-of-function[36], the finding that α-synuclein-null mice are viable and do not have shortened lifespan supports a toxic gain-of-function[37,38]. Not surprisingly, many therapeutic strategies have attempted to remove α-synuclein aggregates as a protective mechanism[39]. These include immunization against α-synuclein[40,41], small molecule inhibition of aggregation[42,43], and the exogenous introduction of protein disaggregases[44]. This last approach is particularly troublesome given the difficulty in introducing these proteins intracellularly and the cofactors that are needed for these large protein complexes to function. The immunoproteasome may provide a novel, endogenous therapeutic target that can be modulated to mitigate α-synuclein-mediated neurodegeneration. Augmentation of the immunoproteasome could accelerate α-synuclein degradation and thus

retard neuron death. Additionally, engineering of the immunoproteasome may increase the activity and selectivity for α-synuclein aggregates.

Determination of the role of the immunoproteasome in enhancing or mitigating synucleinopathies is critical for the ultimate goal of therapeutic development. A key tool that could be used to test this is the immunoproteasome-null mouse. These mice lack all three catalytic subunit of the immunoproteasome and exhibit the expected defects in presenting several classes of MHC-I epitopes[45]. Injection of PFFs into these mice followed by monitoring of motor symptoms, dopaminergic degeneration, and α-synuclein aggregation would clarify the role of the immunoproteasome. We expect decreased α-synuclein-positive aggregates in the immunoproteasome-null injected mice. While enhanced dopaminergic degeneration and motor symptoms would suggest a neuroprotective role for the immunoproteasome, decreased degeneration and motors symptoms would be evidence for a neurotoxic role.

Ultimately, our work contributes three major new findings. First, we further characterized an important mouse model of α-synuclein aggregation that will assist future researchers using this model. Second, we provide a rich source of the relative abundance changes of proteins and phosphosites in the brain in response to the endogenous aggregation of α-synuclein. This could provide a valuable resource for investigators studying how proteostasis pathways respond to α-synuclein aggregation specifically, or protein aggregation broadly. Finally, we document, for the first time, an increase in the levels and activity of the immunoproteasome in a human synucleinopathy, and explore its activity against α-synuclein fibrils compared with the constitutive proteasome. We believe the immunoproteasome is a putative therapeutic target for treating synucleinopathies like PD and DLB, and merits further attention.

References

1. Prince, M. *et al.* World Alzheimer Report 2015. *Alzheimer's Dis. Int.* 1 – 87 (2015).
2. Barker WW, Luis CA, Kashuba A, Luis M, Harwood DG, Loewenstein D, Waters C, Jimison P, Shepherd E, Sevush S, Graff-Radford N, Newland D, Todd M, Miller B, Gold M, Heilman K, Doty L, Goodman I, Robinson B, Pearl G, Dickson D, D. R. Relative frequencies of Alzheimer disease, Lewy body, vascular and frontotemporal dementia, and hippocampal sclerosis in the State of Florida Brain Bank. *Alzheimer Dis Assoc Disord* **16,** 203–212 (2002).
3. The Alzheimer's Association. *http://www.alz.org/facts/*
4. Parkinson's Disease Foundation. *http://www.pdf.org/en/parkinson_statistics*
5. Bower JH, Maraganore DM, McDonnell SDK, R. W. Incidence and distribution of parkinsonism in Olmsted County, Minnesota. *Neurology* **52,** 1214–1220 (1999).
6. Twelves D, Perkins KS, C. C. Systematic review of incidence studies of Parkinson's disease. *Mov. Disord* **18,** 19–31 (2003).
7. Lees, A. J., Hardy, J. & Revesz, T. Parkinson's disease. *Lancet* **373,** 2055–2066 (2009).
8. Aguzzi, A. & Connor, T. O. Protein aggregation diseases: pathogenicity and therapeutic perspectives. *Nat. Rev. Drug Discov.* **9,** 237 – 248 (2010).
9. Jucker, M. & Walker, L. C. Self-propagation of pathogenic protein aggregates in neurodegenerative diseases. *Nature* **501,** 45–51 (2013).
10. Skovronsky, D. M., Lee, V. M. & Trojanowski, J. Q. Neurodegenerative Diseases: New Concepts of Pathogenesis and Their Therapeutic Implications. *Annu. Rev. Pathol.* **1,** 151 – 170 (2006).
11. Mor, D. E., Ugras, S. E., Daniels, M. J. & Ischiropoulos, H. Neurobiology of disease dynamic structural flexibility of α-synuclein. *Neurobiol. Dis.* **88,** 66–74 (2016).
12. Balch, W. E., Morimoto, R. I., Dillin, A. & Kelly, J. W. Adapting Proteostasis for Disease Intervention. *Science* **319,** 916 – 919 (2008).
13. Luk, K. C. *et al.* Pathological α-synuclein transmission initiates Parkinson-like neurodegeneration in nontransgenic mice. *Science* **338,** 949–53 (2012).
14. Fujiwara, H. *et al.* Alpha-Synuclein is phosphorylated in synucleinopathy lesions. *Nat. Cell Biol.* **4,** 160–4 (2002).
15. Anderson, J. P. *et al.* Phosphorylation of Ser-129 is the dominant pathological modification of alpha-synuclein in familial and sporadic Lewy body disease. *J. Biol. Chem.* **281,** 29739–52 (2006).
16. Price, J. C., Guan, S., Burlingame, A., Prusiner, S. B. & Ghaemmaghami, S. Analysis of proteome dynamics in the mouse brain. *Proc. Natl. Acad. Sci. U. S. A.* **107,** 14508 –14513 (2010).
17. Sharma, K. *et al.* Cell type – and brain region – resolved mouse brain proteome. *Nat. Neurosci.* **18,** 1819 – 1831 (2015).
18. Walther, D. M. & Mann, M. Accurate Quantification of More Than 4000 Mouse Tissue Proteins Reveals Minimal Proteome Changes During Aging. *Mol. Cell. Proteomics* 1–7 (2011).
19. Wang, H. *et al.* Characterization of the Mouse Brain Proteome Using Global Proteomic Analysis Complemented with Cysteinyl-Peptide Enrichment. *J. Proteome Res.* 361–369 (2006).
20. Osterberg, V. R. *et al.* Progressive Aggregation of Alpha-Synuclein and Selective

Degeneration of Lewy Inclusion-Bearing Neurons in a Mouse Model of Parkinsonism. *Cell Rep.* **10,** 1252–1260 (2015).
21. Paumier, K. L. *et al.* Intrastriatal injection of pre-formed mouse α-synuclein fibrils into rats triggers α-synuclein pathology and bilateral nigrostriatal degeneration. *Neurobiol. Dis.* **82,** 185–199 (2015).
22. Sacino, A. N. *et al.* Brain Injection of a-Synuclein Induces Multiple Proteinopathies, Gliosis, and a Neuronal Injury Marker. *Neurobiol. Dis.* **34,** 12368–12378 (2014).
23. Tufekci, K. U., Meuwissen, R., Genc, S. & Genc, K. Inflammation in Parkinson's Disease. *Adv. Protein Chem. Struct. Biol.* **88,** 69–132 (2012).
24. Aso, E. *et al.* Amyloid Generation and Dysfunctional Immunoproteasome Activation with Disease Progression in Animal Model of Familial Alzheimer's Disease. *Brain Pathol.* **22,** 636–653 (2012).
25. Orre, M. *et al.* Reactive glia show increased immunoproteasome activity in Alzheimer's disease. *Brain* **136,** 1415–1431 (2013).
26. Dıaz-Hernandez, M. *et al.* Neuronal Induction of the Immunoproteasome in Huntington's Disease. *J. Neurosci.* **23,** 11653–11661 (2003).
27. Ferrington, D. A. & Gregerson, D. S. Immunoproteasomes: Structure, Function, and Antigen Presentation. *Prog. Mol. Biol. Transl. Sci.* **109,** 75–112 (2012).
28. Heink, S., Ludwig, D., Kloetzel, P. & Kru, E. IFN-y-induced immune adaptation of the proteasome system is an accelerated and transient response. *Proc. Natl. Acad. Sci. U. S. A.* **102,** 9241–9246 (2005).
29. Marques, J., Palanimurugan, R., Matias, A. C., Ramos, P. C. & Ju, R. Catalytic Mechanism and Assembly of the Proteasome. *Chem. Rev.* **109,** 1509–1536 (2009).
30. Chapiro, J. *et al.* Destructive Cleavage of Antigenic Peptides Either by the Immunoproteasome or by the Standard Proteasome Results in Differential Antigen Presentation. *J. Immunol.* **176,** 1053–1061 (2006).
31. Cardozo, C. & Kohanski, R. A. Altered Properties of the Branched Chain Amino Acid-preferring Activity Contribute to Increased Cleavages after Branched Chain Residues by the 'Immunoproteasome'. *J. Biol. Chem.* **273,** 16764–16770 (1998).
32. Lei, B. *et al.* Molecular Basis of the Selectivity of the Immunoproteasome Catalytic Subunit LMP2-Specific Inhibitor Revealed by Molecular Modeling and Dynamics Simulations. *J. Phys. Chem.* 12333–12339 (2010).
33. Dalet, A., Stroobant, V. & Vigneron, N. Differences in the production of spliced antigenic peptides by the standard proteasome and the immunoproteasome. *Eur. J. Immunol.* **41,** 39–46 (2011).
34. Cebrian, C. *et al.* MHC-I expression renders catecholaminergic neurons susceptible to T-cell-mediated degeneration. *Nat. Commun.* **5,** 3633 (2014).
35. Raule, M., Cerruti, F. & Cascio, P. Enhanced rate of degradation of basic proteins by 26S immunoproteasomes. *BBA - Mol. Cell Res.* **1843,** 1942–1947 (2014).
36. Winklhofer, K. F. & Haass, C. The two faces of protein misfolding: gain- and loss-of-function in neurodegenerative diseases. *EMBO J.* **27,** 336–349 (2008).
37. Abeliovich, A. *et al.* Mice lacking alpha-synuclein display functional deficits in the nigrostriatal dopamine system. *Neuron* **25,** 239–52 (2000).
38. Cabin, D. E. *et al.* Synaptic Vesicle Depletion Correlates with Attenuated Synaptic a-Synuclein. *J. Neurosci.* **22,** 8797–8807 (2002).
39. Rohn, T. Targeting alpha-synuclein for the treatment of Parkinson's disease. *CNS Neurol*

Disord Drug Targets **11,** 174–179 (2012).
40. Mandler, M. *et al.* Active immunization against alpha-synuclein ameliorates the degenerative pathology and prevents demyelination in a model of multiple system atrophy. *Mol. Neurodegener.* 1–15 (2015).
41. Valera, E. & Masliah, E. Pharmacology & Therapeutics Immunotherapy for nNeurodegenerative Diseases: Focus on α-Synucleinopathies. *Pharmacol. Ther.* **138,** 311–322 (2013).
42. Caruana, M. *et al.* Inhibition and disaggregation of a-synuclein oligomers by natural polyphenolic compounds. *FEBS Lett.* **585,** 1113–1120 (2011).
43. H, C., VL, A.-B., NM, K. & JM, M. Intracellular screening of a peptide library to derive a potent peptide inhibitor of α-synuclein aggregation. *J. Biol. Chem.* **290,** 7426 – 7435 (2015).
44. Doyle, S. M., Genest, O. & Wickner, S. Protein rescue from aggregates by powerful molecular chaperone machines. *Nat. Rev. Mol. Cell Biol.* **14,** 617–629 (2013).
45. Kincaid, E. Z. *et al.* Mice completely lacking immunoproteasomes show major changes in antigen presentation. *Nat. Immunol.* **13,** 129–135 (2012).